過去二十万年間における日本海ＯＤＰ７９７地点堆積物への黄砂（風成塵）寄与率の定量およびそのフラックス変動の復元

入野智久

学 位 論 文

Quantification of Kosa (aeolian dust) contribution to the sediments
and reconstruction of its flux variation at ODP Site 797,
the Japan Sea during the last 200 ky

過去２０万年間における日本海ＯＤＰ７９７地点堆積物への黄砂
（風成塵）寄与率の定量およびそのフラックス変動の復元

平成８年８月博士（理学）申請

東京大学大学院理学系研究科
地質学専攻

入 野 智 久

Quantification of Kosa (aeolian dust) contribution to the sediments and reconstruction of its flux variation at ODP Site 797, the Japan Sea during the last 200 ky

1996

Tomohisa Irino

Geological Institute, Faculty of Science, University of Tokyo

Abstract

Aeolian dust flux and its temporal variation have been studied intensively because of the possible importance of aeolian dust on the marine geochemical cycles and its utility as a paleoclimatic indicator. In order to reconstruct past variations in the Kosa flux to the Japan Sea, and establish the direct linkage between the terrestrial and marine climatic records, the author invented a new procedure for Q-mode factor analysis which is applied to chemical and mineral compositions of the late Quaternary hemipelagic sediments in the Japan Sea. With this procedure, it is possible to distinguish and quantify detrital subcomponents within the detrital component. Four detrital subcomponents were extracted, which are attributed to fine and coarse subcomponents of Kosa and arc-derived detritus, respectively, based on the comparison with the composition of probable source materials. Using these detrital subcomponents, Kosa fraction, Kosa grain size index (KGI), and arc-derived detritus grain size index (AGI) are defined and their variations as well as the variation in mass accumulation rate (MARs) of Kosa and arc-derived detritus during the last 200 ky are reconstructed. The results reveal millennial-scale as well as glacial - interglacial scale variations in Kosa fraction, KGI, and AGI. Close examination of their interrelationships suggests that the millennial-scale variation in Kosa fraction is explained by the changes in coarse arc-derived detritus flux. The examination of Kosa MAR also suggests the importance of the variation in the extent of Kosa source area in controlling the Kosa flux.

Contents

List of Illustrations

Figures

Tables

Appendix

1. Introduction

Kosa is the aeolian dust observed in the Japanese islands and derived from the inland arid area in central Asia [*Iwasaka et al.*, 1983]. It is suggested that higher frequency of dust storm in the arid area of central Asia results in higher flux of aeolian dust to the northwest Pacific [*Gao et al.*, 1992], which is transported by the prevailing westerlies. Consequently, temporal and spatial distribution of aeolian dust flux to the sediments in north Pacific is thought to be controlled by the location and extent of arid source area as well as the strength and pattern of the wind system [*Leinen et al.*, 1986].

Recent high resolution analysis of GRIP and GISP2 ice cores from central Greenland suggests that the climate in high latitude northern hemisphere during the last glacial period was oscillated drastically in millennial-scale which is known as Dansgaard-Oeschger Cycles [*Dansgaard et al.*, 1993, *Taylor et al.*, 1993]. Especially, *Taylor et al.* [1993] pointed out that the atmospheric dust concentration over Greenland changed in millennial-scale. Recently, *Porter and An* [1995] showed that quartz grain size within the loess sequence at the Loess Plateau of China varied in millennial-scale, and suggested the possibility of millennial-scale variation in atmospheric circulation in the northern hemisphere. On the other hand, *Tada et al.* [1995] reported the possible signal of the Dansgaard-Oeschger Cycles from the hemipelagic sediments of the Japan Sea. In order to directly compare such millennial-scale variation in terrestrial records with that of marine records, high resolution reconstruction of aeolian contribution to the marine sediments is necessary.

Aeolian dust flux and its temporal variation have been studied intensively during the last two decades because of the possible importance of aeolian dust on the marine biogeochemical cycles [*Duce et al.*, 1991] and its utility as a paleoclimatic indicator of the aridity of continental interiors as well as the strength of prevailing winds [*Rea et al.*, 1985]. During 1980's, it was believed that the detrital component of the pelagic sediments in the North Pacific is mostly composed of aeolian dust derived from the central Asia (= Kosa), and the

mass accumulation rate and median grain diameter of the detrital component have been widely used as a measure of aeolian flux and wind intensity, respectively [e.g. *Rea and Leinen*, 1988, *Hovan et al.*, 1991]. However, based on the rare earth elements and isotope studies of the North Pacific sediments, it has been pointed out recently that even such pelagic sediments contain significant amount of detrital subcomponent derived from island arcs of the northwest Pacific [*Olivarez et al.*, 1991, *Nakai et al.*, 1993, *Weber II et al.*, 1996]. Thus, in order to estimate Kosa flux from the sedimentary record, it is necessary to distinguish subcomponents within the detrital component, specify their origin, and estimate their contents.

Provenance studies of fine-grained siliciclastic sediments have a long history. The variation in the assemblage of heavy minerals [*Krumbein and Pettijohn*, 1938] and clay minerals [*Chamley*, 1989] has been widely used to distinguish the sources of detrital subcomponents. Rare earth elements are also used recently [*Taylor and McClennan*, 1985, *Olivarez et al.*, 1991, *Nakai et al.*, 1993, *Weber II et al.*, 1996]. Although these methods have been successful in characterizing the detrital sources, they are not necessarily adequate for quantitative estimation of the subcomponents within the detrital component because these methods are based on the elements or minerals which constitute only a small fraction of the total detrital component. Thus, more adequate method to extract the composition and contribution of subcomponents within the detrital component of the sediment samples is required. Statistical analyses such as normative partitioning, linear programming, Q-mode factor analysis [*Leinen*, 1987], and total inversion method [*Kyte et al.*, 1993] has been applied to major and minor elements composition in order to estimate contribution and / or composition of the subcomponents within the detrital component. However, since normative partitioning and linear programming requires number and composition of the subcomponents for the analysis beforehand, these methods are not adequate when composition of the subcomponents is not known or composition of the subcomponents varied with time. Total inversion method allows changes in the composition of subcomponents, but this method assumes random variation in composition. Because it is not certain whether past variation in

composition of subcomponents were random or not, total inversion method may not be adequate for our purpose. Q-mode factor analysis do not require any a priori knowledge on composition of subcomponents although the meaning of extracted subcomponents need to be confirmed by other means.

In this study, the author developed a new procedure to estimate the composition and content of subcomponents within the detrital component by Q-mode factor analysis of selected major elements followed by multi-regression analysis between mineral composition and contents of subcomponents calculated by Q-mode factor analysis, and the author applied it to chemical and mineral composition data obtained for the Japan Sea sediments. Based on the result, the author extracted subcomponents attributable to Kosa, and reconstructed temporal variation in Kosa fraction and its mass accumulation rate during the last 200 ky.

2. Geological Setting of the Studied Site

The Japan Sea is a semi-enclosed marginal sea located in the back arc side of the Japan Island Arc and has total area of approximately 1,000,000 km^2. It is located only 2500 km downwind from the Taklimakan-Gobi Deserts where Kosa is derived from (Figure 1). The sea is connected to the other seas through the Mamiya (15 m water depth), Soya (55 m), Tsugaru (130 m), and Tsushima (130 m) Straits. The Tsushima Warm Current flows into the sea through the Tsushima Strait, flows along the eastern margin of the Japan Sea, and its major part flows out through the Tsugaru Strait. The Japan Sea is composed of the Japan Basin (3000 to 3500 m water depth) to the northwest and the Yamato Basin (2500 to 3000 m) to the southeast which are divided by the Yamato Rise (1000 m). The studied site, Ocean Drilling Program (ODP) Site 797 (36.62 °N, 134.54 °E, 2874 m water depth) is located on the northern rim of the Yamato Basin. It is approximately 500 km to the northeast of the Tsushima Strait, approximately 500 km to the east from the Asian continent, and approximately 250 km to the west from the Japan Arc, respectively (Figure 1).

Because the Japan Sea and Japanese islands are facing to the east margin of the Asian continent and they are the only place where dust haze due to Kosa is clearly observed [*Goudie*, 1983], significant contribution of Kosa to the Japan Sea sediments is expected. Detrital material could also have been transported to the sea through the riverine inputs from the Japan Arc and / or the Japan Sea side of the Asian continent. The drainage area of the Japan Sea side of the Japan Arc including Sakhalin is approximately 146,000 km^2. *Saito and Ikehara* [1992] estimated the present average sediment yield from the Japanese islands as approximately 700 $t/km^2/yr$. Consequently, sediment discharge to the Japan Sea from the Japan Arc is estimated as approximately 10^9 t/yr. On the other hand, the drainage area of the continental side is approximately 205,000 km^2 and the sediment yield is estimated as 10 to 50 $t/km^2/yr$ [*Milliman and Meade*, 1983]. Consequently, the sediment discharge to the sea from the Asian continent is estimated as 0.2 to 1 x 10^8 t/yr. In addition, the distance from Site 797 to the Japan Arc is approximately a half the distance from the Asian continent and the Yamato

Rise would block most of the detrital flux from the continental side to the studied site. From these reasons, the author considers that the riverine detrital flux from the continental side is negligible compared to that from the Arc side at ODP Site 797. The suspended matter discharged from the Huanghe River and transported by Tsushima Warm Current can be another detrital source to the Japan Sea [*Oba et al.*, 1991]. However, *Saito and Yang* [1994], who estimated total sediment discharge of present Huanghe River as 10^9 t/yr, showed that more than 99% of the sediment discharge is deposited within the shelf and less than 1% is exported out of the shelf. Furthermore, present sediment discharge of the Huanghe River could have been enhanced by nearly 10 times due to human agricultural activities during the last 2000 years [*Milliman et al.*, 1987]. Thus, sediment supplied from the Huanghe River through the Tsushima Strait should be less than 10^7 t/yr at present and probably less than 10^6 t/yr before 2000 years ago. Moreover, the distribution of clay minerals in the surface sediments of the Japan Sea is not controlled by the surface currents [*Yin et al.*, 1987]. From these reasons, the author considers that the detrital flux from the Huanghe River through the Tsushima Strait have been also negligible compared to riverine detrital flux from the Japan Arc.

The present Kosa flux to Japan is estimated as 1.4 to 4.3 g/cm^2/ky (1.4 to 4.3 x 10^7 t/yr for the whole Japan Sea area) [*Suzuki and Tsunogai*, 1987] which is more than thirty times larger than the flux to the central North Pacific (0.0013 to 0.045 g/cm^2/ky, [*Suzuki and Tsunogai*, 1987]). Whereas it is comparable to the average mass accumulation rate of 4.1 g/cm^2/ky during Quaternary at Site 797 [*Shipboard Scientific Party*, 1990]. Thus, a significant contribution of Kosa to the sediments is expected, although the detrital flux from the Japan Arc may not be negligible [*Tada et al.*, 1992].

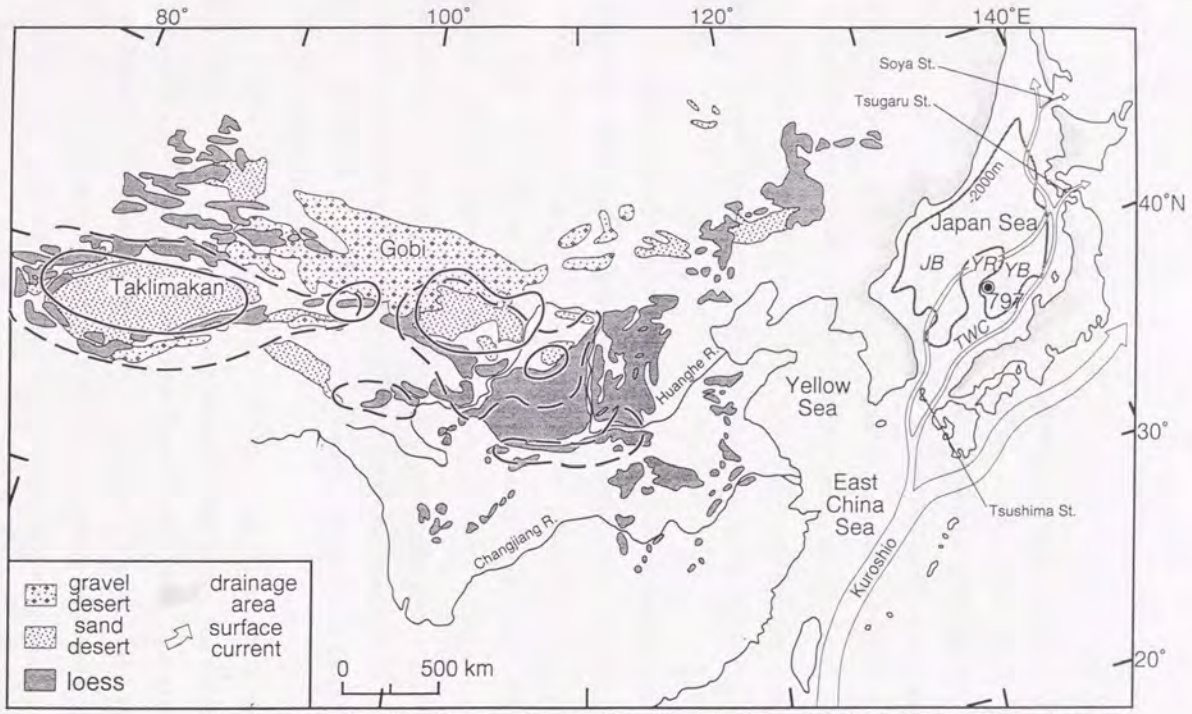

Figure 1 Locality of ODP Site 797 and geological settings of surrounding area. Distribution of loess and major desert in northern China is after *Pye and Zhou* [1989]. Encircled areas by solid and broken lines are areas where annual dust storm frequency and dust haze observation is more than 30 days, respectively [*Pye and Zhou*, 1989].

3. Studied Core and Materials

Continuous late Quaternary sedimentary sequence was recovered at Site 797 (Figure 2). The sediments are composed of clay and silty clay which are occasionally biosiliceous and / or biocalcareous, and thin volcanic ash layers are occasionally intercalated. They show centimeter to decimeter-scale alternationt of the dark and light layers which are correlatable within the Japan Sea [*Tada et al.*, 1992]. The dark layers are mostly laminated whereas the light layers are homogeneous to bioturbated and the boundary between the dark and light layers are generally sharp [*Tada et al.*, 1996]. The sequence is considered as continuous without any interruption by turbidite layers [*Shipboard Scientific Party*, 1990, *Tada et al.*, 1992].

Apparent core recovery exceeds 100% as a result of the expansion of sediments and drilling disturbance in the sediments is minimal [*Tada et al.*, 1992]. Core expansion was estimated as 105% for Core 797B-1H and 104% for Core 797B-2H, respectively [*Tada et al.*, 1996]. *Tada et al.* [1996] also recognized a 35 cm of core gap between Cores 797-1H and 2H which was recovered in Core 797A-1H. In this study, top of Core 797B-1H was set as 0 cmbsf and sample depths were corrected for core expansion and core gaps [*Tada et al.*, 1996]. Depths of samples supplemented from Core 797A-1H were also corrected to the corresponding depths of Cores 797B-1H and 2H based on the correlation of dark and light bands between Cores 797A and 797B (Figure 2).

Approximately 230 samples obtained from the uppermost part of the sequence are used in this study. These samples cover approximately the last 200 ky. The samples are composed of two sets with different sampling dates and ways of storage. First set (50 samples, noted LR and LRA in Tables) was sampled onboard with the average sampling interval of 30 cm and frozen immediately for shipment. Second set (174 samples, noted HR in Tables) was sampled by Associate Professor Ryuji Tada with the average sampling interval of approximately 7 cm one and a half year after the cruise at the Gulf Coast Core Repository of

ODP where cores were stored at 15 °C. One and a half year of the storage caused color alteration of the sediment surface due to oxidation, but original sediment color was preserved a few mm below the cut surface.

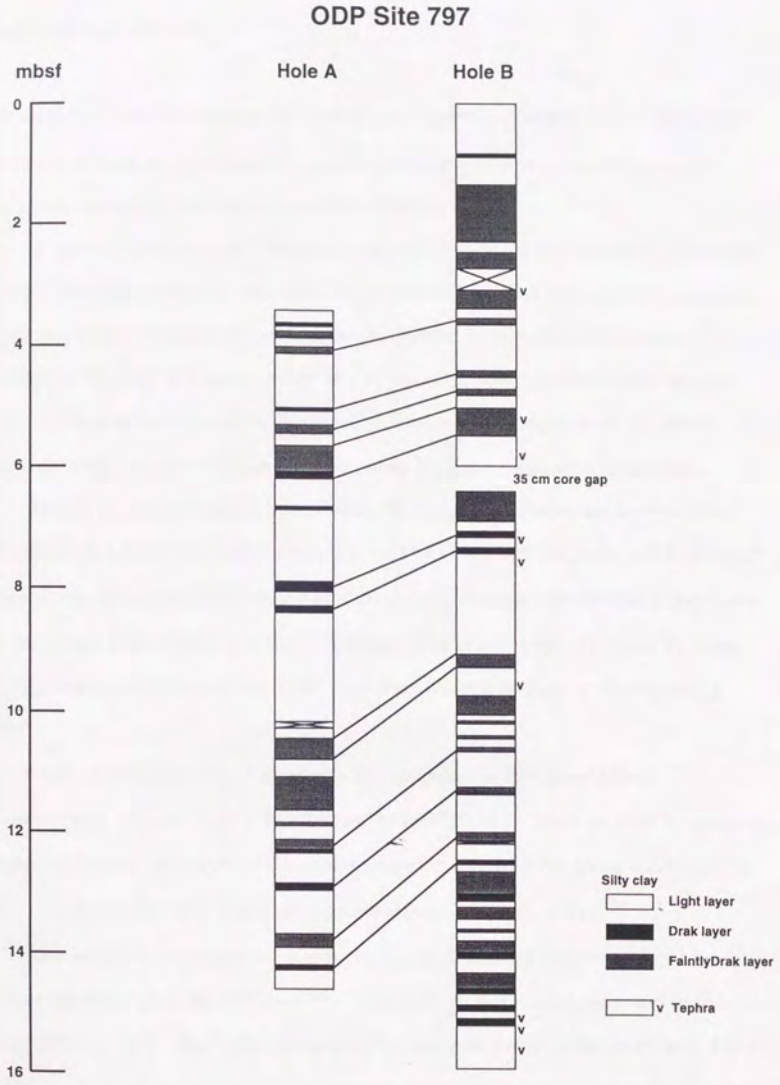

Figure 2 Columnar section of ODP Site 797 Hole A and B.

4. Sediment Age Model

In order to calculate linear sedimentation rate, age model at Site 797 for the last 200 ky is cited from *Tada et al.* [1996] who adopted following 13 datums (Figure 3). Depth (cmbsf) and calendar age (ka) for each sample is listed in Table 1.

Judging from the onboard observation, the top 15 to 20 cm of Core 797B-1H seemed to be originally vacant and filled afterwards with fluidized sediments flowed from top several cm of the sediment. However, the core caught the mudline because brownish oxidized layer of approximately 30 cm thick is preserved at the core top, which is comparable to the reported thickness of the oxidized layer of the Japan Sea sediments which ranges from 0 to 60 cm [*Masuzawa*, 1983]. Thus the horizon 18±2 cm below the apparent core top is set as 0 ka.

Ages of the uppermost dark layer (called TL-1) and the top and near bottom of the second dark layer (called TL-2) are estimated as 9.88±0.17 ka, 14.93±0.22 ka, and 21.01±0.27 ka, respectively, based on AMS^{14}C dating of planktonic foraminifer monospecies (*Globigerina umbilicata*) at the core KH79-3, L-3 from Oki Ridge [*Oba et al.*, 1995]. TL-1 and TL-2 are also recognized at Site 797 and these AMS^{14}C ages are adopted as those of corresponding horizon.

Marker tephra layer Aira-Tanzawa (AT) is identified at 224 cmbsf [*Shirai*, unpublished data]. The age of AT was estimated as 24.33±0.23 ka based on AMS^{14}C dating of planktonic foraminifer monospecies (*Neogloboquadorina dutertrei*) just above and below this tephra at the core KH89-18, P-4 from off Shikoku [*Murayama et al.*, 1993].

Tada et al. [1992] pointed out that the variation curve of the logarithm of diatom abundance (number / g) at Site 797 resembles "standard" oxygen isotope curve and there is no phase lag between them. Thus 7 datums are adopted based on tuning of the logarithmic diatom (especially warm water species) abundance curve to the oxygen isotope curve of *Martinson et al.* [1987] (Figure 3). Adopted datums are oxygen istope stages 5.0 (73.91 ka), 5.2 (90.95 ka), 5.4 (110.79 ka), 6.0 (129.84 ka), 6.3 (142.28 ka), 6.5 (175.05 ka), and 7.0 (189.61 ka) whose

ages are also based on *Martinson et al.* [1987].

Age model is constructed using above 13 datums assuming the constant linear sedimentation rate between datums. In this study, datums estimated using AMS^{14}C dating were corrected to calendar age based on the figure 1 of *Bard et al.* [1993] in order to prevent mass accumulation rates from the underestimation due to the underestimation of linear sedimentation rates.

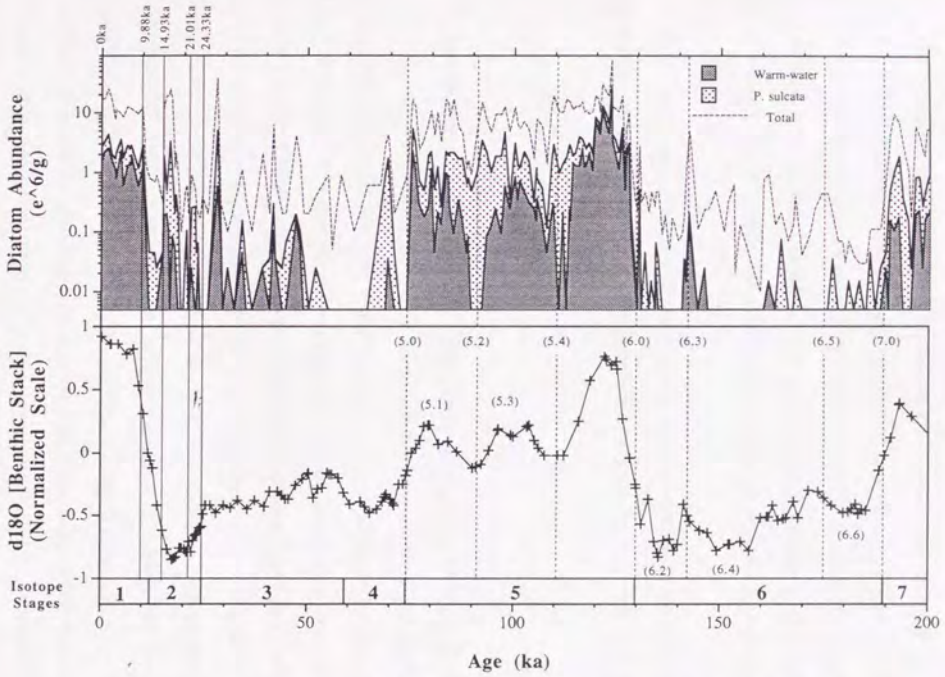

Figure 3. Comparison of the logarithmic diatom abundance curve at Site 797 with "standard" oxygen isotope curve of *Martinson et al.* [1987] Data are cited from *Tada et al.* [1996].

5. Analytical Methods

The samples were dried at 50 °C in an oven immediately after arrival at our laboratory to prevent further alteration. Approximately 5 g of dried samples were washed and centrifuged twice with 50 cc of deionized filtered water to remove sea salt. The residues were dried again at 50 °C for more than 48 hours. Dried samples were ground in an agate mortar and stored in capped glass tubes. These sample treatment and followed analytical procedures are shown in flow chart (Figure 4).

Smear slides were made for all samples and observation of grain composition was made under petrographic microscope. The largest detrital grain diameter was also measured.

5-1. Major Elements Composition

Composition of 10 major elements (SiO_2, TiO_2, Al_2O_3, Fe_2O_3, MnO, MgO, CaO, Na_2O, K_2O, and P_2O_5) were determined for 223 samples by X-ray fluorescence (XRF) analysis using a Rigaku 3270 spectrometer equipped with Rh tube at the Ocean Research Institute, the University of Tokyo. The measurement was carried out on a fused glass bead at the acceleration voltage of 50 kV and the current of 50 mA. To prepare fused glass beads, desalted and powdered samples were dried at 110 °C for more than 4 hours and then ignited at 1000 °C for 6 hours to remove volatiles. Loss on ignition (LOI) was calculated from the weight loss caused by ignition. Approximately 0.4 g of an ignited sample was mixed with approximately 4 g of $Li_2B_4O_7$ flux with the exact ratio of 1.000 : 10.00 and fused at 1150 °C for 7 minutes in platinum crucible to make a glass bead. Fused glass beads were made within 8 hours after ignition so as to avoid weight changes due to absorption of H_2O and CO_2. Calibration curve was constructed using 40 standard samples provided from the Geological Survey of Japan, the United States Geological Survey and the National Bureau of Standards. Details of calibration procedures are described in Appendix I. The reproducibility (95% reliability) of measurement in relative scale is ±0.6% for SiO_2, ±0.8% for TiO_2, ±0.7% for Al_2O_3, ±0.7% for Fe_2O_3, ±1.4%

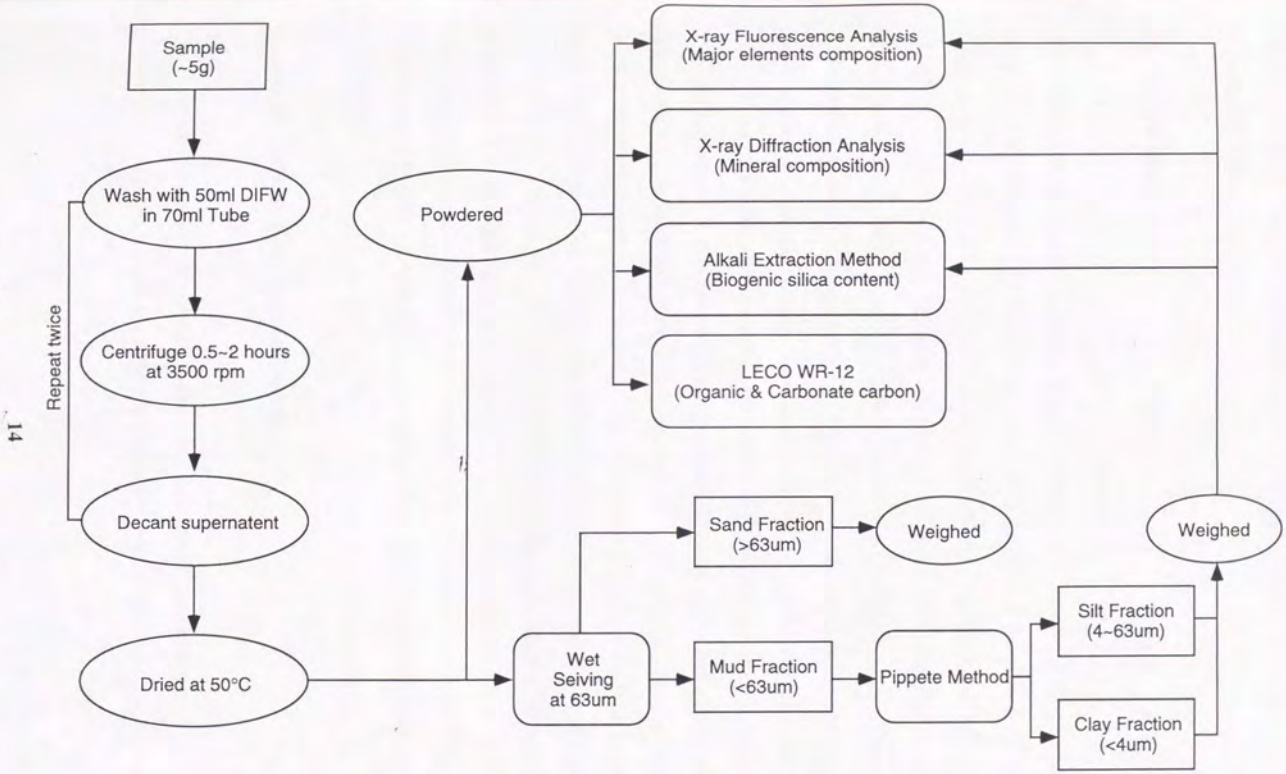

Figure 4 Flow chart of analytical methods.

for MnO, ±1.0% for MgO, ±0.8% for CaO, ±1.6% for Na_2O, ±0.7% for K_2O, and ±1.2% for P_2O_5, respectively.

5-2. Biogenic Silica Content

Biogenic silica content ($bioSiO_2$) was determined for all samples by alkali extraction method after *Mortlock and Froelich* [1989]. The extracted silica was determined by molybdate-blue method of *Fanning and Pilson* [1973]. The time required for complete biogenic silica dissolution was estimated as 6 hours for 40 selected samples based on the method of *DeMaster* [1981]. Even after complete dissolution of biogenic silica, concentration of extracted silica increases linearly as a function of time because of dissolution from soluble detrital silicate minerals and volcanic glass [*DeMaster*, 1981]. Detailed procedures for determination of detrital silica dessolution rate and molybdate-blue method are described in Appendix II. The dissolution rate of silica from detrital silicate minerals and volcanic glass ranges from 0.1 to 0.4 wt%SiO_2/hr with the average of 0.2 ± 0.1 wt%SiO_2/hr for the selected samples. Based on this result, the author adopted 7 hours for the duration of alkali extraction. Seven hours of alkali extraction will cause 1.4 ± 0.7 wt%SiO_2 dissolution of silica from detrital silicates. To correct this effect, the author subtract 1.4 wt%SiO_2 from the total amount of the extracted silica to calculate the biogenic silica content. The error of biogenic silica estimation due to the uncertainty in contribution from detrital silicate dissolution is ±0.7 wt%SiO_2. Since the reproducibility of measurement is ±0.2 wt%SiO_2, total error of biogenic silica estimation is ±1 wt%SiO_2.

5-3. Organic and Carbonate Carbon Content

Evaluation of the calcium carbonate content is necessary to calculate the CaO contribution from the carbonate minerals. Organic carbon content (=Org-C) is also necessary

to chracterize subcomponents within sediments. In this study, organic and carbonate carbon contents (= Carb-C) for 224 samples are cited from *Tada et al.* [1996]. Carbonte carbon contents are calculated from total carbon minus organic carbon which are measured using LECO WR-12 carbon determinator based on the procedure described in *Tada et al.* [1992]. In order to measure total carbon content, 0.1 g of powdered sample was oxidized at 1500 °C for 55 s and the evolved CO_2 gas was measured. For Org-C determination, 0.1 g of powdered sample was treated with 10% HCl for one day, then dried at 60 °C in a permeable crucible. Carb-C content was calculated by the total carbon content minus the Org-C. Analytical precision is ±0.02 wt%.

5-4. Mineral Composition

Quantitative analysis of mineral composition was conducted for all the samples by a MAC Science MXP-3 X-ray diffractometer (XRD) equipped with CuKα tube and monochrometer. Measurements were conducted at tube voltage of 40 kV and tube current of 20 mA with variable slit system which automatically control 25 mm beam width on the sample. Scanning speed is 4 °2θ/min and data sampling step is 0.02 °2θ. A powdered sample was mounted on a glass holder and X-rayed from 2 to 40 °2θ. Before reading out the position and height of each reflection, two steps of data processing were applied. As a first step, original data were smoothed by 5 points averaging which is equivalent to a window width of 0.1 °2θ. This process minimize the error caused by noise. As a second step, a background including amorphous hump was estimated by the background evaluation program which uses a wider smoothing window with 30 points (equivalent to 6 °2θ) between 2 and 40 °2θ. Because the peak width of smectite is approximately 6 °2θ, a smoothing window of 100 points (equivalent to 20 °θ) was used between 2 and 10 °2θ. The background profile which is calculated using 30 points smoothing window is subtracted from the 5 points smoothed intensities to obtain the net peak intensities of crystalline minerals other than smectite. The

background profile which is calculated using 100 points smoothing window is subtracted in case of smectite.

Identification of minerals are based on the following diagnostic peaks; 7.2 ° for smectite, 8.8 ° for illite, 10.4 ° for amphiboles, 11.5 ° for gypsum, 12.1 ° for chlorite + kaolinite, 26.6 ° for quartz, 27.8 ° for feldspars, 29.3 ° for calcite, 30.1 ° for rhodochrosite, and 32.9 ° for pyrite. The 7 Å and 14 Å peaks are considered as mainly contributed by chlorite because the peak ratios between 4.8 Å, 7 Å and 14 Å, which are diagnostic of chlorite are nearly constant. The intensity of diagnostic peak (I) for each mineral was used to estimate the content of each mineral. Because 26.6 ° peak of illite overlaps the main peak of quartz, the quartz peak height at 26.6 ° was corrected for illite based on peak intensity of illite at 8.8 °. The peak intensities of the minerals (I) were transformed to their contents (wt%) using linear calibration equations for each mineral which were determined from meaurements of mixtures of pure reference minerals in various ratios. Detailed calibration methods are described in Appendix III. The reproducibility of measurement are within ±20% for smectite, ±30% for illite, ±30% for chlorite + kaolinite, ±60% for amphiboles, ±7% for quartz, ±15% for feldspars ±20% for calcite, and ±20% for pyrite, respectively.

The content of detrital amorphous material is estimated from the area of amorphous hump (A_{tot}) between 16 and 32.5 ° based on the following procedure. In order to evaluate the aerial contribution of detrital amorphous materials (A_{det}), the background area was corrected for biogenic opal of which content was determined by alkali extraction method as well as for the background of crystalline minerals as follows;

$$A_{det} = A_{tot} - \frac{1.1 \times bioSiO_2(wt\%) \times A_{opal(100)}}{100} - \sum_i \left(\frac{I_i}{I_{i(100)}} \times A_{i(100)} \right) \qquad (1)$$

where I_i and A_i are peak intensity and background area of mineral *i* in the sample, respectively, whereas $I_{i(100)}$, $A_{i(100)}$, and $A_{opal(100)}$ are peak intensity and background areas of pure reference

mineral *i* and opal, respectively. The water content of biogenic opal is assumed as 10% [*Mortlock and Froelich*, 1989]. The content of detrital amorphous material is estimated by dividing A_{det} by $A_{det(100)}$. Background area of pure andesitic volcanic glass from Pliocene section in the northeast Japan was used for a calibration standard for transformation of A_{det} to weight% because the detrital amorphous material in the samples are dominantly composed of altered volcanic glass as will be described later. The reproducibility of estimation in relative scale is within ±10%.

5-5. Grain Size Separation

Grain size separation was conducted for 10 selected samples to evaluate the chemical and mineral compositions of silt (4 - 63 μm) and clay (<4 μm) size fractions of the sediments. First, a fraction larger than 63 μm was removed by wet sieving. Then a fraction less than 63 μm was separated into silt and clay fractions by pipette method [*Krumbein and Pettijohn*, 1938]. Each fraction was weighed after dried, and sand / silt / clay ratio was calculated. The major elements, biogenic silica contents, and mineral compositions of silt and clay fractions were measured by XRF, alkali extraction method, and XRD, respectively. Because sand fraction was too small in amount (less than 11 wt%), the major elements, biogenic silica contents, and mineral compositions of sand fraction were not analyzed.

6. Estimation of Dry Bulk Density

Dry bulk density (DBD) was estimated from GRAPE data which was measured onboard with 2 cm interval [*Shipboard Scientific Party*, 1990]. GRAPE density is an index of wet bulk density of sediment, whereas DBD is a function of wet bulk density and grain density of sediment. In case of late Quaternary sediments at Site 797, GRAPE density shows a linear relationship with DBD (Figure 5) because grain density of sediments are more or less similar between 2.44 and 2.88 g/cm^3. Based on this relation, the author derived the following regression equation to calculate DBD from the GRAPE density data,

$$\mathrm{DBD(g/cm^3)} = 1.5 \times \mathrm{GRAPE\ density} - 1.6\ (r = 0.91). \qquad (2)$$

The estimation error is ±0.16 g/cm^3. The GRAPE density data for top 100 cm of core 797B-1H show abnormally low values. This is probably because top part of the core is disturbed and fluidized during core handling on the deck. Onboard observation of core disturbance also support this idea. Although the author calculated DBDs from the above equation for the top 100 cm of the core, the estimated DBD for this part of the core could involve a large error.

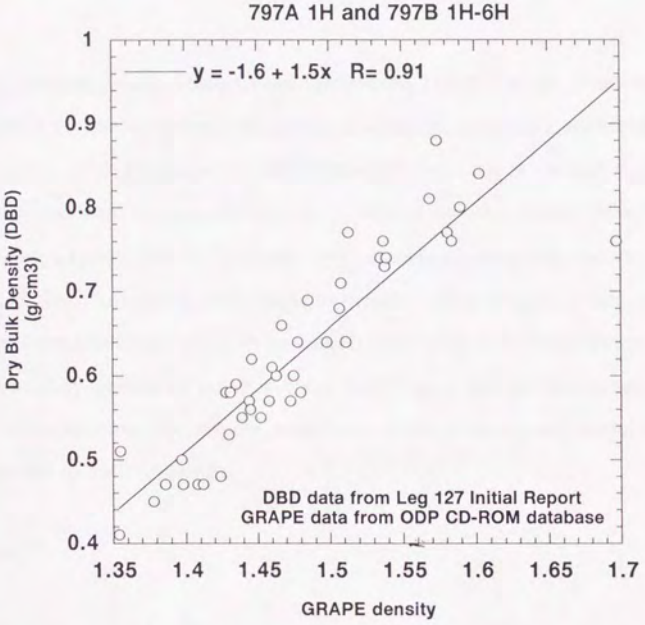

Figure 5 Relationship between GRAPE density and dry bulk density (DBD) measured onboard.

7. Estimation of Detritus Content

The author estimated content of the detrital component (= Detritus%) within the samples from LOI, $bioSiO_2$, and Carb-C, based on the following equation,

$$\text{Detritus\%} = 100 - \text{LOI} - \text{bioSiO}_2 - \frac{56}{12} \times \text{Carb} - \text{C}. \quad (3)$$

Organic matter, water in biogenic opal, and the CO_2 in carbonate are included in LOI. In equation (3), total carbonate is subtracted as calcite whose content is calculated from Carb-C. However, calcite fraction within Site 797 samples consist not only of biogenic calcite which is mainly composed of foraminifers but also of angular inorganic calcite grains. Since Kosa often contains several% of calcite [*Ishizaka*, 1991], those inorganic carbon could be of aeolian origin. Thus, subtraction of all carbonates from the detrital component may result in underestimation of the detritus in the samples by as much as 2%. The detritus content estimated by equation (3) agrees well within ±20% error with the total amount of detrital materials (smectite, illite, chlorite, amphiboles, quartz, feldspars, and detrital amorphous) estimated by XRD (Figure 6).

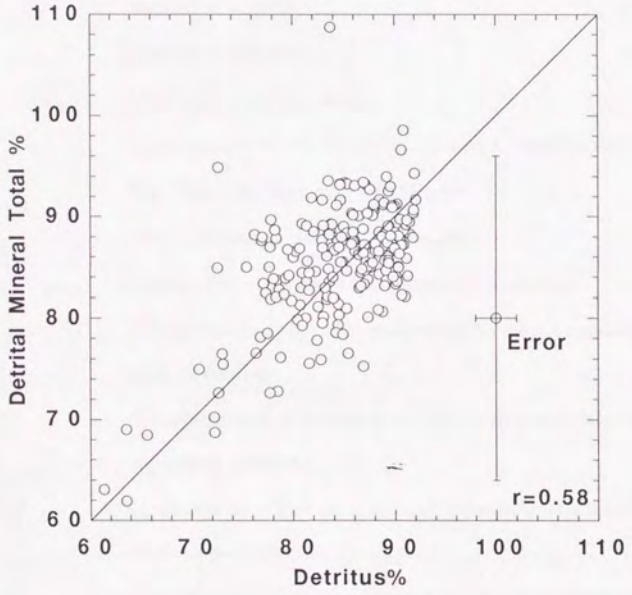

Figure 6 Relationship between content of detritus (Detritus%) calculated from equation (3) and total sum of detrital mineral contents.

8. Q-mode Factor Analysis

Q-mode factor analysis was applied for the major element composition of samples in order to extract subcomponents within the detrital component and evaluate the possible range of composition of the subcomponents and their contents within individual samples. The author adopted the data transformation routine described by *Miesch* [1976], and used Systat™ 5.2.1 for Macintosh™ to calculate factor loadings and factor scores. Symbols used here are listed below.

l	Number of samples
m	Number of elements
n	Number of subcomponents
x_{ik} (x''_{ik})	Concentration of k-th element in i-th sample (transformed)
$x\max_k$	Maximum concentation of k-th element
$x\min_k$	Minimum concentration of k-th element
$x\text{mean}_k$ ($x''\text{mean}_k$)	Average concentration of k-th element (transformed)
a_{ij} (a''_{ij})	Concentration of j-th subcomponent in i-th sample (transformed) based on varimax rotation
f_{jk} (f''_{jk})	Concentration of k-th element in j-th subcomponent (transformed) based on varimax rotation
g_{jk} (g''_{jk})	Concentration of k-th element in j-th subcomponent (transformed) based on oblique rotation
b_{ij} (b''_{ij})	Concentration of j-th subcomponent in i-th sample (transformed) based on oblique rotation
S (S'')	Samples - elements matrix composed of x_{ik} (x''_{ik})
A (A'')	Samples - composition loadings matrix composed of a_{ij} (a''_{ij})
F (F'')	Composition score - elements matrix composed of f_{jk} (f''_{jk})
G (G'')	Composition score - elements matrix composed of g_{jk} (g''_{jk})

$B\,(B'')$	Composition score -elements matrix composed of b_{ij} (b''_{ij})
${}^{t}X$	Transpose matrix of matrix X
X^{-1}	Inverse matrix of matrix X
λ_j	Eigen value of matrix $S''{}'S''$
s_j	Scaling factor [*Miesch*, 1976]
α_j	Constant which defines the oblique rotation angle of j-th subcomponent

8-1. Q-mode Factor Analysis with Varimax Rotation

For m elements, n subcomponents, and l samples, Q-mode factor analysis was used here to find the composition loading matrix A and the composition score matrix F from sample matrix S which satisfy

$$S = AF\,, \tag{4}$$

where S is the l x m matrix composed of x_{ik} which represent the concentration of k-th element in i-th sample, A is the l x n matrix composed of a_{ij} which represents concentration of j-th subcomponent in i-th sample, and F is the n x m matrix composed of f_{jk} which represents concentration of k-th element in j-th subcomponent. Previous to analysis, sum of element composition for each sample was normalized to unity to prepare S. Then, re-scaling of concentrations of individual elements are conducted based on the following data transformation [*Miesch*, 1976] in order to equalize the variation of each element and obtain the transformed sample matrix S'' $(= (x''_{ik}))$.

$$x''_{ik} = x'_{ik} \Big/ \sqrt{\sum_k x'^{2}_{ik}}\,, \tag{5}$$

and

$$x'_{ik} = (x_{ik} - x_{\min_k})/(x_{\max_k} - x_{\min_k}) \tag{6}$$

where $x\max_k$ and $x\min_k$ are maximum and minimum concentrations of k-th element, respectively. For the transformed sample matrix S'', transformed factor loading matrix A'' ($= (a''_{ij})$) is calculated, which satisfies

$$S''^t S'' = A''^t A'', \tag{7}$$

where ${}^tS''$ and ${}^tA''$ are transpose matrices of S'' and A'', respectively, and S''^tS'' is called the matrix of cosine theta.

In the course of Q-mode factor analysis, number of subcomponents to explain the original data set should be determined. the author set criteria to determine the minimum number of subcomponent n as such that they explain more than 98.5% of the total variance. Namely,

$$\sum_{j=1}^{n} \lambda_j \Big/ \sum_{j=1}^{m} \lambda_j \geq 0.985, \tag{8}$$

where λ_j ($\lambda_1 \geq \lambda_2 \geq \cdots \geq \lambda_m$) is eigen values of the matrix of cosine theta (S''^tS'') which is calculated during the course of factor calculation. The number of non-zero eigen values is less than or equal to m. Because the maximum relative error for element concentrations used here is ±1.5%, this criteria should give enough precision for the factor analysis.

In the next step, an l x n matrix A'' is calculated from S''^tS'' based on n-

subcomponents model to satisfy varimax criteria which is defined to make $\sum_{j=1}^{n}\left(\sum_{i=1}^{l} a''^{2}_{ij}\right)^{2}$

maximized. Transformed factor score matrix F'' (= (f''_{jk})) is defined to satisfy

$$S''= A''F'', \tag{9}$$

and F'' can be calculated as

$$F''=({}^{t}A''A'')^{-1\,t}A''S''. \tag{10}$$

Row vectors of F'' gives characteristic chemical composition of subcomponents and are regarded as reference axes which are orthogonal in the n-dimensional space. Composition loadings (a_{ij}) and composition scores (f_{jk}) can be calculated from factor loadings (a''_{ij}) and factor scores (f''_{jk}) using following equations

$$a_{ij} = \frac{a''_{ij}/s_j}{\sum_j (a''_{ij}/s_j)} \tag{11}$$

and

$$f_{jk} = s_j f''_{jk} (x_{\max_k} - x_{\min_k}) + x_{\min_k} \tag{12}$$

where $s_j = \left(1 - \sum_k x_{\min_k}\right) \Big/ \sum_k \left(f''_{jk}\left(x_{\max_k} - x_{\min_k}\right)\right)$ [*Miesch*, 1976].

8-2. Oblique Rotation of Factor Scores

Some of composition loadings (a_{ij}) and composition scores (f_{jk}) calculated from varimax factor loadings (a''_{ij}) and factor scores (f''_{jk}) may have negative values. However, negative composition loadings (a_{ij}) and composition scores (f_{jk}) could not be accepted as geologically reasonable content and composition of the subcomponents. To solve this problem, *Leinen and Pisias* [1984] proposed an objective criteria to re-define the reference axes (compositions of subcomponents). According to their criteria, every new reference axis $\vec{g}''_j = (g''_{j1}, g''_{j2}, \cdots, g''_{jm})$ (j=1,2,···,n) can be set on the plane made by corresponding varimax reference axis $\vec{f}''_j = (f''_{j1}, f''_{j2}, \cdots, f''_{jm})$ and mean sample vector $\vec{x}''_{\text{mean}} = (x''_{\text{mean}_1}, x''_{\text{mean}_2}, \cdots, x''_{\text{mean}_m})$ which is calculated from $\vec{x}_{\text{mean}} = (x_{\text{mean}_1}, x_{\text{mean}_2}, \cdots, x_{\text{mean}_m})$ using equations (5) and (6). Namely,

$$\vec{g}''_j = \frac{(1-\alpha_j)\vec{x}''_{\text{mean}} + \alpha_j \vec{f}''_j}{\left|(1-\alpha_j)\vec{x}''_{\text{mean}} + \alpha_j \vec{f}''_j\right|} \qquad (13)$$

where α_j is a constant. For n x m matrix of the new reference axes $G'' = \begin{pmatrix} \vec{g}''_1 \\ \vdots \\ \vec{g}''_n \end{pmatrix}$ which is composed of the new factor scores g''_{jk}, an m x m matrix R is defined as to satisfy

$$G'' = RF''. \tag{14}$$

Because F'' is orthogonal, R is calculated as

$$R = G''^{t}F'', \tag{15}$$

where ${}^{t}F''$ is transpose matrix of F''. Using the inverse matrix of R, equation (9) can be rewritten as

$$\begin{aligned} S'' &= A''F'' \\ &= A''R^{-1}RF'' \\ &= B''G'' \end{aligned} \tag{16}$$

where B'' $(=(b''_{ij})) = A''R^{-1}$, and b''_{ij} are regarded as the new factor loadings. Newly defined composition loading matrix B $(=(b_{ij}))$ and composition score matrix G $(= (g_{jk}))$ can be calculated using transformations similar to equations (11) and (12), respectively.

Leinen and Pisias [1984] conducted oblique rotation of varimax reference axes until the negative composition scores (f_{jk}) calculated from varimax factor scores (f''_{jk}) become zero. In this case, some of composition loadings (b_{ij}) may have negative values which are not geologically acceptable. For this reason, the author adopted tighter criteria that both B and G have no negative value. Our criteria do not define unique composition loadings (b_{ij}) nor scores (g_{jk}) but could constrain α_j into certain ranges. In general, the maximum α_j gives the non-negative composition score limit whereas the minimum α_j gives the non-negative composition loading limit. Resulted composition loadings (b_{ij}) and scores (g_{jk}) are interpreted as contents and element concentration of subcomponents for samples, respectively. The meaning of

subcomponents extracted by Q-mode factor analysis is explored through comparing composition loadings (b_{ij}) with mineral contents, which could give further constraint on α_j as will be described in the next section.

9. Estimation of Mineral Composition of Subcomponents based on Multi-regression Analysis

To characterize the subcomponents extracted by Q-mode factor analysis using chemical composition data, it is useful to estimate the mineral composition of these subcomponents. Multi-regression analysis between the contents (composition loadings) of the subcomponents and the mineral composition for individual samples was performed to estimate the mineral composition of each subcomponent. Symbols used here are listed below.

l	Number of samples
p	Number of minerals
y_{ir}	Concentration of r-th mineral in i-th sample
b_{ij}	Concentration of j-th subcomponent in i-th sample based on oblique rotation
h_{jr}	Concentration of r-th mineral in j-th subcomponent
Y	Sample - mineral matrix composed of y_{ir}
B	Composition score -elements matrix composed of b_{ij}
H	Multi-regression coefficient matrix composed of h_{jr}

Mineral composition matrix of p minerals for l samples is defined as Y ($=(y_{ir})$) where y_{ir} is r-th mineral content of i-th sample. Total of mineral contents for individual samples are normalized to unity. Multi-regression analysis was conducted to calculate multi-regression coefficient matrix H ($= (h_{jr})$) which satisfy

$$Y = BH \tag{17}$$

where B is composition loadings calculated by Q-mode factor analysis with oblique rotation. Since H should satisfy the least square criteria, H is calculated as

$$H = ({}^{t}BB)^{-1}{}^{t}BY \tag{18}$$

where ${}^{t}B$ is transpose matrix of B. In this H, h_{jr} can be interpreted as r-th mineral content of j-th subcomponent. The calculation was performed by Systat™ 5.2.1 for Macintosh™. If B represents actual contents of the subcomponents, H should be zero or positive. This criteria may further constrain possible range of α_j.

10. Estimation of Silt / Clay Ratio of Each Subcomponent

In order to examine the grain size (silt / clay ratio) of each subcomponent (factor), the content of each factor in the clay fraction and the silt fraction is estimated as follows. First, the total of chemical composition of each selected sample is normalized to unity. Then, each composition value is transformed using equations (5) and (6). This transformed composition vector can be treated as $\vec{g}_j$ and factor loadings of each selected sample is calculated using equation (15). Composition loadings (content of each factor) within silt and clay fractions of each sample can be calculated using equation (11).

Using the content of each factor in the silt and clay fractions and silt / clay ratio of the bulk samples, the silt / clay ratio of each factor is calculated as

$$\left(\frac{\text{Silt}}{\text{Clay}}\right)_{\text{Factor } j} = \frac{(\text{Factor } j\ (\%))_{\text{silt}}}{(\text{Factor } j\ (\%))_{\text{clay}}} \times \left(\frac{\text{Silt}}{\text{Clay}}\right)_{\text{bulk}} . \tag{19}$$

11. Results

11-1. Grain Composition

Smear slide observation shows that late Quaternary sediments at Site 797 mainly consist of a detrital component with subordinate amount of biogenic and diagenetic components. Detrital grain compositions are listed in Table 1. The detrital component in the clay size fraction consists dominantly of clay minerals, whereas that in silt and sand size fractions consist dominantly of subangular to subrounded monocrystalline quartz, feldspars, and light brownish rounded altered volcanic glass, with small amounts of flaky fresh or altered mica (biotite and/or muscovite), rutile, and amphiboles. Largest detrital grain was quartz, feldspars, or flaky mica. The reproducibility of measurement of largest grain size is ±31 μm based on comparison between measurement of *Tada et al.* [1992] and this work (Figure 7a). The grain size is larger during Stage 2 and substage 6.2 which are glacial maxima (Figure 7b). Ten samples contain significant amount of angular transparent fresh volcanic glass shards. Inorganic calcite are clay to silt size and irregular in shape. Biogenic component consists dominantly of siliceous microfossils such as diatoms with minor amount of radiolarians and sponge spicules. Calcareous microfossils such as foraminifers and cocolith occur only sporadically. Diagenetic component consists mostly of framboidal pyrite.

11-2. Major Elements Composition

The result of XRF analysis are listed in Table 2. The range and average concentration of each element are also listed in the last four rows in Table 2. Elements such as SiO_2, TiO_2, MgO, Na_2O, and K_2O show positive correlation with Al_2O_3 except for 10 tuffaceous samples and one sample with extremely high MgO (Figure 8). Tuffaceous samples have wide range of chemical composition suggestive of different volcanic sources. One sample with high MgO content is from a thick dark layer, and this sample contains relatively high CaO and carbonate

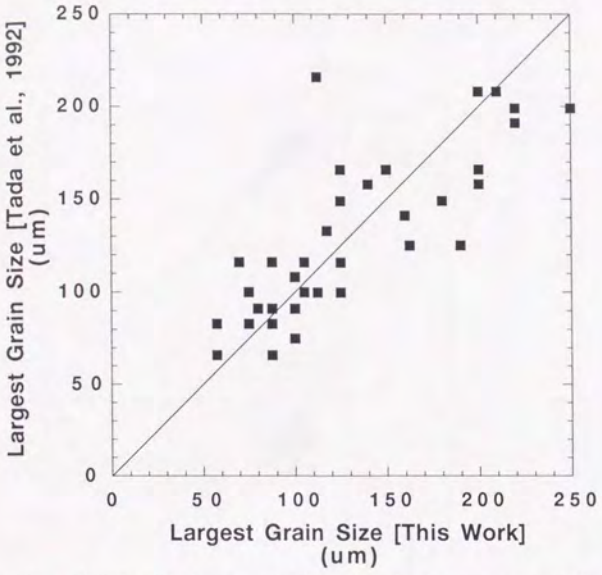

Figure 7a Relationship between the largest grain size measurement by Tada et al. [1992] and by this work.

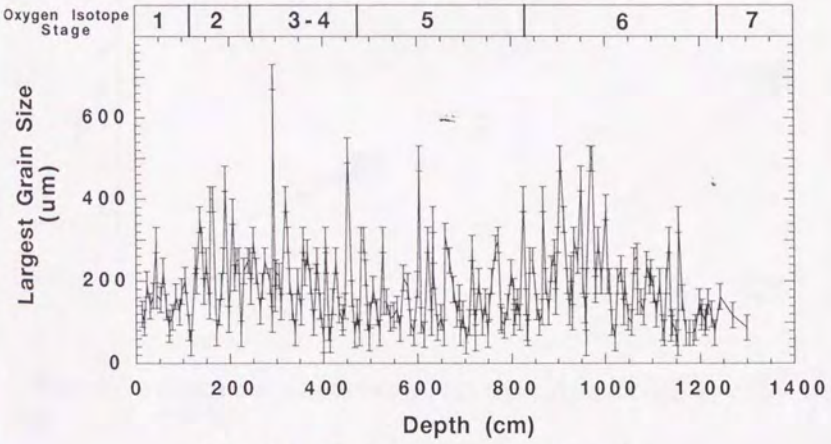

Figure 7b Depth profile of the largest grain size.

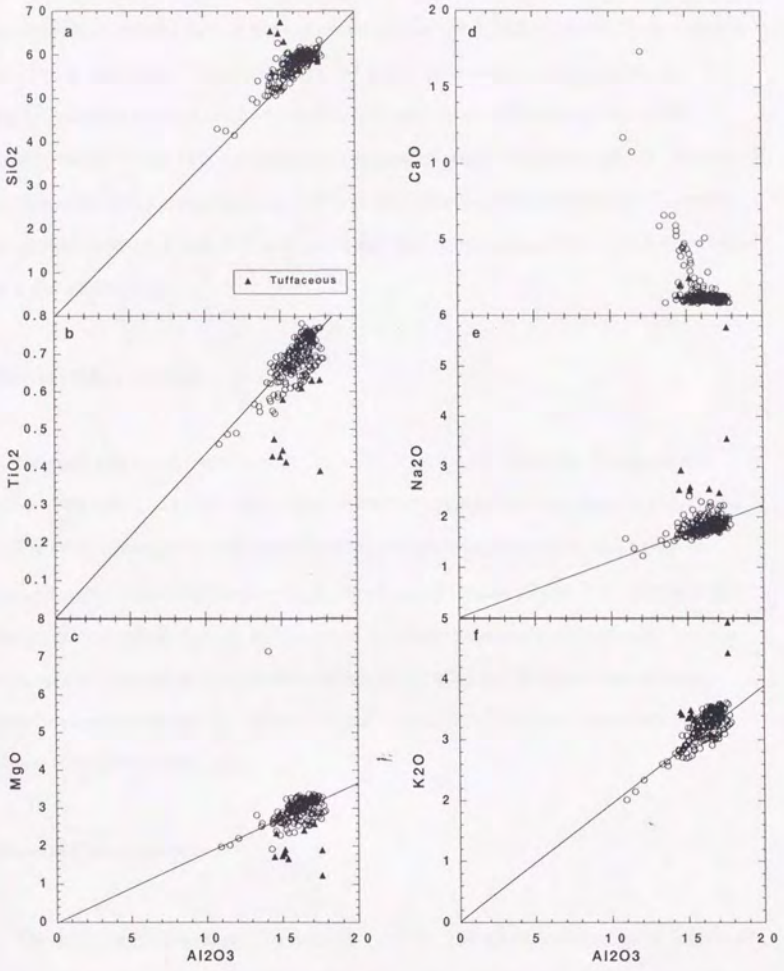

Figure 8 Relationships between SiO_2 (a), TiO_2 (b), MgO (c), CaO (d), Na_2O (e), K_2O (f) and Al_2O_3.

carbon [*Tada et al.*, 1996]. Thus high MgO is considered to be originated from Mg-carbonate. LOI and CaO show the negative correlation with Al_2O_3, and LOI shows positive correlation with the contents of organic carbon and carbonate carbon. Fe_2O_3, MnO, and P_2O_5 do not show clear correlation with Al_2O_3. Extremely high (>1 wt%) MnO samples occur within the stratigraphic intervals between 0 and 60 cmbsf, 700 and 790 cmbsf, and at 1108 cmbsf, respectively, and these intervals correspond to interglacial stage 1 and substage 5.5. Almost all samples shows the P_2O_5 content between 0.076 and 0.179 wt%, however there are 2 samples with P_2O_5 contents of 0.546 and 2.25 wt% at 44 and 480 cmbsf, respectively, which correspond to stage 1 and substage 5.1.

11-3. Biogenic Silica Content

Biogenic silica content is ranging from 2.5 to 18.9 wt% (Table 3). It is generally higher at 0 - 100 cmbsf and 500 - 850 cmbsf which correspond to oxygen isotope stage 1 and stage 5 (Figure 9). Samples at 224 and 239 cmbsf also show high biogenic silica contents. Samples with high biogenic silica show high abundance of diatom [*Tada et al.*, 1996] except for a sample at 224 cmbsf. Sample at 224 cmbsf shows rare diatom frustules based on smear slide observation, however it is just below tuffaceous samples and is considered to contain extremely fine volcanic glass. Its "biogenic silica" content could be overestimation due to faster dissolution of these fine glass.

11-4. Mineral Composition

The result of XRD analysis are listed in Table 4. The range and average of content of each mineral (including detrital amorphous material) are also listed in the last four rows in Table 4. XRD analysis shows that major detrital components are clay minerals (average 36%), detrital amorphous (av. 27%), quartz (av. 16%), and feldspars (av. 4%). Within clay minerals, smectite and illite are dominant (av. 18% and 15%, respectively) followed by chlorite +

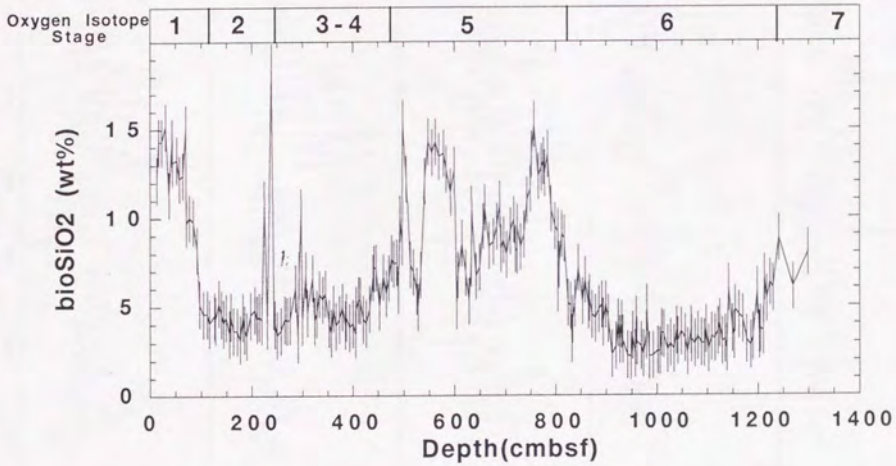

Figure 9 Depth profile of biogenic silica ($bioSiO_2$) content. Corresponding oxygen isotope stages are from *Tada et al.* [1996].

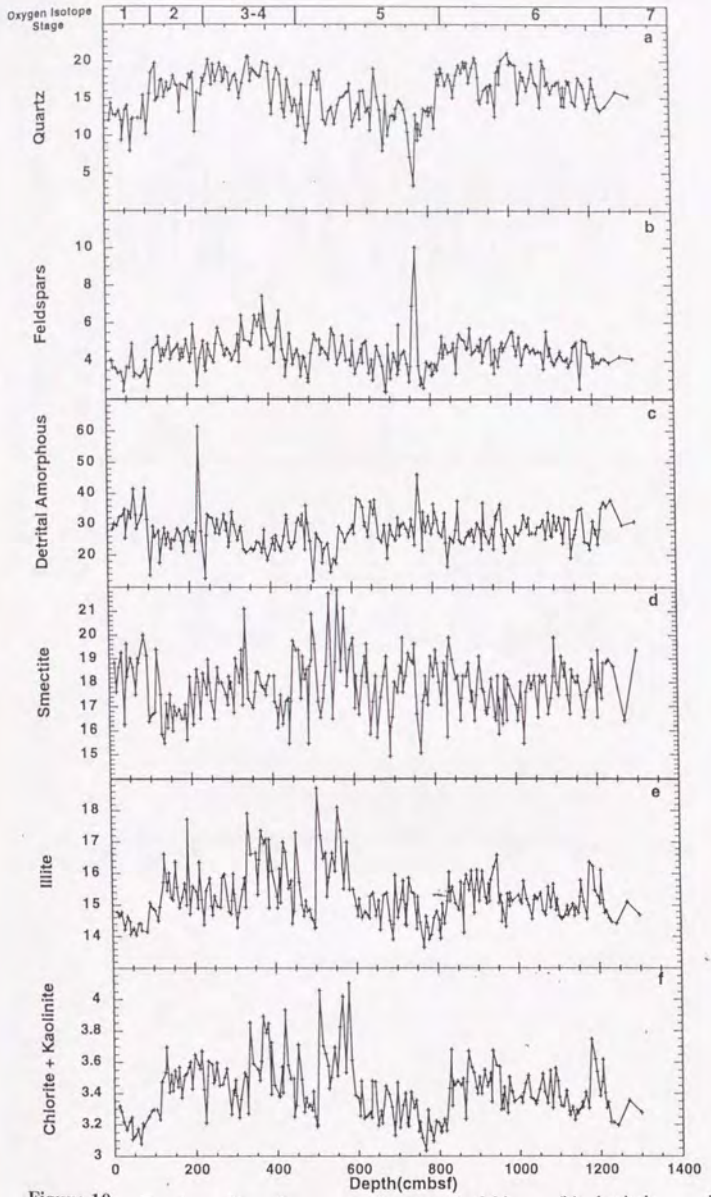

Figure 10 Depth profiles of contents of quartz (a), feldspars (b), detrital amorphous (c), smectite (d), illite (e), chlorite + kaolinite (f), amphiboles (g), calcite (h), pyrite (i), and rhodochrosite (j). Corresponding oxygen isotope stages are from *Tada et al.* [1996].

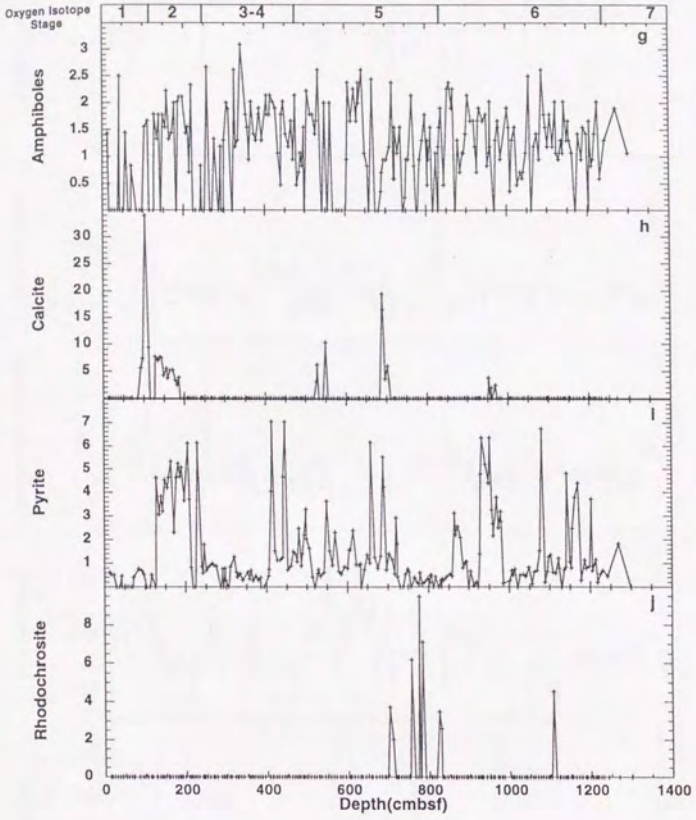

Figure 10 (*continued*)

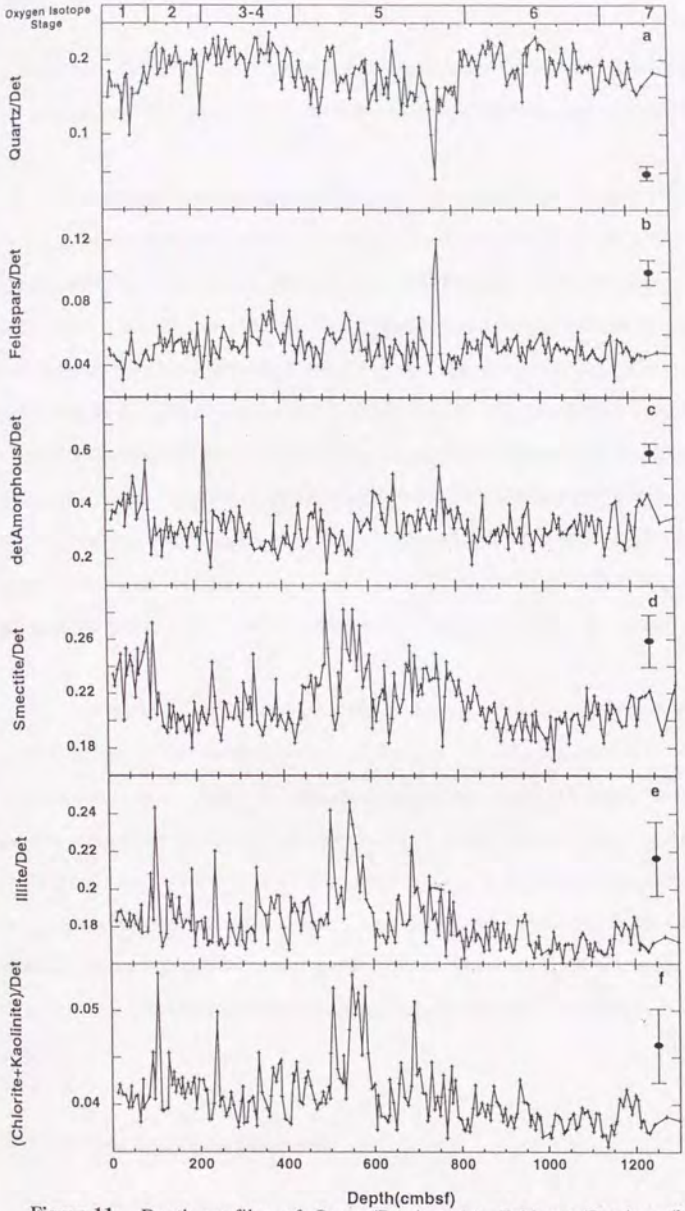

Figure 11 Depth profiles of Quartz/Detritus (a), Feldspars/Detritus (b), (detrital Amorphous)/Detritus (c), Smectite/Detritus (d), Illite/Detritus (e), and (Chlorite + Kaolinite)/Detritus (f). Corresponding oxygen isotope stages are from *Tada et al.* [1996].

kaolinite (av. 3%). Contents of quartz and feldspars are lower between 0 and 100 cmbsf and between 600 and 800 cmbsf which correspond to oxygen isotope stages 1 and 5 (Figure 10a, b).

Since these fluctuation patterns are mirror image of biogenic silica (Figure 9), it could be due to the dilution effect by biogenic silica. To remove this effect, the author normalized mineral contents by Detritus%. Quartz/detritus and feldspars/detritus are higher between 100 and 450 cmbsf and between 850 and 1300 cmbsf which correspond to glacial stages 2 to 3 and 6 whereas they are lower between 0 and 100 cmbsf and between 450 and 850 cmbsf which correspond to interglacial stages 1 and 5 (Figure 11a, b). On the other hand, detrital amorphous/detritus and smectite/detritus are lower during glacial stages and higher during interglacial stages (Figure 11c, d). Illite/detritus and (chlorite+kaolinite)/detritus are higher at 80-150, 500-600, and 650-800 cmbsf which corresponds to interglacial stage 5 and it is generally lower in other intervals (Figure 11e, f). These results show that the detrital mineral composition within detrital component tends to change in harmony with glacial - interglacial cycles.

Twenty five samples show detectable calcite peak and the content ranges from 2.4 to 34%. Other samples show no detectable calcite peak. Amphiboles and pyrite are minor but common constituents. Pyrite is of diagenetic origin and rich in dark layers. Small amount of gypsum and jarosite are found in several samples from the second sample set especially those rich in calcite and pyrite as is noted in remarks in Table 4. They were considered to be formed by oxidation of pyrite and reaction with calcite during sample storage. Some samples in the interval between 700 and 840 cmbsf and at 1108 cmbsf contain a minor amount of rhodochrosite. They correspond to MnO rich samples and are considered as of diagenetic origin.

11-5. Result of Grain Size Separation

Grain size composition of 10 selected samples are listed in Table 5. Content of sand

(>63 μm) fraction ranges from 0 to 11% but most of samples contain less than 3% of sand. Silt (4 to 63 μm) content ranges from 24 to 41% and varies by factor of 1.7. Clay (<4 μm) fraction show negative correlation with silt fraction and ranges from 56 to 71%. Thus the variation in silt / clay ratio rather than the variation of sand fraction is considered as a major cause of variations in the bulk chemical composition of sediments. Biogenic silica contents and major elements composition of silt and clay fraction are also listed in Table 5 and mineral composition of these two fractions are listed in Table 6. $BioSiO_2$ in the silt fraction is generally lower (0 to 6%) than that of clay fraction (3 to 10%) in spite of higher total SiO_2 content of silt fraction than that of clay fraction (Table 5). This is because silt fraction contains more quartz than clay fraction (Table 6). Higher Al_2O_3 content of clay fraction suggests the higher clay mineral content in this fraction (Table 5). Table 6 shows that clay fraction is chracterized by higher smectite and detrital amorphous content.

11-6. Dry Bulk Density

Estimated DBD values for all samples are listed in Table 3. DBD is ranging from 0.3 to 0.85 g/cm^3 except for the interval between 0 and 100 cmbsf where it is abnormally low (0.2 to 0.4 g/cm^3) (Figure 12a). This is probably because top part of the core is disturbed and fluidized during core handling on the deck as is described previously. Below 100 cmbsf, DBD tends to be low within the interval of 500 to 850 cmbsf, moderate within 1000 to 1300 cmbsf, and high within 100 to 500 cmbsf and 850 to 1000 cmbsf. DBD at Site 797 has negative correlation ($r = -0.73$) with $bioSiO_2$ (Figure 12b) which is interpreted as caused by the higher content of porous diatom frustules in higher $bioSiO_2$ samples [*Tada and Iijima*, 1983].

11-7. Content of Detrital Material

Estimated content of detrital material (=Detritus%) for all the samples are listed in Table 3. Detritus% in the studied samples ranges from 61 to 92 wt%. The detritus content is higher in the intervals between 100 and 450 cmbsf and 850 and 1300 cmbsf which correspond to glacial stages 2 to 4 and 6 (Figure 13). It is a mirror image with the variation of $bioSiO_2$.

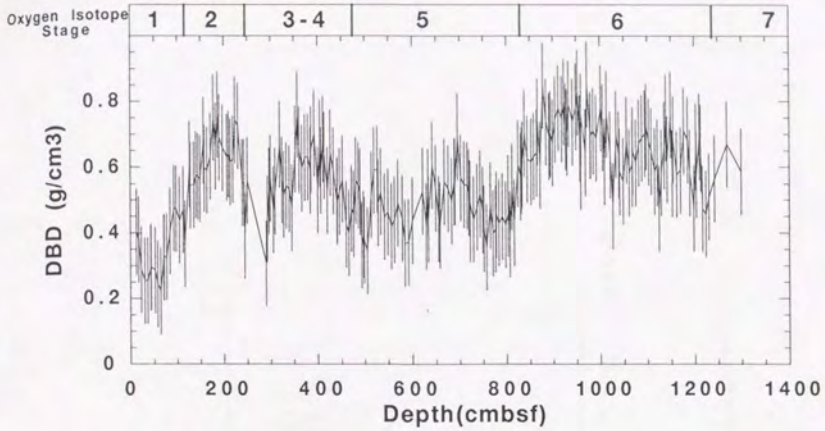

Figure 12a Depth profile of dry bulk density (DBD). Corresponding oxygen isotope stages are from *Tada et al.* [1996].

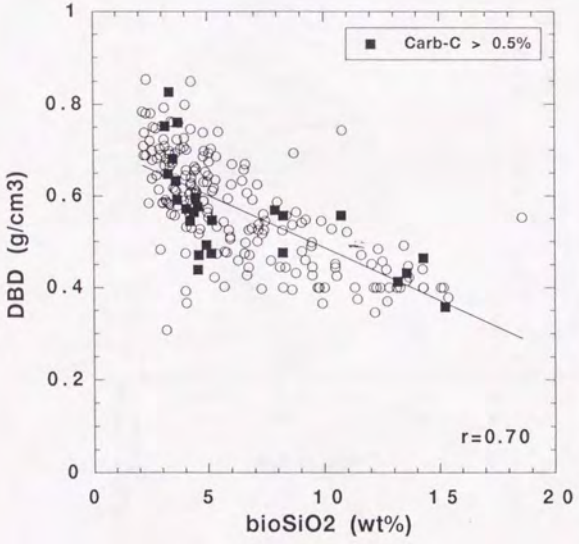

Figure 12b Relationship between biogenic silica ($bioSiO_2$) content and dry bulk density (DBD).

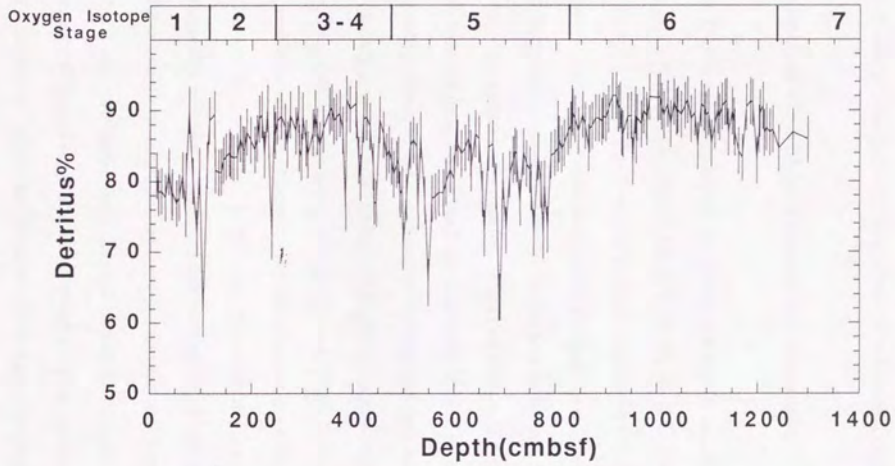

Figure 13 Depth profile of content of detritus (Detritus%) calculated from equation (3).

12. Partitioning of the Detrital Component

Q-mode factor analysis of the major elements was performed in order to identify the detrital subcomponents and estimate their composition and contents in each sample. Since our major interest is focused on the quantitative estimation of Kosa contribution within the detrital component, the author conducted two step factor analysis as is described below (Figure 14).

12-1. STEP1: Factor Analysis of All Major Elements for All Samples

As a first step, Q-mode factor analysis was conducted for all samples using all 11 major elements (SiO_2, TiO_2, Al_2O_3, Fe_2O_3, MnO, MgO, CaO, Na_2O, K_2O, P_2O_5, and LOI). Result of preliminary analysis shows that five factors could explain 98.8% of the total variance. Thus, the author repeated Q-mode factor analysis again based on a 5 factor model with varimax rotation. Extracted 5 factors are named as Factors A through E in descending order of variance explained by each varimax factor. After calculation of composition loadings and composition scores from varimax factor loadings and factor scores, respectively, the author conducted multi-regression analysis of the composition loadings for each sample with its content of minerals including smectite, illite, chlorite + kaolinite, amphiboles, quartz, feldspars, detrital amorphous, bioSiO_2, calcite, organic carbon, pyrite and rhodochrosite. Composition loadings and multi-regression coefficients should give the contents of elements and minerals of each subcomponents (Factors A through E). In this step, the author did not apply oblique rotation to extract geologically reasonable chemical and mineral composition of subcomponents because the result obtained was enough to examine the chemical and mineralogical character of each subcomponents. Several negative composition scores and negative multi-regression coefficients suggest smaller contents of the elements and minerals whereas large positive composition scores and positive multi-regression coefficients suggests larger contents. Calculated composition scores of each elements for each factor are shown in Table 7 in which the factor with composition scores larger than the average of samples has

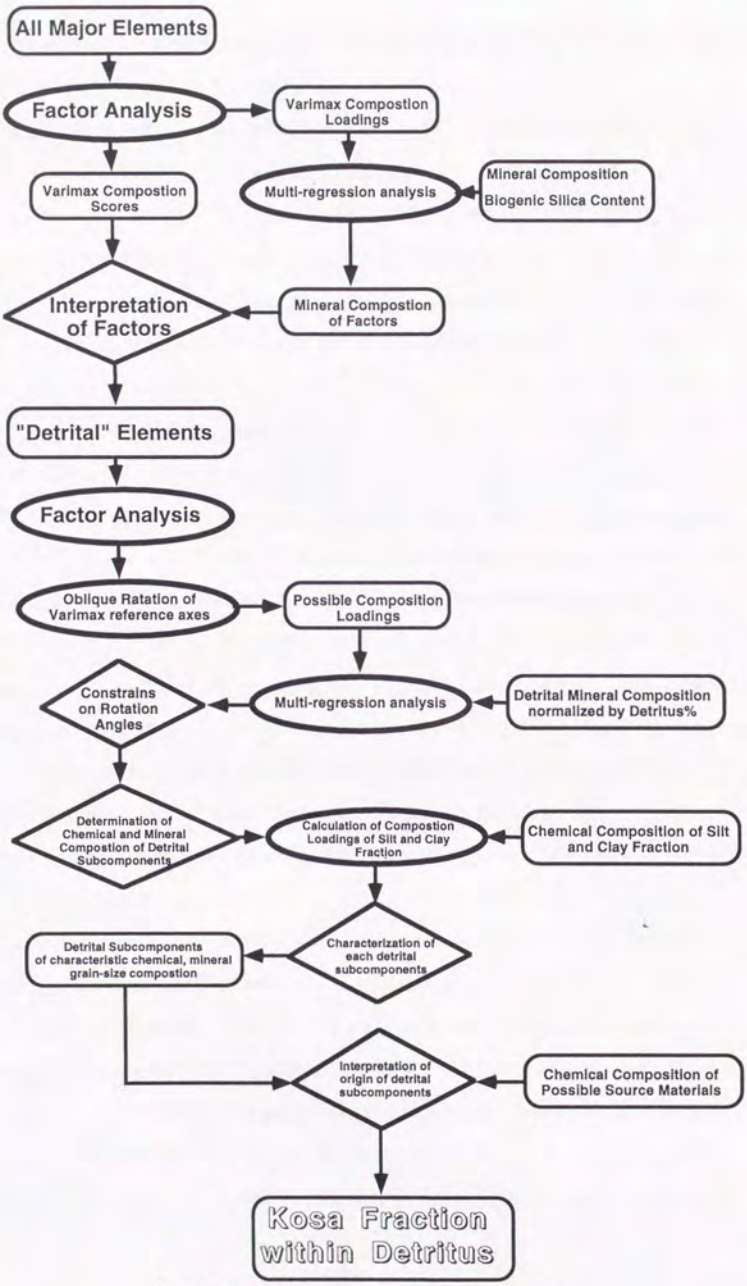

Figure 14 Flow chart of statistical analysis.

positive contribution to the elements (Figure 15). Multi-regression coefficients are also listed in Table 7 in which the factor with multi-regression coefficients larger than the average mineral contents of samples has positive contribution to the minerals (Figure 16). Calculated composition scores and multi-regeression coefficients are listed in Table 7.

Factor A has strong positive contribution to TiO_2, Al_2O_3, SiO_2, K_2O, and MgO, and strong negative contribution to LOI, Fe_2O_3, MnO, CaO, and P_2O_5 (Figure 15). It shows strong positive contribution to smectite, illite, chlorite + kaolinite, amphiboles, quartz, and feldspars (Figure 16). Thus, this factor is attributable to a subcomponent characterized by detrital material. Factor B has strong positive contribution to LOI, CaO, moderate contribution to TiO_2 and MgO, and strong negative contribution to SiO_2 and MnO (Figure 15). It shows strong positive contribution to calcite and organic carbon, and moderate positive contribution to illite, chlorite + kaolinite, amphiboles, and quartz (Figure 16). Based on these relationships, Factor B is mainly attributable to a subcomponent characterized by calcite and organic carbon with small contribution of detrital material. Factor C has strong positive contribution to SiO_2, Na_2O, and K_2O, moderate contribution to LOI and Al_2O_3, and strong negative contribution to TiO_2, MgO, and CaO (Figure 15). It shows strong positive contribution to biogenic silica and detrital amorphous, and moderate positive contribution to smectite and feldspars (Figure 16). Some of samples with high contribution of Factor C contain abundant fresh volcanic glass shards under the microscope. Thus, this factor is attributable to a subcomponent characterized by biogenic silica and volcanic glass with low TiO_2 and MgO and high Na_2O and K_2O contents. Factor D has strong positive contribution to Fe_2O_3 and P_2O_5, moderate contribution to LOI and Na_2O, and strong negative contribution to MnO and CaO (Figure 15). It shows strong positive contribution to pyrite and organic matter, and moderate positive contribution to smectite and detrital amorphous (Figure 16). Thus, this factor is attributable to a subcomponent characterized by diagenetic pyrite suggestive of reducing condition with small contribution of detrital material. Factor E has strong positive contribution to MnO and P_2O_5, and moderate contribution to MgO and Na_2O (Figure 15). It shows positive contribution to rhodochrosite and biogenic silica (Figure 16). However, moderately negative contribution of this factor to

Figure 15: Composition scores of factors calculated by Q-mode factor analysis for all analyzed samples using all elements with varimax rotation.

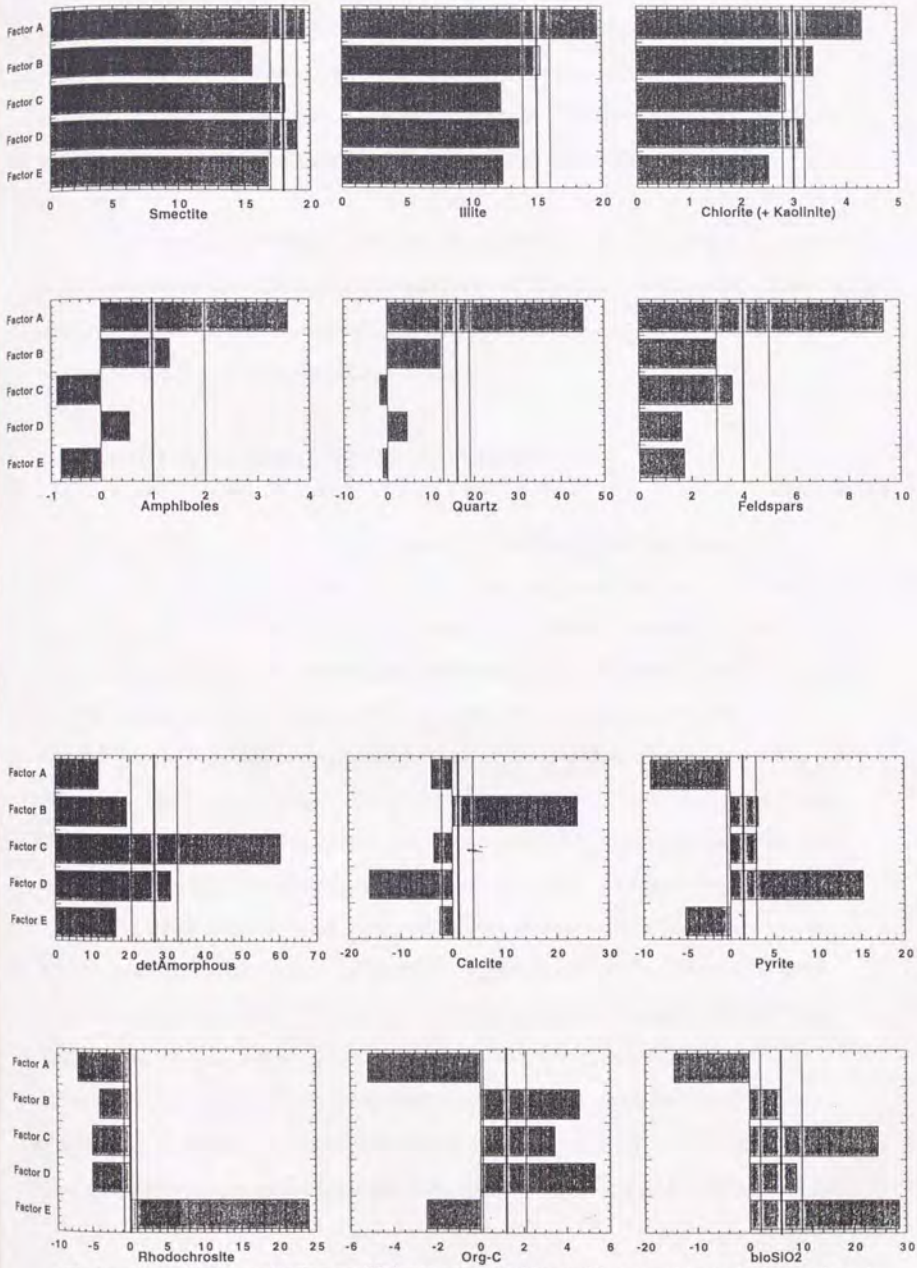

Figure 16 Multi-regression coefficients calculated by multi-regression analysis of mineral composition to the composition loadings calculated by Q-mode factor analysis for all analyzed samples using all elements with varimax rotation.

SiO_2 (Figure 15) suggests that positive contribution to bioSiO_2 could be superficial. Thus, Factor E is attributable to a subcomponent characterized by diagenetic manganese oxi-hydroxide or manganese carbonate with small contribution of detrital material, and the former could have been originally precipitated as manganese oxide under oxic bottom water conditions.

These result suggests that contribution of the detrital component is largely included in Factor A and Factor C with minor inclusions in Factor B, D, and E. Consequently, it is not possible to extract the detrital component and partition it into subcomponents by Q-mode factor analysis using all major elements of all samples.

12-2. STEP2: Factor Analysis Using "Detrital" Elements

In order to extract the detrital component and partition it into subcomponents of different origin by Q-mode factor analysis, the elements which contribute mostly to "detrital" factors (Factors A and C) such as TiO_2, Al_2O_3, MgO, Na_2O, and K_2O are selected (Figure 15). Detrital SiO_2 (detSiO_2) is also included which are calculated by subtracting biogenic SiO_2 from total SiO_2. The elements which are strongly affected either by biogenic components (CaO, P_2O_5, LOI) or by diagenetic components (Fe_2O_3, MnO) are excluded. The sum of detSiO_2, TiO_2, Al_2O_3, MgO, Na_2O, and K_2O accounts for approximately 90% of the detrital component. This means that detrital subcomponents partitioned from these 6 elements by themselves could explain approximately 90% of the bulk detrital materials within the samples (Figure 17).

Ten samples which contain significant amount of fresh volcanic glass were excluded because those fresh volcanic glass was probably supplied by ash fall from various volcanoes and could have a wide compositional range. The wide compositional range of volcanic glass would violate the basic assumption that each subcomponent have the specific chemical composition. One sample with high MgO content was also excluded from analysis because relatively high content of CaO and carbonate carbon of this sample suggest that the origin of MgO in this sample is magnesium-calcium carbonate although 31 °2θ peak of dolomite is not

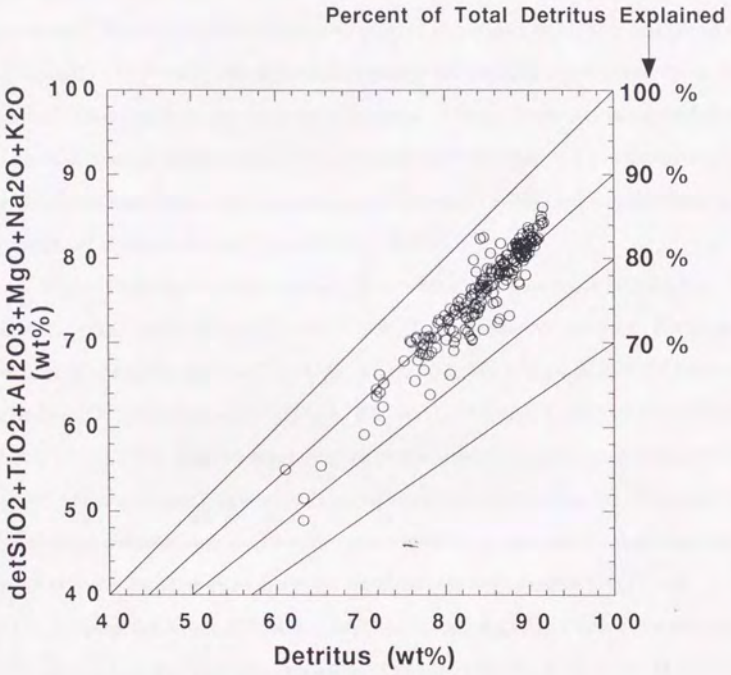

Figure 17 Interrelationship between the content of detritus and the total sum of "detrital" elements (detSiO$_2$, TiO$_2$, Al$_2$O$_3$, MgO, Na$_2$O, and K$_2$O)

clear due to overlapping with feldspars peak.

As a second step, Q-mode factor analysis was conducted again using the 6 selected "detrital" elements for 213 selected samples. Preliminary result of analysis shows that four factors explain the 98.7% of the total variance. Based on this result, the author conducted Q-mode factor analysis based on a 4 factor model with varimax rotation. Extracted factors are named Factor 1 through 4 in descending order of variance explained by each varimax factor. The result gave a negative value of MgO composition score for Factor 4. To avoid the negative value, the author applied oblique rotation of all varimax factor axes and obtain the rotation angles which satisfy the requirements that all composition scores are positive. The author calls these angles as non-negative score limits (NNSs). Then, the author rotated one factor axis at one time while another 3 factors are fixed at NNSs to find a non-negative loading limit (NNL) for each factor. The possible range (from NNS to NNL) of compositions scores of each factor are shown in Figure 18 and listed in Table 8.

Figure 18 shows the interrelationships between element ratios $detSiO_2/Al_2O_3$, MgO/Al_2O_3, Na_2O/Al_2O_3, K_2O/Al_2O_3 and TiO_2/Al_2O_3 for the selected samples. The diagrams show general trend from high $detSiO_2/Al_2O_3$, TiO_2/Al_2O_3, MgO/Al_2O_3, K_2O/Al_2O_3 ratios and low Na_2O/Al_2O_3 ratio to low $detSiO_2/Al_2O_3$, TiO_2/Al_2O_3, MgO/Al_2O_3, K_2O/Al_2O_3 ratios and high Na_2O/Al_2O_3 ratio. Factor 1 represents the detrital subcomponent characterizing one end of this trend, whereas Factor 2 represents the subcomponent characterizing the other end. The major trend of compositional variation shown in Figure 18 is explained by these two factors. Factor 3 explains deviation from this major trend towards higher $detSiO_2/Al_2O_3$ and Na_2O/Al_2O_3 ratios, and lower TiO_2/Al_2O_3, MgO/Al_2O_3, and K_2O/Al_2O_3 ratios. Factor 4 explains the deviation toward the other side characterized by high TiO_2/Al_2O_3 ratio, low MgO/Al_2O_3, Na_2O/Al_2O_3, and K_2O/Al_2O_3 ratios, and moderate $detSiO_2/Al_2O_3$ ratio.

12-3. Mineral Composition of the Detrital Subcomponents

The result of the multi-regression analysis between composition loadings (contribution

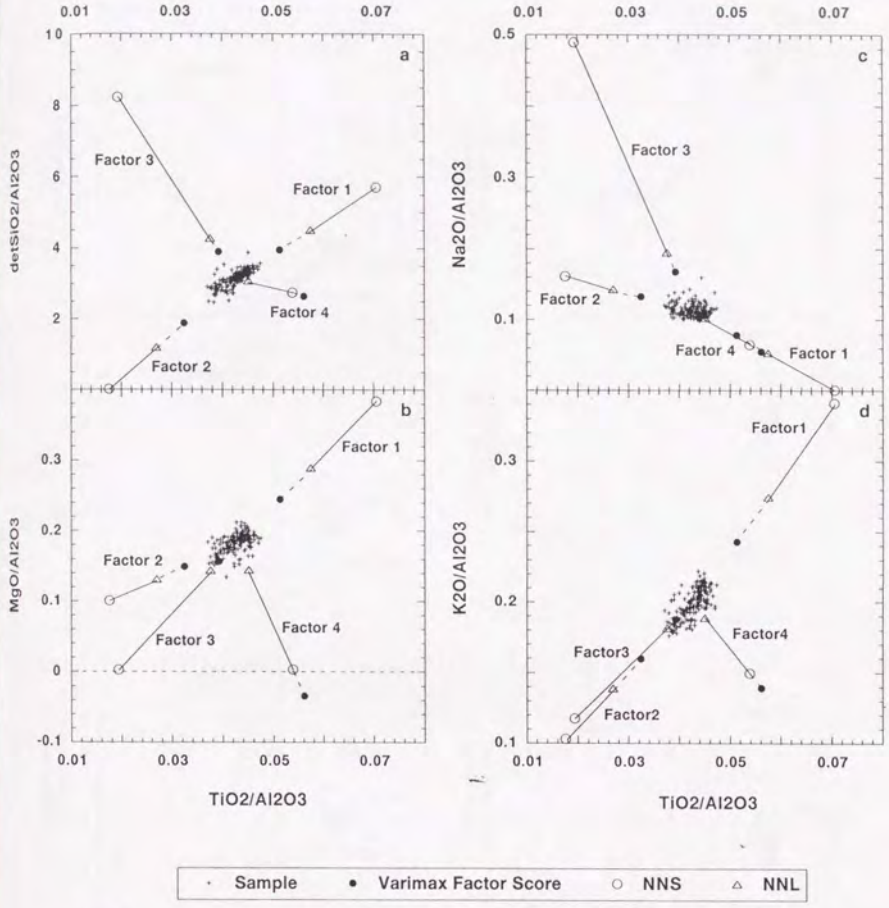

Figure 18 $DetSiO_2/Al_2O_3$ (a), MgO/Al_2O_3 (b), Na_2O/Al_2O_3 (c), K_2O/Al_2O_3 (d) versus TiO_2/Al_2O_3 plots of samples and detrital subcomponents (Factors 1 through 4) estimated by Q-mode factor analysis of "detrital" elements. Possible ranges of composition for each factor is shown between non-negative score limit (NNS) and non-negative loading limit (NNL).

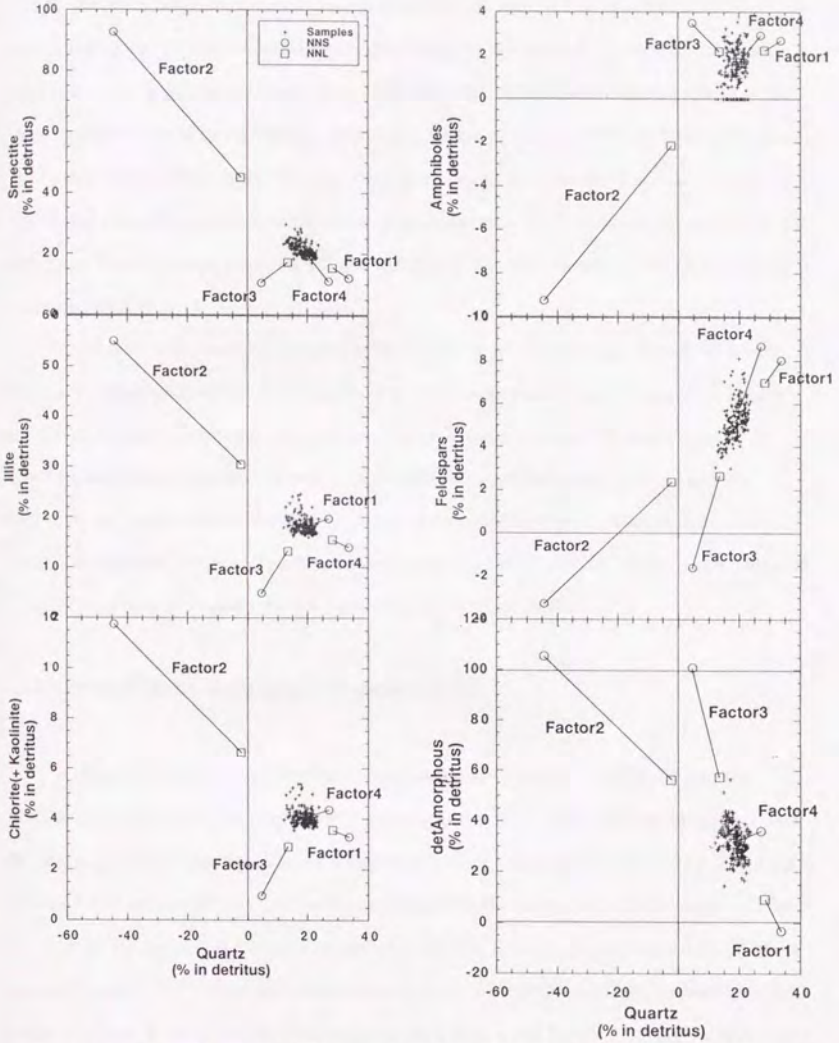

Figure 19 Mineral composition ranges of each detrital subcomponent calculated by multi-regression analysis of detrital mineral composition and composition loadings.

of each factor) and the bulk detrital mineral contents normalized by the detrital content for each sample gives the ranges of mineral composition for each factor as is listed in Table 9 and shown in Figure 19. Mathematically possible ranges of mineral composition may include negative values which are geologically unrealistic. To eliminate such mineral compositions, rotation angles should be further adjusted within the range between NNS and NNL. Figure 19 shows that Factor 2 have negative range of quartz content between -45% and -2% which is significant even after taking into account of estimation error (±2%). Accommodation of this constraint further narrow the chemical and mineral composition ranges of the factors which is listed in Table 10.

As is obvious from Figure 19, Factor 1 is characterized by high contents of quartz, feldspars, amphiboles, illite, and chlorite + kaolinite, moderate content of smectite, and low content of detrital amorphous. By contrast, Factor 2 is characterized by high contents of smectite and detrital amorphous, and low contents of quartz, feldspars, illite, chlorite + kaolinite, and amphiboles. Factor 3 is characterized by high contents of amphiboles and detrital amorphous, and low contents of other crystalline minerals. The composition of Factor 4 is similar to that of Factor 1 except its lower content of smectite.

12-4. Silt / Clay Ratio of the Detrital Subcomponents

The silt / clay ratio of 10 selected samples ranges from 0.31 to 0.71 (Table 11). Major element compositions of the clay fraction are characterized by relatively low TiO_2/Al_2O_3 and $detSiO_2/Al_2O_3$ ratios whereas those of the silt fraction are characterized by higher TiO_2/Al_2O_3, $detSiO_2/Al_2O_3$ and Na_2O/Al_2O_3 ratios as compared with the ratios for the bulk samples (Figure 20). Figure 20 shows that chemical composition of clay fraction are approximately on the mixing line of Factor 1 and Factor 2 whereas those of silt fraction are in the mixing triangle of Factor 1, Factor 3, and Factor4. This suggest that Factor 1 and Factor 2 largely contributed to clay fraction and Factor 3 and Factor 4 largely contributed to silt fraction. Figure 21 shows that samples with high Factor 3 and Factor 4 content tend to have higher silt / clay ratio.

In order to evaluate this tendency, silt / clay ratio of each factor was estimated. Although the result may contain large error, the silt / clay ratios are estimated as 0.21 to 0.55 for Factor 1, 0.12 to 0.43 for Factor 2, 0.5 to 3.1 for Factor 3 and 1.0 to 5.6 for Factor 4, respectively (Table 11). The result suggests that Factor 3 and Factor 4 are composed dominantly of silt size grains whereas Factor 1 and Factor 2 are composed dominantly of clay size grains.

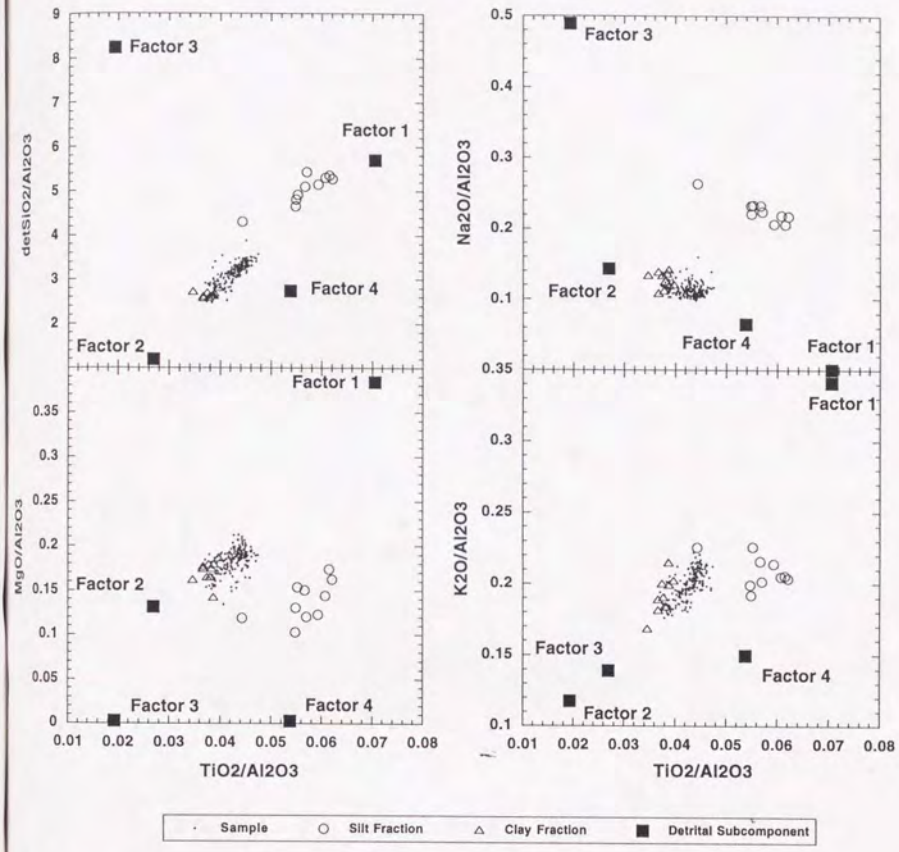

Figure 20 $DetSiO_2/Al_2O_3$ (a), MgO/Al_2O_3 (b), Na_2O/Al_2O_3 (c), K_2O/Al_2O_3 (d) versus TiO_2/Al_2O_3 plots of selected 213 bulk samples and silt and clay fraction of selected 10 samples.

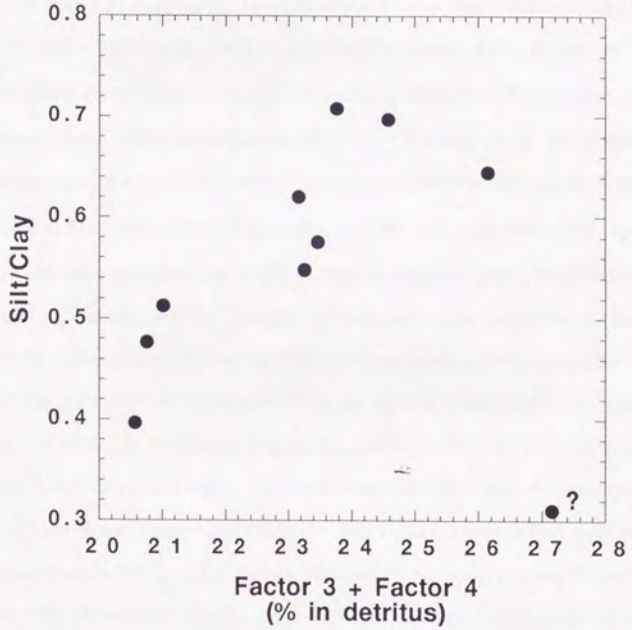

Figure 21 Interrelationship between silt /clay ratio and Factor 3 + Factor 4 (%) for selected 10 samples

13. Origin of Detrital Subcomponents

Based on the result of examination of chemical and mineral composition and grain size of the detrital subcomponents estimated by factor analysis, the characteristics of each factor is summarized in Table 10.

In order to estimate the origin of these factors (= detrital subcomponents), chemical and mineral composition as well as silt / clay ratio of the factors are compared with those of possible source materials. Because these four factors are characterized with significantly different chemical composition, their difference is most clearly demonstrated by x-y plots of $detSiO_2/Al_2O_3$, MgO/Al_2O_3, Na_2O/Al_2O_3, $K2O/Al_2O_3$ and TiO_2/Al_2O_3 (Figure 18). The author compares the composition of the subcomponents with those of Kosa [*Inoue and Naruse*, 1987, *Kanamori et al.*, 1991], suspended dust from Gobi [*Parungo et al.*, 1994], Pliocene neritic mudstone collected from the Northern Japan which represents fine-grained detritus derived from Japan Arc [*Irino*, 1992MS, *Sakamoto*, unpublished data], and various Quaternary tephra from Japan [*Machida and Arai*, 1992] on these diagrams (Figure 22). Cited data are also listed in Table 12. $DetSiO_2$ was not available for Kosa and neritic mudstone. As is obvious from Figure 22, composition of Kosa and Gobi dust are plotted on the mixing line between Factors 1 and 4 whereas that of detritus derived from the Japan Arc fall on the mixing line between Factors 2 and 3. These relations suggest that Factors 1 and 4 are attributable to Kosa, whereas Factors 2 and 3 are attributable to the detritus derived from Japan Arc, respectively. Silt / clay ratio of each factor further suggests that Factors 1 and 4 represent fine and coarse fraction of Kosa whereas Factors 2 and 3 represent fine and coarse fraction of arc-derived detritus, respectively. In addition, Factors 1 and 4 are rich in quartz and feldspars which are main constituents of Kosa [*Ishizaka*, 1991] whereas Factor 2 and Factor 3 are rich in detrital amorphous and smectite which are consistent with the smear slide observation that altered volcanic glass and weathered volcanoclastics are common in the studied sediments and are most likely derived from the Japan Arc.

Based on these estimation on the origin of each factor, the author defines percentage of Kosa within the detrital component as

$$\text{Kosa fraction (\%)} = \text{Factor 1 (\%)} + \text{Factor 4 (\%)}. \tag{20}$$

The author also defines Kosa grain size index (KGI) and arc-derived detritus grain size index (AGI) as follows,

$$\text{KGI} = \frac{\text{Factor 4 (\%)}}{(\text{Factor 1 (\%)} + \text{Factor 4 (\%)})}, \tag{21}$$

$$\text{AGI} = \frac{\text{Factor 3 (\%)}}{(\text{Factor 2 (\%)} + \text{Factor 3 (\%)})}. \tag{22}$$

Composition loadings of each detrital subcomponents, Kosa fraction, KGI, and AGI for each sample are listed in Table 13.

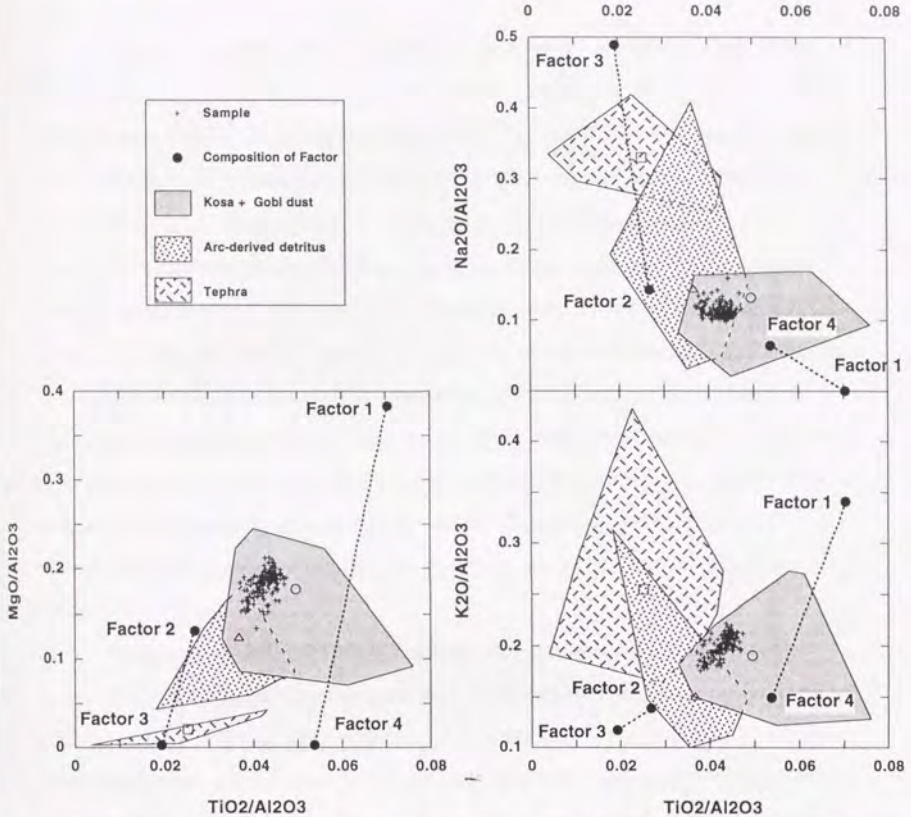

Figure 22 Comparison of chemical composition of each detrital subcomponent with possible source materials: The data included in Kosa category are Kosa collected in Japan (n=21) [*Inoue and Naruse*, 1987, *Kanamori et al.*, 1991], and air-suspended dust from Gobi (n=3) [*Parungo et al.*, 1995], whereas the data included in arc-derived detritus category are neritic mudstones of the Japan Sea side (n=195) [*Irino*, 1992MS, *Sakamoto*, unpublished data]. Data for various Quaternary tephra (n=8) is from *Machida and Arai* [1992]. Open circle, open triangle, and open square indicate the average composition of Kosa and Gobi dust, arc-derived detritus, and tephra, respectively.

14. Variation in Kosa Fraction, KGI, and AGI during the Last 200 ky

Figure 23a shows the temporal variation in Kosa fraction at Site 797 during the last 200 ky. Variation in Kosa fraction is generally in harmony with glacial-interglacial cycles with higher fraction of up to 62% during glacial stages and lower fraction of 40% during interglacial stages. Although overall profile of Kosa fraction resembles "typical" oxygen isotope curve [e.g. *Martinson et al.*, 1987], millennial scale fluctuation is superimposed on the glacial-interglacial changes with the magnitude almost as large as that of the latter. Kosa grain size index (KGI) shows 10 ky-scale variation with the larger values of 0.18 to 0.35 at stages 1, 2, and 4, and substage 6.2, and the smaller values of 0 to 0.15 at the end of stage 3, and substages 5.5 and 6.3 to 6.5 (Figure 23b). KGI shows millennial-scale fluctuation with the amplitude as large as that for 10ky-scale changes. Arc-derived detritus grain size index (AGI) tends to have larger values of 0.5 to 0.7 during stages 2 to 3 and substages 6.2 to 6.5, and the smaller values of 0.2 to 0.5 during stage 1, and substages 5.3 and 6.6 (Figure 23c). AGI also shows millennial-scale fluctuation but the amplitude tend to be smaller than that for 10 ky-scale changes.

Variation in Kosa fraction can be caused by changes either in Kosa flux or in arc-derived detritus flux. In order to examine which is more important, the author compared the fluctuation pattern of Kosa fraction with those of KGI and AGI. Close inspection of the phase relationship between the millennial-scale oscillations in Kosa fraction and KGI suggests that the minima in Kosa fraction tend to agree with the millennial-scale minima in KGI although KGI minima lag by one sample behind the minima in Kosa fraction in several cases. Phase delays are less than 2 ky. On the other hand, the maxima in AGI shows excellent agreement with the minima in Kosa fraction without any phase shift. Amplitude of the millennial-scale decrease in Kosa fraction is most easily explained by relative increase in coarse arc-derived detritus (Factor 3) because its variation shows the mirror image with the variation in Kosa fraction and the amplitude of the two are approximately the same (Figure 23d). Millennial-scale variation in AGI also seems to be mainly caused by variation in the fraction of coarse

arc-derived detritus. On the other hand, the millennial-scale variation in KGI tend to lag behind the variation in Kosa fraction, and the amplitude of variation in coarse Kosa does not seem enough to explain the millennial-scale variation in Kosa fraction (Figure 23d). From these reasons, the author consider changes in the flux of arc-derived detritus is more responsible for the millennial changes in Kosa fraction.

Then, what caused the millennial-scale increase in coarse arc-derived detritus flux ? There are two possible explanations. First explanation is the enhanced lateral transport of suspended load along the pycnocline [*Harlett and Kulm*, 1973] at the time of stronger density stratification in the Japan Sea. *Tada et al.* [1996] suggest that dark layers were deposited in the Japan Sea when the relative contribution of the East China Sea Coastal Water (ECSCW) influx increased. Stronger density stratification in the water column caused by the influx of the ECSCW with slightly lower salinity could have enhanced lateral transport of suspended load along the pycnocline. This is consistent with general coincidence of AGI maxima with the maxima of ECSCW influx suggested by diatom assemblage [*Tada et al.*, 1996]. The other explanation is that the increase in precipitation on the Japanese islands resulted in the increase in the total arc-derived detritus discharge to the Japan Sea including its coarser fraction. Generally speaking, increasing river discharge tend to increase the capacity of rivers to carry coarser detritus which may result in the increase in AGI [*Allen*, 1970]. From currently available data alone, the author cannot specify which explanation is more likely.

The decrease in KGI could be caused either by the increase in distance to the dust source area or by the weakening of wind intensity. The increase in the distance to the source area is caused by retreat of the eastern margin of the desert due to increasing vegetation cover on the Loess Plateau. *Tada et al.* [1996] suggested that the strong ECSCW influx to the Japan Sea during deposition of the dark layers could have been resulted from increasing precipitation within inland China and the consequent increase in discharge of Huanghe and Changjiang Rivers. If this interpretation is correct, the decrease in KGI within the dark layers suggests that the retreat of the eastern margin of the desert area occurred during these periods. Then, the phase delay of KGI minima from the start of the dark layers deposition might have reflected

the duration which was necessary for the recovery of vegetation cover. In order to further explore the possible influence of wind intensity on KGI, the author compared KGI record from Site 797 with the loess-paleosol sequences in China [*Kukla and An*, 1989] and their high resolution grain size record [*Porter and An*, 1995] (Figure 24). In 10 ky-scale, KGI at Site 797 tends to be lower during the periods of soil formation in the Loess Plateau (Figure 24). In millennial-scale, the maxima in KGI between 10 and 80 ka agree in timing, within the uncertainty of age determination, with the maxima in the quartz grain size observed in the loess sequence of China, which *Porter and An* [1995] believe is corresponding to Heinrich events except for H-1 (15 ka). Even during the period of soil formation at the Loess Plateau, millennial-scale KGI fluctuation is observed at Site 797. These observations suggest that variation in KGI seem to have been caused at least in part by variation in wind intensity. Thus, decrease of KGI could have reflected changes both in wind intensity and in the proximity to the dust source area, the latter being controlled by changes in precipitation within inland China.

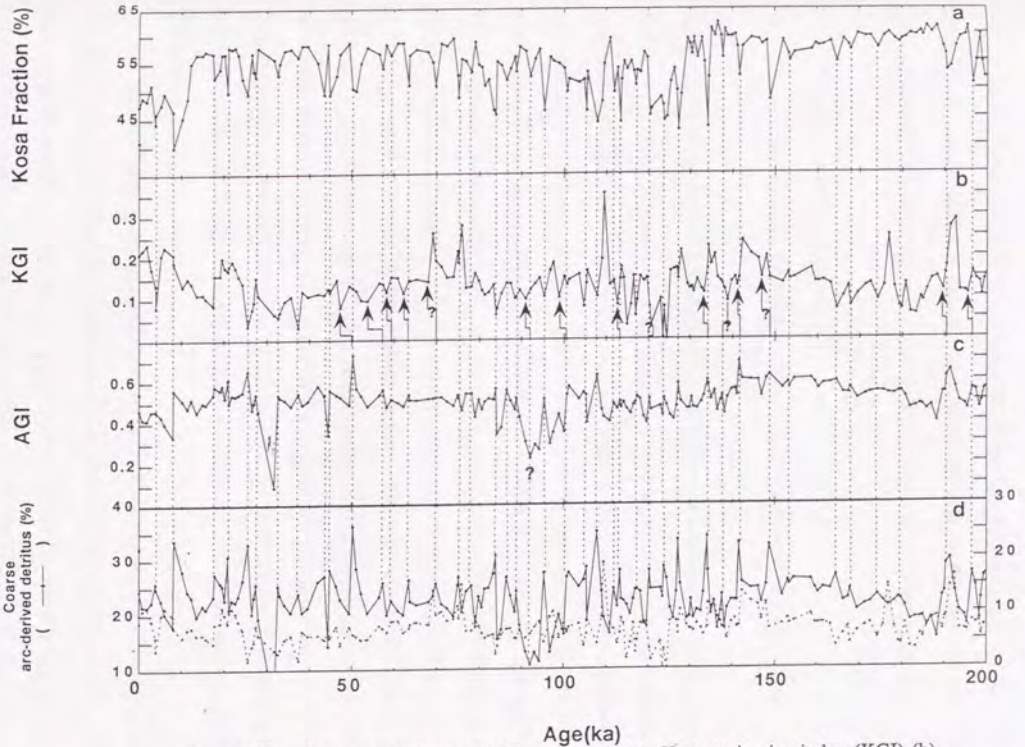

Figure 23 Temporal variations of Kosa fraction (a), Kosa grain size index (KGI) (b), arc-derived detritus grain size index (AGI) (c), and coarse arc-derived detritus fraction and coarse Kosa fraction (d) at ODP Site 797. In phase relationship between millennial-scale minima in Kosa fraction, KGI, and AGI are shown by vertical tie lines. Arrows in KGI profile indicate lag of KGI minima.

15. Variation in Kosa Flux during the Last 200 ky

In order to evaluate the Kosa flux to the Japan Sea and its variation in the past, the author calculated the mass accumulation rate (MAR) for each detrital subcomponent. The MAR of each detrital subcomponent is calculated based on the following equation.

(MAR of a subcomponent)

= (fraction of the subcomponent) x (detrital content) x DBD x LSR (23)

It is not possible to calculate LSR for individual samples because number of the datums in the sediments is limited [*Tada et al.*, 1996]. On the other hand, discussion in the previous section suggests the possibility of millennial-scale fluctuations in the fluxes of subcomponents. Thus, it is misleading to assume constant LSR between the datums and calculate MARs of subcomponents for each sample. For this reason, the author only calculates average MARs of the detrital subcomponents between the datums. Preceding the calculation of MARs, DBD, detrital content, and fraction of each detrital subcomponent were averaged for every stratigraphic interval defined by two adjacent datums. The results are listed in Table 14. The MARs for Holocene interval may have a large error because of the uncertainties involved in estimation of LSR and DBD. This error is probably caused by the underestimation of either LSR due to a slight lack of core top or DBD due to disturbance of core. Considering these uncertainties, MARs during Holocene could be as much as 1.5 times larger than described in Table 14.

Figure 24 shows the temporal variation in the MARs of Kosa and arc-derived detritus during the last 190 ky. Kosa MAR varied by factor of 3 and was high (2.5 to 3.0 $g/cm^2/ky$) during glacial stage 2 and substage 6.2, intermediate (1.7 $g/cm^2/ky$) during interglacial substage 5.5 and glacial substage 6.6, and low (0.8 to 1.2 $g/cm^2/ky$) during Holocene, glacial stages 3 and 4, and glacial substages 6.3 to 6.5. There was no evidence of soil formation in the Loess Plateau during glacial maxima (stage 2 and substage 6.2) whereas there is an evidence of

soil formation during the other intervals [*Kukla and An*, 1989]. This suggest that a larger Kosa source area developed during glacial maxima, that is consistent with observed higher Kosa MAR during these periods. Figure 1 shows that, at present, Kosa event is initiated as dust storms in the Taklimakan - Gobi desert area where the area with more than 30 days of annual frequency of dust storm and floating dust is approximately 4000 km^2 [*Pye and Zhou*, 1989]. If this dust storm area extended to whole area of the Loess Plateau during glacial maxima [*Bowler et al.*, 1987], the Kosa source area would have increased to approximately 9600 km^2 which is 2.4 times larger than the present area. This is consistent with our observation that Kosa MAR at Site 797 was three times larger during glacial maxima. On the other hand, the average Kosa MAR is nearly constant during the periods when the soil formation occurred in the Loess Plateau.

The present Kosa flux to the Japan Sea side of central to southwestern Japan is estimated as 1.4 to 3.2 $g/cm^2/ky$ based on the atmospheric dust concentration measurement [*Suzuki and Tsunogai*, 1987]. On the other hand, *Inoue and Naruse* [1989] estimated the Kosa flux as 0.5 to 1.0 $g/cm^2/ky$ based on the dust concentration within precipitation in northeastern to southwestern Japan. They also estimate the Kosa flux during the last glacial age as 1.9 to 3.2 $g/cm^2/ky$ based on the calculation of mass accumulation rate for Japanese paleosols which they believe was derived from the aeolian dust. Our estimation of Kosa MAR during Holocene is 0.8 $g/cm^2/ky$ and it could be as high as 1.2 $g/cm^2/ky$ considering the uncertainty of the estimation, whereas the MAR for the last glacial periods is estimated as 2.5 $g/cm^2/ky$. These values are consistent with the above estimation.

Arc-derived detritus MAR was high (2 to 2.3 $g/cm^2/ky$) during glacial maxima (stage 2 and substage 6.2), intermediate (1.7 $g/cm^2/ky$) during interglacial substage 5.5, and low (0.9 to 1.1 g/cm2/ky) during Holocene, stage 3 to substage 5.3 and substages 6.3 to 6.6 (Figure 24). The higher arc-derived detritus MARs during glacial maxima such as stage 2 and substage 6.2 are probably related to enhanced lateral transport of suspended load due to salinity stratification in the Japan Sea during these periods rather than the increasing discharge of Japanese rivers, because there are no evidence of increased precipitation during these intervals

[*Yasuda*, 1987] whereas there is good evidence of density stratification caused by the development of low salinity water cap during these periods [*Oba*, 1991, *Oba et al.*, 1995]. Higher AGI during the glacial maxima are also consistent with above explanation. Excluding the glacial maxima, arc-derived detritus MARs were higher during the last interglacial period. This suggests that the increase in river discharge due to enhanced precipitation on the Japanese islands during interglacial periods resulted in the increase in arc-derived detritus flux. Relatively low MAR of arc-derived detritus during Holocene could be underestimation.

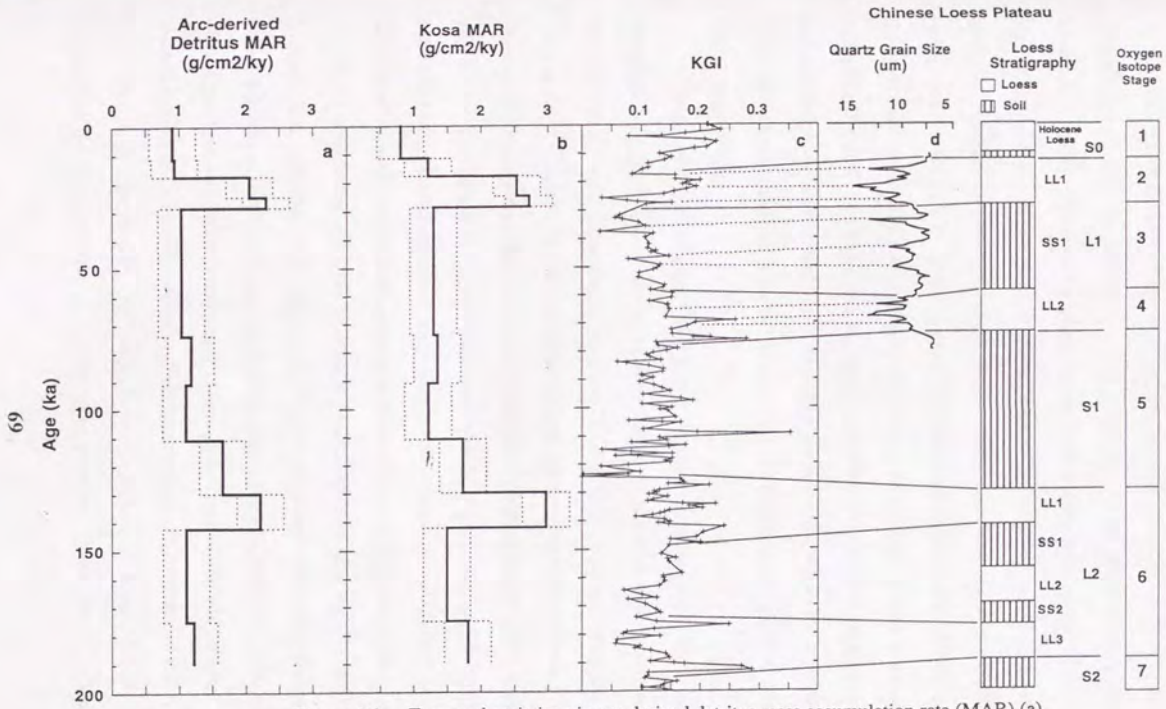

Figure 24 Temporal variations in arc-derived detritus mass accumulation rate (MAR) (a), Kosa MAR (b), and KGI (c) at ODP Site 797, and their comparison with quartz grain size in loess sequence [*Porter and An*, 1995] (d), and loess-paleosol sequence in China [*Kukla and An*, 1989].

16. Conclusions

The author developed a new procedure for Q-mode factor analysis to partition the detrital component of the sediment into subcomponents using chemical composition of selected "detrital" elements. The author applied this procedure to the hemipelagic sediments from ODP Site 797 in the Japan Sea to extract subcomponents attributable to aeolian dust (Kosa). Four detrital subcomponents were extracted, their chemical and mineral compositions and silt / clay ratios were estimated, and the origin of the each subcomponent was identified by comparing the estimated compositions with actual compositions of probable source materials. The extracted 4 detrital subcomponents are attributed to fine and coarse subcomponents of Kosa and arc-derived detritus, respectively. Based on these results, the author reconstructed the temporal variations of Kosa fraction, Kosa grain size (KGI), and arc-derived detritus grain size (AGI), respectively.

Reconstructed Kosa fraction is higher during glacial stages and lower during interglacial stages. Kosa fraction also shows millennial-scale variation whose amplitude is as large as that of glacial - interglacial variation. KGI tends to be larger during the periods of loess deposition and smaller during the periods of soil formation in the Loess Plateau. It also show millennial-scale variation with the amplitude as large as that of 10 ky-scale variation. AGI tend to be larger during glacial stages and smaller during interglacial stages. It also shows millennial-scale fluctuation whose amplitude is smaller than that of longer time scale variation. Millennial-scale minima in KGI coincide with the minima in Kosa fraction or lag by as much as 2 ky whereas millennial-scale maxima in AGI coincide exactly with the minima in Kosa fraction. The millennial-scale variation in Kosa fraction and AGI could be explained by the changes in coarse arc-derived detritus flux considering nearly perfect in phase relationship among the three and the large amplitude of coarse arc-derived detritus variation within the detrital component which is enough to explain variations in Kosa fraction and AGI. Variation in KGI could be controlled by the changes in proximity to the source area caused by advance or retreat of the eastern margin of arid area or by changes in wind intensity. Variation in AGI

could be caused by changes in efficiency of lateral transportation of suspended load along pycnocline in response to variation in the strength of salinity stratification of the water column in the Japan Sea, or alternatively by the changes in river discharge from the Japanese islands.

The author estimated MAR of Kosa and arc-derived detritus. Kosa MARs were 2.5 to 3.0 $g/cm^2/ky$ during glacial maxima which are 2 to 3 times larger than 0.8 to 1.7 $g/cm^2/ky$ during other periods. This suggests that significantly larger extent of Kosa source area developed during glacial maxima. Arc-derived detritus MAR was high between 2 and 2.3 $g/cm^2/ky$ during glacial maxima, intermediate at 1.7 $g/cm^2/ky$ during substage 5.5, and low between 0.9 and 1.1 $g/cm^2/ky$ during other periods. The high MAR during glacial maxima are probably related to enhanced lateral transport of suspended load due to salinity stratification in the Japan Sea. Relatively high MAR of arc-derived detritus during interglacial period suggests the increase in river discharge due to enhanced precipitation on the Japanese islands.

Acknowledgments. I am deeply grateful to Associate Professor Ryuji Tada for his helpful advice, many encouraging discussions, critical reading of the manuscript, providing the samples, and finacial support throughout this work. I would like to express my sincere thanks to all the participants and onboard stuffs of ODP Leg 127 and stuffs of Gulf Coast Core Repository of ODP for their assistance to take samples and associated data. I also express my thanks to Drs. Tom Pedersen, Tadamichi Oba, Itaru Koizumi, Minoru Utada, Ryo Matsumoto, Satoru Nakashima, S. Ogihara, E. Tajika, and J. Ashi for their helpful discussions and constructive review of this manuscript and Dr. Teruaki Ishii for providing an access to the XRF facility at ORI. Dr. Hidehiko Shimazaki and Masaaki Shimizu provided facilities to use mineral reference samples stored in the University Museum. Mr. Ahagon, Hyon, Yamagishi, Shirai, Takayama, and Sato kindly helped laboratory and drawing works. Dr. T. Sakamoto provided his unpublished chemical composition data.

References

Allen, J. R. L., *Physical Processes of Sedimentation*, 248 pp., George Allen and Unwin Ltd., London, 1970.

Bowler, J. M., K. Chen, and B. Yuan, Systematic variations in loess source areas: Evidence from Qaidam and Qinghai Basins, Western China, in *Aspects of Loess Research*, edited by T. Liu, pp. 39-51, China Ocean Press, Beijing, 1987.

Chamley, H., *Clay Sedimentology*, 623 pp., Springer-Verlag, Heidelberg, 1989.

Dansggaard, W., S. J. Johnsen, H. B. Clausen, D. Dahl-Jensen, N. S. Gundestrup, C. U. Hammer, C. S. Hvidberg, J. P. Steffensen, A. E. Sveinbjornsdottir, J. Jouzel, and G. Bond, Evidence for general instability of past climate from a 250-kyr ice-core record, *Nature , 364*, 218-220, 1993.

DeMaster, D. J., The supply and accumulation of silica in the marine environment, *Geochim. Cosmochim. Acta , 45*, 1715-1732, 1981.

Duce, R. A., P. S. Liss, J. T. Merrill, E. L. Atlas, P. Buat-Menard, B. B. Hicks, J. M. Miller, J. M. Prospero, R. Arimoto, T. M. Church, W. Ellis, J. N. Galloway, L. Hansen, T. D. Jickells, A. H. Knap, K. H. Reinhardt, B. Schneider, A. Soudine, J. J. Tokos, S. Tsunogai, R. Wollast, and M. Zhou, The atmospheric input of trace species to the world ocean, *Global Biogeochem. Cycles, 5*, 193-259, 1991.

Fanning, K. A. and M. E. Q. Pilson, On the spectro-photometric determination of dissolved silica in natural waters, *Analytical Chemistry, 45*, 136-140, 1973.

Gao, Y., R. Arimoto, M. Zhou, J. T. Merrill, and R. A. Duce, Relationships between the dust concentrations over Eastern Asia and the remote North Pacific, *J. Geophys. Res., 97* , 9867-9872, 1992.

Goudie, A. S., Dust storms in space and time, *Progress in physical geography; an international review of geographical work in the natural and environmental sciences, 7*, 502-530, 1983.

Harlett, J. C. and L. D. Kulm, Suspended sediment transport on the Northern Oregon Continental Shelf, *Geol. Soc. Am. Bull., 84*, 3815-3826, 1973.

Hovan, S. A. and D. K. Rea, Late Pleistocene continental climate and oceanic variability recorded in Northwest Pacific sediments, *Paleoceanography, 6*, 349-370, 1991.

Inoue, K. and T. Naruse, Physical, chemical, and mineralogical characteristics of modern eolian dust in Japan and rate of dust deposition, *Soil Sci. Plant Nutri., 33*, 327-345, 1987.

Irino, T. Nature of sedimentary cycles from late Miocene to Pliocene diatomaceous mudstones of Ajigasawa area, Northeast Japan, Master Thesis, University of Tokyo, 1992.

Ishizaka, Y., Kosa as chemical species (In Japanese), in *Kosa*, edited by Institute for Hydrospheric-Atmospheric Sciences, Nagoya Univ., pp. 109-123, Kokin Shoin, Tokyo, 1991.

Iwasaka, Y., H. Minoura, and K. Nagaya, The transport and spacial scale of Asian dust-storm clouds: a case study of the dust-storm event of April 1979, *Tellus, 35B*, 189-196, 1983.

Kanamori, S., N. Kanamori, M. Nishikawa, and T. Mizoguchi, Chemical composition of Kosa (In Japanese), in *Kosa*, edited by Institute for Hydrospheric-Atmospheric Sciences, Nagoya Univ., pp. 124-156, Kokin Shoin, Tokyo, 1991.

Krumbein, W. C. and F. J. Pettijohn, *Manual of Sedimentary Petrography*., 549 pp., Appleton-Century-Crofts, Inc., New York, 1938.

Kukla, G. and Z. An, Loess stratigraphy in central China, *Palaeogeogr. Palaeoclimatol. Palaeoecol., 72*, 203-225, 1989.

Kyte, F. T., M. Leinen, G. R. Heath, and L. Zhou, Cenozoic sedimentation history of the central North Pacific: Inferences from the elemental geochemistry of core LL44-GPC3, *Geochim. Cosmochim. Acta, 57*, 1719-1740, 1993.

Leinen, M., The origin of paleochemical signatures in North Pacific pelagic clays: Partitioning experiments, *Geochim. Cosmochim. Acta, 51*, 305-319, 1987.

Leinen, M., D. Cwienk, G. R. Heath, P. E. Biscaye, V. Kolla, J. Thiede, and J. P. Dauphin, Distribution of biogenic silica and quartz in recent deep-sea sediments, *Geology, 14*,

199-203, 1986.

Leinen, M. and N. Pisias, An objective technique for determining end-member compositions and for partitioning sediments according to their sources, *Geochim. Cosmochim. Acta, 48*, 47-62, 1984.

Machida, H. and F. Arai, *Atlas of Tephra in and around Japan* (In Japanese), 276 pp., University of Tokyo Press, Tokyo, 1992.

Martinson, D. G., N. G. Pisias, J. D. Hays, J. Imbrie, T. C. J. Moore, and N. J. Shackleton, Age dating and the orbital theory of the ice ages: Development of a high-resolution 0 to 300,000-year chronostratigraphy, *Quat. Res., 27*, 1-29, 1987.

Miesch, A. T., *Q-mode factor analysis of geochemical and petrologic data matrices with constant row-sums, U.S. Geol. Surv. Prof. Paper 574-G*, 47 pp., 1976.

Milliman, J. D. and R. H. Meade, World-wide delivery of river sediment to the oceans, *J. Geol., 91*, 1-21, 1983.

Milliman, J. D., Y. Qin, M. Ren, and Y. Saito, Man's influence on the erosion and transport of sediment by Asian rivers: the Yellow River (Huanghe) example, *J. Geol., 95*, 751-762, 1987.

Mortlock, R. A. and P. N. Froelich, A simple method for the rapid determination of biogenic opal in pelagic marine sediments, *Deep Sea Res., 36*, 1415-1426, 1989.

Nakai, S., A. N. Halliday, and D. K. Rea, Provenance of dust in the Pacific Ocean, *Earth Planet. Sci. Lett., 119*, 143-157, 1993.

Oba, T., Paleoenvironmental changes indicated by oxygen and carbon isotope (In Japanese), in *Environment and Civilization, 1*, edited by Y. Yasuda, pp. 38-46, The International Research Center for Japanese Studies, Kyoto, 1991.

Oba, T., M. Kato, H. Kitazato, I. Koizumi, A. Omura, T. Sakai, and T. Takayama, Paleoenvironmental changes in the Japan Sea during the last 85,000 years, *Paleoceanography, 6*, 499-518, 1991.

Oba, T., M. Murayama, E. Matsumoto, and T. Nakamura, AMS-^{14}C ages of Japan Sea cores

from the Oki Ridge (In Japanese with English abstract), *The Quaternary Research, 34*, 289-296, 1995.

Olivarez, A. M., R. M. Owen, and D. K. Rea, Geochemistry of eolian dust in Pacific pelagic sediments: Implications for paleoclimatic interpretations, *Geochim. Cosmochim. Acta, 55*, 2147-2158, 1991.

Parungo, F., Z. Li, X. Li, D. Yang, and J. Harris, Gobi dust storms and the Great Green Wall, *Geophys. Res. Lett., 21*, 999-1002, 1994.

Porter, S. C. and Z. An, Correlation between climate events in the North Atlantic and China during the last glaciation, *Nature, 375*, 305-308, 1995.

Pye, K. and L. Zhou, Late Pleistocene and Holocene aeolian dust deposition in north China and the Northwest Pacific Ocean, *Palaeogeogr. Palaeoclimatol. Palaeoecol., 73*, 11-23, 1989.

Rea, D. K. and M. Leinen, Asian aridity and the zonal westerlies: Late Pleistocene and Holocene record of eolian deposition in the Northwest Pacific Ocean, *Palaeogeogr. Palaeoclimatol. Palaeoecol., 66*, 1-8, 1988.

Rea, D. K., M. Leinen, and R. Janecek, Geologic approach to the long-term history of atmospheric circulation, *Science, 227*, 721-725, 1985.

Saito, Y. and K. Ikehara, Sediment discharge of Japanese rivers, and sedimentation rate and carbon content of marine sediments around the Japanese Islands (In Japanese), *Chishitsu News, 452*, 59-64, 1992.

Saito, Y. and Z. Yang, The Huanghe River: its water discharge, sediment discharge, and sediment budget (In Japanese with English abstract), *J. Sed. Soc. Japan, 40*, 7-17, 1994.

Shipboard Scientific Party, Site 797, in *Proc. Ocean Drill. Program, Init. Repts., 127*, edited by K. Tamaki, K. Pisciotto, J. Allan *et al.*, pp. 71-167. College Station, TX (Ocean Drilling Program), 1990.

Suzuki, T. and S. Tsunogai, Transport of chemical species from land to sea through atmosphere (In Japanese), *Marine Sciences Monthly, 19*, 657-662, 1987.

Tada, R. and A. Iijima, Petrology and diagenetic changes of Neogene siliceous rocks in

northern Japan, *J. Sediment. Petrol., 53*, 911-930, 1983.

Tada, R., T. Irino, and I. Koizumi, Possible Dansgaard-Oeschger oscillation signal recorded in the Japan Sea sediments, in *Global Fluxes of Carbon and Its Related Substances in the Coastal Sea-Ocean-Atmosphere System*, edited by S. Tsunogai, K. Iseki, I. Koike, and T. Oba, pp. 517-522, M&J International, Yokohama, 1995.

Tada, R., T. Irino, and I. Koizumi, Land - ocean linkage in association with Dansgaard - Oeschger cycles recorded in the late Quaternary sediments of the Japan Sea, *Paleoceanography*, submitted, 1996.

Tada, R., I. Koizumi, A. Cramp, and A. Rahman, Correlation of dark and light layers, and the origin of their cyclicity in the Quaternary sediments from the Japan Sea, in *Proc. Ocean Drill. Program, Sci. Results, 127/128, Pt1*, edited by K. A. Pisciotto, J. C. Ingle Jr., M. T. von Breymann, and J. Barron, pp. 577-601, College Station, TX (Ocean Drilling Program), 1992.

Taylor, K. C., G. W. Lamorey, G. A. Doyle, R. B. Alley, P. M. Grootes, P. A. Mayewski, J. W. C. White, and L. K. Barlow, The 'flickering switch' of late Pleistocene climatic change, *Nature, 361*, 432-436, 1993.

Taylor, S. R. and S. M. McLenann, *The Continental Crust: its Composition and Evolution*, 312 pp., Blackwell, Oxford, 1985.

Weber II, E. T., R. M. Owen, G. R. Dickens, A. N. Halliday, C. E. Jones, and D. K. Rea, Quantitative resolution of eolian continental crustal material and volcanic detritus in North Pacific surface sediment, *Paleoceanography, 11*, 95-127, 1996.

Yasuda, Y., The cold climate of the last glacial age in Japan (In Japanese with English abstract), *The Quaternary Research, 25*, 277-294, 1987.

Yin, J., H. Okada, and L. Labeyrie, Clay mineralogy of slope sediments around the Japanese islands (In Japanese with English abstract), *Geosci. Repts. Shizuoka Univ., 13*, 41-65, 1987.

Table 1 Age, grain composition, and remarks on all analyzed samples from ODP Site 797. Depth is corrected for core expansion. Age is based on the age model of *Tada et al.* [1996].

Type	No	Hole	Core	Sec	Interval	Depth (cmbsf)	Age (ka)	Largest Detrital Grain Size (µm)	Mineral	Detrital Grain Composition: Mica	Fresh Volcanic Glass	Carbonate: Inorganic	Carbonate: Diagenic	Others	Others	Remarks
HR	1	797A	1H	1	23 25	297	84.4	158	Qtz or Feld							
HR	2	797A	1H	2	86 88	499	84.2	118	Qtz or Feld						Gyp?	
HR	3	797A	1H	2	93 95	505	85.2	180	Qtz or Feld							
HR	4	797A	1H	2	130 132	542	90.9	110	Qtz or Feld							
HR	5	797A	1H	2	137 139	549	92.1	118	Qtz or Feld							
HR	6	797A	1H	2	144 146	556	93.2	133	Qtz or Feld							
HR	7	797A	1H	3	1 3	563	94.3	85	Qtz or Feld					Horn	Gyp?	
HR	8	797A	1H	3	8 10	570	95.4	208	Qtz or Feld							
HR	9	797A	1H	3	18 20	579	96.8	168	Qtz or Feld							
HR	10	797A	1H	3	22 24	584	97.6	100	Qtz or Feld							
HR	11	797A	1H	3	29 31	592	98.8	75	Qtz or Feld						Glauconite	
HR	12	797A	1H	3	36 38	600	100.1	193	Qtz or Feld							
HR	13	797A	1H	3	71 73	634	105.4	213	Qtz or Feld						Glauconite	
HR	14	797A	1H	3	98 100	659	109.4	310	Qtz or Feld						Gyp?	
HR	15	797A	1H	3	108 110	668	110.8	250	Qtz or Feld							
HR	16	797B	1H	1	17 19	17	0.0	100	Qtz or Feld							Core disturbance
HR	17	797B	1H	1	23 25	23	0.8	193	Qtz or Feld							Core disturbance
HR	18	797B	1H	1	31 33	30	1.8	140	Qtz or Feld						Gyp?	Core disturbance
HR	19	797B	1H	1	38 40	37	2.9	165	Qtz or Feld							Core disturbance
HR	20	797B	1H	1	45 47	44	4.0	165	Qtz or Feld							Core disturbance
HR	21	797B	1H	1	54 56	52	5.2	155	Qtz or Feld							Core disturbance
HR	22	797B	1H	1	59 61	57	6.0	225	Qtz or Feld							Core disturbance
HR	23	797B	1H	1	66 68	64	7.1	158	Qtz or Feld							Core disturbance
HR	24	797B	1H	1	73 75	70	8.0	83	Qtz or Feld	○						
HR	25	797B	1H	1	80 82	77	9.1	113	Qtz or Feld							XRD, XRF not analyzed
HR	26	797B	1H	1	87 89	84	10.2	163	Qtz or Feld							
HR	27	797B	1H	1	96 98	92	11.4	125	Qtz or Feld			○○○				
HR	28	797B	1H	1	101 103	97	12.3	175	Qtz or Feld			○○○				
HR	29	797B	1H	1	108 110	104	13.5	203	Qtz or Feld				○○			
HR	30	797B	1H	1	117 119	112	15.0	88	Qtz or Feld				○○			
HR	31	797B	1H	1	121 123	116	15.7	50	Qtz or Feld						Gyp?	
HR	32	797B	1H	1	131 133	126	17.4	250	Qtz or Feld							
HR	33	797B	1H	1	141 143	135	18.5	350	Qtz or Feld			○○○	○		Gyp?	
HR	34	797B	1H	1	146 148	140	19.1	300	Qtz or Feld				○○		Gyp?	
HR	35	797B	1H	2	0 2	144	19.5	175	Qtz or Feld	Biotite			○○			
HR	36	797B	1H	2	6 8	149	20.1	250	Qtz or Feld				○			
HR	37	797B	1H	2	15 17	158	21.1	400	Qtz or Feld			○○○	○			
HR	38	797B	1H	2	21 23	164	21.8	400	Qtz or Feld	Altered			○		Gyp?	
HR	39	797B	1H	2	29 31	171	22.6	75	Qtz or Feld			○○	○		Gyp?	
HR	40	797B	1H	2	35 37	177	23.3	125	Qtz or Feld			○○		Horn	Gyp?	
HR	41	797B	1H	2	40 42	182	23.9	188	Qtz or Feld		○				Gyp?	
HR	42	797B	1H	2	49 51	190	24.8	450	Qtz or Feld		○				Gyp?	
HR	43	797B	1H	2	56 58	197	25.6	108	Qtz or Feld						Gyp?	
HR	44	797B	1H	2	66 68	206	26.5	370	Qtz or Feld		○					
HR	45	797B	1H	2	70 72	210	27.0	208	Qtz or Feld		○					
HR	46	797B	1H	2	79 81	219	28.0	250	Qtz or Feld							
HR	47	797B	1H	2	84 86	224	28.5	73	Qtz or Feld		○					
HR	48	797B	1H	2	91 93	230	29.8	225	Qtz or Feld		○					
HR	49	797B	1H	2	100 102	239	31.8	250	Qtz or Feld							
HR	50	797B	1H	2	106 108	245	33.1	175	Qtz or Feld							
HR	51	797B	1H	2	112 114	250	34.2	300	Qtz or Feld							
HR	52	797B	1H	2	119 121	257	35.7	225	Qtz or Feld							
HR	53	797B	1H	2	127 129	265	37.4	128	Qtz or Feld							
HR	54	797B	1H	2	132 134	269	38.3	188	Qtz or Feld							
HR	55	797B	1H	2	138 140	275	39.6	250	Qtz or Feld							
HR	56	797B	1H	3	0 2	286	42.0	200	Qtz or Feld							
HR	57	797B	1H	3	7 9	293	43.3	700	Flaky Mica	Biotite						
HR	58	797B	1H	3	21 23	306	46.3	213	Qtz or Feld							
HR	59	797B	1H	3	25 27	310	47.2	138	Qtz or Feld							
HR	60	797B	1H	3	35 37	320	49.4	400	Qtz or Feld					Horn		
HR	61	797B	1H	3	40 42	324	50.2	300	Qtz or Feld					Horn	Gyp?	
HR	62	797B	1H	3	49 51	333	52.2	138	Qtz or Feld							
HR	63	797B	1H	3	56 58	340	53.7	75	Qtz or Feld							
HR	64	797B	1H	3	63 64	345	54.8	200	Altered Mica	Altered		○				XRD, XRF not analyzed
HR	65	797B	1H	3	70 72	353	56.5	125	Qtz or Feld							
HR	66	797B	1H	3	78 80	361	58.3	220	Qtz or Feld					Horn		
HR	67	797B	1H	3	84 86	366	59.4	270	Qtz or Feld							
HR	68	797B	1H	3	91 93	373	60.9	200	Altered Mica	Altered						
HR	69	797B	1H	3	97 99	379	62.2	100	Qtz or Feld					Horn		
HR	70	797B	1H	3	105 107	386	63.7	250	Qtz or Feld	Biotite						
HR	71	797B	1H	3	112 114	393	65.2	140	Qtz or Feld							
HR	72	797B	1H	3	120 121	400	66.8	58	Qtz or Feld							XRD, XRF not analyzed
HR	73	797B	1H	3	126 128	406	68.1	250	Qtz or Feld	Biotite						
HR	74	797B	1H	3	131 133	411	69.2	88	Qtz or Feld							
HR	75	797B	1H	3	140 142	420	71.1	150	Altered Mica	Altered						
HR	76	797B	1H	3	147 149	426	72.4	250	Qtz or Feld							
HR	77	797B	1H	4	4 6	433	73.9	130	Qtz or Feld							
HR	78	797B	1H	4	11 13	440	75.0	100	Qtz or Feld							
HR	79	797B	1H	4	18 20	446	75.9	140	Qtz or Feld							
HR	80	797B	1H	4	24 26	452	76.9	320	Qtz or Feld	Biotite						
HR	81	797B	1H	4	32 34	460	78.1	170	Qtz or Feld	Biotite						
HR	82	797B	1H	4	39 41	466	79.1	70	Qtz or Feld							
HR	83	797B	1H	4	49 51	476	80.6	75	Qtz or Feld							
HR	84	797B	1H	4	53 55	480	81.3	300	Flaky Mica	Biotite, Altered						
HR	85	797B	1H	4	60 62	486	82.2	300	Altered Mica	Altered						
HR	86	797B	1H	4	67 69	493	83.3	113	Qtz or Feld							
HR	87	797B	1H	4	88 90	513	86.4	125	Qtz or Feld			○○○				
HR	88	797B	1H	4	94 96	519	87.3	75	Qtz or Feld							
HR	89	797B	1H	4	102 104	526	88.4	300	Qtz or Feld			○○				
HR	90	797B	1H	4	109 111	533	89.5	150	Flaky Mica	Biotite						
HR	91	797B	2H	1	17 19	607	101.2	105	Qtz or Feld							Core disturbance
HR	92	797B	2H	1	24 26	614	102.3	70	Qtz or Feld	○						Core disturbance
HR	93	797B	2H	1	32 34	622	103.5	300	Altered Mica	Altered						
HR	94	797B	2H	1	39 41	629	104.7	100	Qtz or Feld	Altered			○			
HR	95	797B	2H	1	53 55	642	106.7	88	Qtz or Feld			○				XRF not analyzed
HR	96	797B	2H	1	60 62	649	107.8	113	Qtz or Feld			○				
HR	97	797B	2H	1	67 69	656	108.9	75	Qtz or Feld			○				
HR	98	797B	2H	1	88 90	676	111.7	180	Qtz or Feld			○				
HR	99	797B	2H	1	95 97	683	112.6	120	Altered Mica	Altered		○				
HR	100	797B	2H	1	104 106	691	113.5	75	Qtz or Feld			○○○	○			
HR	101	797B	2H	1	109 111	696	114.1	120	Qtz or Feld							
HR	102	797B	2H	1	115 117	702	114.8	53	Qtz or Feld				○○			
HR	103	797B	2H	1	123 125	710	115.7	100	Altered Mica	Altered						
HR	104	797B	2H	1	130 132	716	116.4	280	Altered Mica	Altered						
HR	105	797B	2H	1	137 139	723	117.3	63	Qtz or Feld					Horn		
HR	106	797B	2H	1	144 146	730	118.1	200	Altered Mica	Muscovite, Altered						
HR	107	797B	2H	2	1 3	737	118.9	100	Qtz or Feld	Biotite		○○				
HR	108	797B	2H	2	8 10	743	119.6	150	Altered Mica	Altered						
HR	109	797B	2H	2	17 19	752	120.7	138	Qtz or Feld							
HR	110	797B	2H	2	22 24	757	121.3	200	Qtz or Feld	○	○○○					
HR	111	797B	2H	2	30 32	765	122.2	260	Qtz or Feld	Biotite	○	○○				
HR	112	797B	2H	2	36 38	771	122.9	300	Altered Mica	Altered		○○				
HR	113	797B	2H	2	42 44	776	123.5	113	Qtz or Feld	Biotite		○○○				
HR	114	797B	2H	2	50 52	784	124.4	93	Qtz or Feld			○○○				
HR	115	797B	2H	2	57 59	791	125.3	138	Qtz or Feld			○○○				
HR	116	797B	2H	2	64 66	798	126.1	220	Flaky Mica	Biotite						
HR	117	797B	2H	2	71 73	804	126.8	175	Qtz or Feld	Biotite						
HR	118	797B	2H	2	79 81	812	127.7	150	Qtz or Feld				○	Horn		
HR	119	797B	2H	2	84 86	817	128.3	113	Qtz or Feld	Biotite	○					
HR	120	797B	2H	2	92 94	825	129.3	400	Qtz or Feld							
HR	121	797B	2H	2	98 100	830	129.8	150	Altered Mica	Altered					Glauconite	
HR	122	797B	2H	2	106 108	838	130.8	250	Altered Mica	Altered						
HR	123	797B	2H	2	113 115	845	131.7	250	Horn?					Horn?		
HR	124	797B	2H	2	121 123	853	132.6	138	Qtz or Feld							
HR	125	797B	2H	2	127 129	858	133.2	100	Qtz or Feld			○○○		Horn		
HR	126	797B	2H	2	136 138	867	134.3	400	Altered Mica	Altered				Horn		
HR	127	797B	2H	2	141 143	872	134.9	200	Altered Mica	Altered				Horn?		
HR	128	797B	2H	2	148 150	879	135.8	125	Qtz or Feld			○○○				
HR	129	797B	2H	3	5 7	885	136.5	230	Altered Mica	Altered		○○○	○			
HR	130	797B	2H	3	11 13	891	137.2	270	Qtz or Feld							
HR	131	797B	2H	3	19 21	899	138.2	300	Qtz or Feld							
HR	132	797B	2H	3	24 26	904	138.8	500	Qtz or Feld							

Table 1 (*continued*)

Type	No.	Hole	Core	Sec.	Interval	Depth (cmbsf)	Age (ka)	Largest Detrital Grain Size (mm)	Detrital Grain Composition: Mineral	Mica	Fresh Volcanic Glass	Carbonate: Inorganic	Carbonate: [Foram]	Others	Diluvs	Remarks	
HR	133	797B	2H	3	33 35	912	139.7	350	Qtz or Feld			cc					
HR	134	797B	2H	3	40 42	919	140.6	200	Qtz or Feld								
HR	135	797B	2H	3	48 50	927	141.6	230	Qtz or Feld						Gyp?		
HR	136	797B	2H	3	54 56	933	142.3	300	Altered Mica	Biotite, Altered							
HR	137	797B	2H	3	64 66	942	144.4	250	Altered Mica	Altered				Horn			
HR	138	797B	2H	3	71 73	949	146.1	450	Altered Mica	Altered				Horn			
HR	139	797B	2H	3	79 81	957	147.9	130	Qtz or Feld								
HR	140	797B	2H	3	82 84	960	148.6	200	Qtz or Feld			cc	cc				
HR	141	797B	2H	3	92 94	969	150.8	500	Qtz or Feld	Biotite	c						
HR	142	797B	2H	3	96 98	973	151.7	500	Qtz or Feld			cc					
HR	143	797B	2H	3	103 105	980	153.4	200	Qtz or Feld								
HR	144	797B	2H	3	108 110	985	154.5	300	Qtz or Feld					Horn?			
HR	145	797B	2H	3	116 117	992	156.2	200	Qtz or Feld					Horn			
HR	146	797B	2H	3	126 128	1002	158.6	300	Qtz or Feld					Rutile			XRD, XRF not analyzed
HR	147	797B	2H	3	131 133	1006	159.5	200	Qtz or Feld								
HR	148	797B	2H	3	138 140	1014	161.4	100	Altered Mica								
HR	149	797B	2H	3	145 147	1021	163.0	63	Qtz or Feld					Zircon			
HR	150	797B	2H	4	2 4	1027	164.4	200	Qtz or Feld								
HR	151	797B	2H	4	9 11	1034	166.1	230	Qtz or Feld	Biotite				Horn			
HR	152	797B	2H	4	16 18	1041	167.8	200	Qtz or Feld					Zircon			
HR	153	797B	2H	4	23 25	1048	169.4	113	Qtz or Feld								
HR	154	797B	2H	4	32 34	1056	171.3	100	Qtz or Feld					Horn?			
HR	155	797B	2H	4	37 39	1061	172.5	250	Qtz or Feld								
HR	156	797B	2H	4	46 47	1069	174.4	150	Flaky Mica	Biotite							XRD, XRF not analyzed
HR	157	797B	2H	4	51 53	1073	175.6	150	Altered Mica	Altered				Horn, Zircon			
HR	158	797B	2H	4	58 60	1081	176.8	125	Qtz or Feld					Horn			
HR	159	797B	2H	4	65 67	1088	178.1	240	Qtz or Feld								
HR	160	797B	2H	4	71 73	1094	179.2	200	Qtz or Feld	Altered							
HR	161	797B	2H	4	79 81	1102	180.7	180	Qtz or Feld								
HR	162	797B	2H	4	86 88	1108	181.9	120	Altered Mica	Altered		cc		Horn, Zircon			
HR	163	797B	2H	4	93 95	1115	183.2	200	Qtz or Feld			cc	cc				
HR	164	797B	2H	4	99 101	1121	184.3	88	Qtz or Feld								
HR	165	797B	2H	4	107 109	1129	185.8	200	Qtz or Feld					Horn			
HR	166	797B	2H	4	114 116	1135	187.0	300	Altered Mica	Altered							
HR	167	797B	2H	4	121 123	1142	188.3	100	Qtz or Feld								
HR	168	797B	2H	4	128 130	1149	189.6	75	Qtz or Feld								
HR	169	797B	2H	4	132 134	1153	190.2	50	Qtz or Feld								
HR	170	797B	2H	4	142 144	1162	191.5	160	Qtz or Feld								
HR	171	797B	2H	5	0 2	1170	192.6	75	Qtz or Feld								
HR	172	797B	2H	5	7 9	1177	193.6	75	Qtz or Feld								
HR	173	797B	2H	5	16 18	1186	194.9	75	Qtz or Feld								
HR	174	797B	2H	5	21 23	1190	195.5	88	Qtz or Feld								
HR	175	797B	2H	5	29 31	1198	196.6	150	Altered Mica	Altered							
HR	176	797B	2H	5	35 37	1204	197.5	125	Qtz or Feld	Altered							
HR	177	797B	2H	5	41 43	1210	198.3	100	Altered Mica	Altered							
HR	178	797B	2H	5	49 51	1217	199.3	150	Altered Mica	Altered							
HR	179	797B	2H	5	56 58	1224	200.3	120	Altered Mica	Altered				Rutile			
HR	180	797B	2H	5	62 64	1230	201.2	75	Qtz or Feld								
LR	1	797B	1H	1	13 13	13	0.0	120	Altered Mica	Biotite, Altered						Core disturbance	
LR	2	797B	1H	1	44 46	43	3.8	300	Altered Mica	Altered							
LR	3	797B	1H	1	74 76	73	8.2	100	Qtz or Feld			cc					
LR	4	797B	1H	1	134 136	128	17.7	200	Qtz or Feld			cc	cc				
LR	5	797B	1H	2	13 15	136	20.9	140	Qtz or Feld			ccc	cc	Horn, Zircon			
LR	6	797B	1H	2	44 46	186	24.3	250	Altered Mica	Altered		cc	c	Zircon	Glauconite		
LR	7	797B	1H	2	74 76	214	27.4	250	Qtz or Feld	Biotite							
LR	8	797B	1H	2	104 106	243	32.6	250	Altered Mica	Biotite							
LR	9	797B	1H	3	13 15	299	44.8	220	Qtz or Feld	Altered				Rutile			
LR	10	797B	1H	3	44 46	328	51.1	200	Qtz or Feld	Biotite							
LR	11	797B	1H	3	74 76	357	57.4	300	Qtz or Feld	Altered		ccc		Horn, Rutile			
LR	12	797B	1H	3	104 106	385	63.5	210	Qtz or Feld	Altered		cc		Horn			
LR	13	797B	1H	3	134 136	414	69.8	58	Qtz or Feld			ccc	c				
LR	14	797B	1H	4	13 15	443	75.2	113	Qtz or Feld			cc		Horn, Zircon			
LR	15	797B	1H	4	44 46	471	79.8	125	Altered Mica	Altered					Glauconite		
LR	16	797B	1H	4	71 73	497	83.9	63	Flaky Mica	Biotite		c					
LR	17	797B	1H	4	104 106	528	88.8	150	Flaky Mica	Biotite		cc	cc				
LR	18	797B	2H	1	14 16	604	100.7	500	Flaky Mica	Biotite							
LR	19	797B	2H	1	44 46	633	105.3	350	Altered Mica	Biotite, Altered		cc	c	Horn	Glauconite		
LR	20	797B	2H	1	102 104	689	113.3	160	Altered Mica	Altered		cc	cc				
LR	21	797B	2H	1	134 136	720	116.9	150	Altered Mica	Altered				Zircon	Glauconite		
LR	22	797B	2H	2	14 16	746	120.3	70	Qtz or Feld						Glauconite		
LR	23	797B	2H	2	102 104	834	130.3	75	Qtz or Feld					Rutile			
LR	24	797B	2H	2	134 136	865	134.1	125	Qtz or Feld								
LR	25	797B	2H	2	44 46	778	123.7	105	Qtz or Feld						Glauconite		
LR	26	797B	2H	2	74 76	807	127.1	125	Qtz or Feld								
LR	27	797B	2H	3	14 16	894	137.6	150	Qtz or Feld					Zircon			
LR	28	797B	2H	3	44 46	923	141.1	125	Qtz or Feld			cc			Glauconite		
LR	29	797B	2H	3	74 76	952	146.8	200	Flaky Mica	Biotite		ccc	cc				
LR	30	797B	2H	3	102 104	979	153.1	180	Qtz or Feld			cc					
LR	31	797B	2H	3	134 136	1009	160.2	200	Qtz or Feld	Biotite		cc					
LR	32	797B	2H	4	14 16	1039	167.3	125	Qtz or Feld								
LR	33	797B	2H	4	44 46	1068	174.1	260	Qtz or Feld	Muscovite				Rutile			
LR	34	797B	2H	4	74 76	1097	179.8	220	Qtz or Feld			cc		Horn			
LR	35	797B	2H	4	102 104	1124	184.9	75	Qtz or Feld			ccc	cc				
LR	36	797B	2H	4	134 136	1153	190.3	350	Flaky Mica	Muscovite		cc	cc		Glauconite		
LR	37	797B	2H	5	44 46	1213	198.8	113	Qtz or Feld	Biotite					Glauconite		
LR	38	797B	2H	5	74 76	1242	202.9	163	Qtz or Feld			c			Glauconite		
LR	39	797B	2H	5	102 104	1269	206.8	118	Qtz or Feld	Biotite		ccc					
LR	40	797B	2H	5	134 136	1299	211.1	88	Qtz or Feld	Biotite				Horn			
LRA	1	797A	1H	1	14 16	291	43.1	106	Qtz or Feld							Core disturbance	Grain Size Separation
LRA	5	797A	1H	1	134 136	405	67.8	300	Qtz or Feld	Biotite, Altered		cc					Grain Size Separation
LRA	8	797A	1H	2	74 76	489	82.7	220	Qtz or Feld	Biotite	c		cc		Glauconite		Grain Size Separation
LRA	16	797A	1H	4	14 16	721	117.3	100	Qtz or Feld					Zircon			Grain Size Separation
LRA	19	797A	1H	4	104 106	804	126.8	100	Altered Mica	Altered		cc					Grain Size Separation
LRA	20	797A	1H	4	134 136	832	130.1	88	Qtz or Feld						Glauconite		Grain Size Separation
LRA	23	797A	1H	5	74 76	930	141.9	113	Qtz or Feld	Altered							Grain Size Separation
LRA	24	797A	1H	5	104 106	959	146.4	50	Qtz or Feld								Grain Size Separation
LRA	30	797A	1H	6	134 136	1139	182.7	85	Qtz or Feld				cc	Zircon			Grain Size Separation
LRA	32	797A	1H	7	44 46	1202	197.3	113	Qtz or Feld	Altered							Grain Size Separation

Table 2 Major elements composition of all analyzed samples from ODP Site 797.

Type	No	Hole	Core	Sec	Interval	L.O.I.	SiO2	TiO2	Al2O3	Fe2O3	MnO	MgO	CaO	Na2O	K2O	P2O5	Total
HR	1	797A	1H	1	23 25	5.61	60.1	0.716	16.9	6.11	0.061	3.17	1.22	1.81	3.41	0.119	99.2
HR	2	797A	1H	2	86 88	13.04	54.0	0.547	13.6	10.50	0.110	2.60	0.84	1.45	2.57	0.129	99.4
HR	3	797A	1H	2	93 95	8.80	57.0	0.660	15.7	7.02	0.122	3.02	1.91	1.76	2.86	0.124	99.0
HR	4	797A	1H	2	130 132	9.98	56.8	0.655	15.8	7.20	0.077	3.02	1.15	1.70	3.09	0.128	99.6
HR	5	797A	1H	2	137 139	14.01	49.0	0.561	13.6	6.57	0.283	2.52	6.62	1.67	2.65	0.126	97.7
HR	6	797A	1H	2	144 146	8.48	58.3	0.683	16.2	6.81	0.183	3.01	1.13	1.85	3.16	0.124	100.0
HR	7	797A	1H	3	1 3	7.59	59.3	0.689	16.3	6.81	0.093	2.98	0.99	1.81	3.22	0.117	99.9
HR	8	797A	1H	3	8 10	7.95	59.1	0.595	14.9	8.45	0.150	2.61	0.98	1.94	3.07	0.116	99.9
HR	9	797A	1H	3	18 20	7.66	59.1	0.683	16.7	6.48	0.094	2.90	0.97	1.84	3.22	0.121	99.8
HR	10	797A	1H	3	22 24	7.15	59.9	0.691	16.9	6.06	0.068	2.85	0.99	1.86	3.26	0.114	99.9
HR	11	797A	1H	3	29 31	6.53	60.5	0.682	15.7	7.20	0.078	3.05	1.09	1.87	3.32	0.121	100.1
HR	12	797A	1H	3	36 38	6.55	60.3	0.689	17.0	5.87	0.088	2.95	1.05	1.91	3.32	0.109	99.9
HR	13	797A	1H	3	71 73	7.26	59.5	0.690	17.4	5.75	0.082	2.92	1.08	1.90	3.28	0.113	99.9
HR	14	797A	1H	3	98 100	15.41	50.6	0.582	14.3	10.41	0.051	1.92	1.34	1.58	2.73	0.121	99.0
HR	15	797A	1H	3	108 110	6.30	59.8	0.726	16.7	6.35	0.186	3.17	1.31	1.76	3.37	0.121	99.8
HR	16	797B	1H	1	17 19	6.81	60.6	0.643	16.5	5.99	0.860	2.57	0.97	1.99	3.05	0.157	100.2
HR	17	797B	1H	1	23 25	6.68	60.1	0.647	16.7	6.15	0.803	2.58	0.96	1.94	3.09	0.159	99.8
HR	18	797B	1H	1	31 33	6.89	60.3	0.642	16.7	6.19	1.042	2.54	0.97	1.93	3.03	0.173	100.4
HR	19	797B	1H	1	38 40	7.01	57.6	0.646	15.7	6.15	3.742	2.67	1.01	1.87	3.04	0.179	99.7
HR	20	797B	1H	1	45 47	7.87	55.0	0.575	14.4	11.45	1.299	2.64	1.05	1.89	2.81	0.546	99.5
HR	21	797B	1H	1	54 56	9.41	58.9	0.646	16.8	6.32	0.075	2.64	1.09	1.97	3.01	0.178	101.0
HR	22	797B	1H	1	59 61	9.49	57.9	0.658	17.0	5.91	0.119	2.64	1.07	1.93	3.03	0.167	99.9
HR	23	797B	1H	1	66 68	6.33	58.6	0.632	17.6	5.51	0.087	1.90	1.29	3.56	4.44	0.148	100.1
HR	24	797B	1H	1	73 75	9.02	57.8	0.633	17.0	6.21	0.108	2.61	1.06	2.01	3.08	0.156	99.7
HR	25	797B	1H	1	80 82												
HR	26	797B	1H	1	87 89	9.45	57.0	0.609	16.2	6.91	0.103	2.66	1.36	1.94	3.02	0.148	99.4
HR	27	797B	1H	1	96 98	15.46	51.9	0.594	15.2	5.34	0.057	2.57	4.06	1.76	2.74	0.157	99.8
HR	28	797B	1H	1	101 103	9.14	55.1	0.659	15.9	5.91	0.142	2.84	4.74	1.69	3.07	0.136	99.3
HR	29	797B	1H	1	108 110	17.53	41.5	0.491	12.1	4.49	0.061	2.21	17.31	1.23	2.34	0.105	99.3
HR	30	797B	1H	1	117 119	8.78	55.5	0.664	16.2	6.05	0.078	2.99	5.12	1.63	3.10	0.128	100.2
HR	31	797B	1H	1	121 123	6.26	58.1	0.707	16.9	6.50	0.094	3.19	1.74	1.74	3.39	0.134	98.8
HR	32	797B	1H	1	131 133	5.70	59.8	0.717	16.1	6.78	0.060	3.27	1.47	1.79	3.42	0.138	99.3
HR	33	797B	1H	1	141 143	9.10	50.6	0.624	14.1	7.19	0.088	7.15	6.57	1.52	2.78	0.122	99.9
HR	34	797B	1H	1	146 148	9.08	51.8	0.623	14.4	7.20	0.092	2.59	5.93	1.64	2.84	0.119	96.3
HR	35	797B	1H	2	0 2	8.26	53.4	0.676	14.4	6.78	0.075	2.63	5.61	1.66	2.84	0.129	96.5
HR	36	797B	1H	2	6 8	8.58	52.2	0.647	14.8	7.90	0.081	2.64	4.60	1.61	2.93	0.136	96.2
HR	37	797B	1H	2	15 17	8.23	52.3	0.673	14.9	7.98	0.072	2.73	4.75	1.64	2.92	0.123	96.3
HR	38	797B	1H	2	21 23	9.58	52.1	0.665	14.8	8.31	0.065	2.65	4.42	1.61	2.90	0.122	97.3
HR	39	797B	1H	2	29 31	9.26	53.8	0.696	15.1	6.56	0.063	2.83	4.37	1.68	2.99	0.126	97.4
HR	40	797B	1H	2	35 37	7.95	54.4	0.695	15.3	7.44	0.067	2.90	3.66	1.73	3.10	0.122	97.3
HR	41	797B	1H	2	40 42	8.82	64.9	0.429	15.0	4.48	0.064	1.74	1.27	1.69	3.36	0.078	101.8
HR	42	797B	1H	2	49 51	8.54	63.0	0.413	15.4	4.36	0.063	1.66	1.27	1.66	3.34	0.076	99.8
HR	43	797B	1H	2	56 58	7.66	59.2	0.621	15.4	6.69	0.057	2.96	1.34	1.81	3.27	0.130	99.1
HR	44	797B	1H	2	66 68	9.04	54.9	0.652	15.9	9.11	0.072	3.04	1.28	1.64	3.22	0.142	99.0
HR	45	797B	1H	2	70 72	8.62	56.3	0.692	16.1	7.13	0.064	3.12	1.37	1.90	3.34	0.134	98.8
HR	46	797B	1H	2	79 81	5.73	59.0	0.737	17.4	6.59	0.069	3.30	1.33	1.82	3.52	0.125	99.6
HR	47	797B	1H	2	84 86	5.16	67.5	0.446	15.2	4.66	0.066	1.81	1.32	2.53	3.50	0.081	102.2
HR	48	797B	1H	2	91 93	5.08	65.4	0.429	14.5	4.52	0.065	1.72	1.32	2.54	3.46	0.079	99.1
HR	49	797B	1H	2	100 102	8.45	58.7	0.616	16.1	6.63	0.057	2.93	1.33	1.74	3.24	0.129	99.9
HR	50	797B	1H	2	106 108	8.62	55.2	0.655	15.4	9.15	0.072	3.05	1.29	1.72	3.24	0.143	98.5
HR	51	797B	1H	2	112 114	7.18	57.2	0.703	16.1	7.24	0.065	3.17	1.39	1.75	3.40	0.136	98.4
HR	52	797B	1H	2	119 121	6.28	58.7	0.733	17.1	6.55	0.068	3.28	1.32	1.81	3.50	0.125	99.5
HR	53	797B	1H	2	127 129	7.21	57.7	0.667	15.3	8.35	0.073	3.24	1.32	1.71	3.39	0.133	99.1
HR	54	797B	1H	2	132 134	9.82	57.0	0.710	16.3	6.44	0.063	3.12	1.31	1.73	3.33	0.118	99.9
HR	55	797B	1H	2	138 140	5.56	59.9	0.734	17.0	6.67	0.066	3.29	1.27	1.77	3.46	0.124	99.8
HR	56	797B	1H	3	0 2	6.27	60.2	0.697	15.6	6.88	0.062	3.05	1.22	1.80	3.26	0.120	99.1
HR	57	797B	1H	3	7 9	7.92	58.1	0.673	15.8	7.34	0.080	2.93	1.20	2.06	3.34	0.133	99.6
HR	58	797B	1H	3	21 23	7.26	60.1	0.701	16.9	6.53	0.076	2.98	1.23	1.91	3.29	0.133	101.1
HR	59	797B	1H	3	25 27	10.91	55.3	0.650	15.4	8.00	0.068	3.02	1.17	1.60	3.09	0.143	99.4
HR	60	797B	1H	3	35 37	5.79	59.9	0.722	16.3	7.02	0.074	3.12	1.25	1.74	3.36	0.121	99.4
HR	61	797B	1H	3	40 42	5.59	62.6	0.676	15.0	6.48	0.059	2.82	1.27	1.90	3.20	0.118	99.7
HR	62	797B	1H	3	49 51	8.18	58.7	0.705	15.7	6.87	0.065	3.18	1.46	1.85	3.26	0.139	100.0
HR	63	797B	1H	3	56 58	6.51	59.4	0.725	16.3	7.30	0.074	3.27	1.27	1.80	3.48	0.130	100.3
HR	64	797B	1H	3	63 64												
HR	65	797B	1H	3	70 72	5.37	60.3	0.760	16.4	6.49	0.107	3.20	1.29	1.93	3.50	0.125	99.5
HR	66	797B	1H	3	78 80	5.62	59.4	0.738	16.5	7.06	0.332	3.23	1.35	1.83	3.56	0.126	99.8
HR	67	797B	1H	3	84 86	6.39	59.4	0.750	17.1	5.90	0.103	3.14	1.26	1.90	3.46	0.128	99.6
HR	68	797B	1H	3	91 93	5.41	60.8	0.768	17.3	5.96	0.097	3.23	1.27	1.85	3.54	0.125	100.4
HR	69	797B	1H	3	97 99	7.25	58.5	0.724	16.1	7.04	0.097	3.19	1.18	1.77	3.46	0.125	99.5
HR	70	797B	1H	3	105 107	3.27	61.6	0.768	17.5	6.13	0.102	3.25	1.28	1.96	3.62	0.124	99.6
HR	71	797B	1H	3	112 114	5.29	59.6	0.757	16.9	5.95	0.081	3.18	1.27	1.89	3.51	0.120	98.5
HR	72	797B	1H	3	120 121												
HR	73	797B	1H	3	126 128	5.27	60.3	0.752	16.7	6.59	0.094	3.19	1.29	1.89	3.47	0.122	99.6
HR	74	797B	1H	3	131 133	11.23	54.6	0.691	16.0	8.15	0.048	2.54	1.03	1.79	2.99	0.132	99.2
HR	75	797B	1H	3	140 142	6.18	58.9	0.749	16.5	6.91	0.076	3.03	1.42	1.80	3.33	0.131	99.0
HR	76	797B	1H	3	147 149	5.66	59.6	0.770	16.7	6.24	0.092	3.22	1.80	1.89	3.47	0.125	99.6
HR	77	797B	1H	4	4 6	6.86	59.5	0.755	16.9	6.89	0.086	3.18	1.21	1.79	3.41	0.119	100.7
HR	78	797B	1H	4	11 13	10.91	56.8	0.687	16.2	5.91	0.063	2.68	1.11	1.87	3.04	0.133	99.4
HR	79	797B	1H	4	18 20	14.78	50.8	0.626	14.8	9.95	0.051	2.28	0.91	1.63	2.78	0.126	98.7
HR	80	797B	1H	4	24 26	5.62	59.4	0.707	16.8	7.62	0.113	3.09	1.10	1.80	3.30	0.120	99.7
HR	81	797B	1H	4	32 34	6.30	57.5	0.667	15.8	9.60	0.093	2.91	0.92	1.78	3.07	0.141	98.8
HR	82	797B	1H	4	39 41	10.81	56.4	0.718	16.4	5.79	0.097	3.01	1.13	1.76	3.28	0.116	99.5
HR	83	797B	1H	4	49 51	9.43	56.5	0.672	16.1	6.95	0.082	3.01	1.11	1.77	3.02	0.138	98.8
HR	84	797B	1H	4	53 55	10.36	51.7	0.592	14.6	7.85	0.137	2.67	4.29	1.67	2.71	2.251	98.8
HR	85	797B	1H	4	60 62	9.30	57.1	0.659	15.7	7.04	0.063	2.92	1.11	1.84	3.09	0.125	99.0

Table 2 (*continued*)

Type	No	Hole	Core	Sec	Interval	L.O.I.	SiO2	TiO2	Al2O3	Fe2O3	MnO	MgO	CaO	Na2O	K2O	P2O5	Total
HR	86	797B	1H	4	67 69	11.10	55.5	0.605	15.3	7.80	0.076	2.62	1.07	1.91	2.89	0.135	99.0
HR	87	797B	1H	4	88 90	6.09	63.3	0.714	17.7	5.50	0.097	3.07	1.25	1.96	3.41	0.113	103.2
HR	88	797B	1H	4	94 96	5.84	61.4	0.730	17.2	5.62	0.098	3.14	1.31	1.97	3.44	0.119	100.9
HR	89	797B	1H	4	102 104	6.79	58.2	0.719	16.4	5.85	0.122	3.25	2.87	1.86	3.35	0.117	99.5
HR	90	797B	1H	4	109 111	5.92	59.5	0.744	16.9	6.05	0.064	3.30	1.40	1.85	3.39	0.118	99.3
HR	91	797B	2H	1	17 19	7.54	59.2	0.688	15.6	7.16	0.065	2.88	1.17	1.93	3.20	0.120	99.6
HR	92	797B	2H	1	24 26	7.34	56.6	0.611	16.4	7.99	0.095	2.41	1.06	2.56	3.55	0.110	98.7
HR	93	797B	2H	1	32 34	8.23	57.4	0.667	16.9	6.96	0.092	2.85	0.97	1.84	3.09	0.117	99.2
HR	94	797B	2H	1	39 41	8.08	57.1	0.670	15.7	7.56	0.082	3.08	1.14	1.88	3.19	0.116	98.5
HR	95	797B	2H	1	53 55												
HR	96	797B	2H	1	60 62	6.42	59.7	0.616	16.0	7.41	0.076	2.68	0.96	2.02	3.22	0.100	99.2
HR	97	797B	2H	1	67 69	11.57	56.3	0.649	16.6	5.60	0.055	2.66	1.01	1.97	3.05	0.118	99.6
HR	98	797B	2H	1	88 90	5.67	59.8	0.708	16.4	6.43	0.145	2.96	1.35	2.19	3.48	0.124	99.2
HR	99	797B	2H	1	95 97	10.78	56.0	0.627	15.0	7.45	0.086	2.90	1.04	1.70	2.99	0.106	98.6
HR	100	797B	2H	1	104 106	17.48	42.6	0.487	11.5	6.76	0.084	2.02	10.77	1.37	2.15	0.116	95.3
HR	101	797B	2H	1	109 111	8.42	58.0	0.676	15.3	5.72	0.089	2.84	2.93	1.80	3.18	0.114	99.0
HR	102	797B	2H	1	115 117	11.93	49.8	0.567	13.3	5.92	3.434	2.81	5.92	1.53	2.60	0.154	98.0
HR	103	797B	2H	1	123 125	8.25	57.1	0.661	15.5	6.91	1.786	3.08	1.58	1.74	3.05	0.136	99.7
HR	104	797B	2H	1	130 132	6.73	60.0	0.680	16.4	6.21	0.197	2.88	1.00	1.86	3.21	0.106	99.2
HR	105	797B	2H	1	137 139	7.54	58.1	0.651	15.4	8.44	0.190	2.95	0.96	1.76	3.11	0.111	99.2
HR	106	797B	2H	1	144 146	14.06	56.0	0.639	15.2	5.21	0.144	2.69	1.03	1.75	3.02	0.099	99.8
HR	107	797B	2H	2	1 3	6.17	61.3	0.720	17.5	5.82	0.255	3.14	1.06	1.81	3.33	0.113	101.2
HR	108	797B	2H	2	8 10	6.04	60.0	0.685	16.8	5.95	0.286	2.94	0.99	1.80	3.27	0.108	98.8
HR	109	797B	2H	2	17 19	6.40	60.1	0.610	15.7	6.50	0.969	2.92	0.99	1.98	3.22	0.111	99.5
HR	110	797B	2H	2	22 24	8.31	56.0	0.474	14.6	5.37	4.037	2.34	2.03	2.94	3.42	0.195	99.7
HR	111	797B	2H	2	30 32	4.16	59.1	0.390	17.6	5.67	0.288	1.23	1.28	5.77	4.94	0.106	100.5
HR	112	797B	2H	2	36 38	6.96	60.7	0.631	16.3	5.45	0.910	2.87	1.16	1.88	3.08	0.110	100.1
HR	113	797B	2H	2	42 44	9.75	54.9	0.550	14.5	5.29	5.014	2.76	2.18	1.72	2.79	0.160	99.6
HR	114	797B	2H	2	50 52	9.04	56.6	0.543	14.6	5.52	4.099	2.70	1.91	1.76	2.84	0.136	99.8
HR	115	797B	2H	2	57 59	5.90	60.3	0.680	17.5	6.02	0.159	2.88	0.89	1.93	3.30	0.102	99.6
HR	116	797B	2H	2	64 66	6.11	59.8	0.688	17.8	5.95	0.236	2.93	0.88	1.84	3.29	0.100	99.6
HR	117	797B	2H	2	71 73	6.05	60.3	0.690	17.7	6.30	0.096	2.90	0.88	2.00	3.27	0.108	100.3
HR	118	797B	2H	2	79 81	6.26	59.8	0.681	17.5	5.93	0.414	2.72	0.93	2.00	3.23	0.112	99.6
HR	119	797B	2H	2	84 86	5.72	59.5	0.631	17.1	7.21	0.095	2.59	0.85	2.48	3.57	0.105	99.9
HR	120	797B	2H	2	92 94	6.33	59.2	0.733	17.1	5.85	0.893	3.20	1.33	1.74	3.38	0.126	99.9
HR	121	797B	2H	2	98 100	6.00	59.4	0.742	17.1	5.83	0.633	3.27	1.29	1.81	3.45	0.125	99.7
HR	122	797B	2H	2	106 108	5.41	60.8	0.751	17.1	6.09	0.183	3.33	1.16	1.79	3.54	0.125	100.2
HR	123	797B	2H	2	113 115	5.12	60.9	0.744	17.0	6.04	0.139	3.14	1.27	1.98	3.58	0.128	100.1
HR	124	797B	2H	2	121 123	5.08	61.1	0.739	16.9	6.31	0.143	3.23	1.03	1.76	3.56	0.120	100.0
HR	125	797B	2H	2	127 129	5.29	61.0	0.709	16.4	6.23	0.132	3.10	1.15	1.89	3.53	0.123	99.6
HR	126	797B	2H	2	136 138	6.89	58.3	0.709	15.7	7.43	0.082	2.59	1.55	2.02	3.33	0.125	98.7
HR	127	797B	2H	2	141 143	7.24	58.3	0.738	16.2	7.26	0.106	2.97	1.37	1.68	3.33	0.134	99.3
HR	128	797B	2H	2	148 150	6.63	58.7	0.742	16.3	7.21	0.085	2.89	1.28	1.72	3.27	0.125	98.9
HR	129	797B	2H	3	5 7	5.63	60.1	0.753	17.1	6.23	0.141	3.20	1.21	1.68	3.54	0.121	99.7
HR	130	797B	2H	3	11 13	5.85	60.7	0.739	17.0	6.77	0.335	3.15	1.21	1.74	3.51	0.130	101.1
HR	131	797B	2H	3	19 21	5.53	60.4	0.758	17.1	5.91	0.155	3.33	1.23	1.76	3.60	0.122	99.9
HR	132	797B	2H	3	24 26	5.59	59.6	0.714	16.2	8.06	0.093	3.22	0.96	1.69	3.54	0.120	99.8
HR	133	797B	2H	3	33 35	5.30	61.7	0.770	17.6	5.85	0.116	3.29	1.13	1.78	3.59	0.120	101.2
HR	134	797B	2H	3	40 42	5.10	61.1	0.760	17.0	6.00	0.106	3.17	1.04	1.76	3.59	0.119	99.8
HR	135	797B	2H	3	48 50	6.24	60.2	0.650	16.7	6.55	0.063	2.70	0.87	1.72	3.37	0.112	99.1
HR	136	797B	2H	3	54 56	9.99	53.5	0.668	14.6	11.42	0.075	2.40	1.38	1.64	3.07	0.113	98.8
HR	137	797B	2H	3	64 66	8.29	55.9	0.711	15.6	9.00	0.084	2.75	1.69	1.63	3.12	0.121	98.9
HR	138	797B	2H	3	71 73	8.20	55.7	0.704	15.6	8.80	0.085	2.78	2.06	1.63	3.11	0.119	98.7
HR	139	797B	2H	3	79 81	7.70	56.6	0.702	15.9	8.19	0.066	2.73	1.58	1.64	3.21	0.119	98.4
HR	140	797B	2H	3	82 84	7.38	57.9	0.675	16.1	6.63	0.089	2.78	1.98	2.06	3.33	0.116	99.1
HR	141	797B	2H	3	92 94	9.18	52.6	0.579	15.2	9.04	0.072	1.91	2.50	2.59	3.41	0.113	97.2
HR	142	797B	2H	3	96 98	7.06	58.5	0.735	16.2	7.44	0.178	3.14	1.33	1.74	3.41	0.120	99.9
HR	143	797B	2H	3	103 105	6.46	58.8	0.707	15.7	8.53	0.112	2.94	1.14	1.86	3.38	0.117	99.7
HR	144	797B	2H	3	108 110	5.49	61.4	0.763	16.8	5.80	0.093	3.18	1.25	1.88	3.50	0.125	100.3
HR	145	797B	2H	3	116 117												
HR	146	797B	2H	3	126 128	5.06	61.7	0.780	16.5	5.76	0.086	3.13	1.21	1.92	3.49	0.123	99.7
HR	147	797B	2H	3	131 133	5.31	61.1	0.761	16.6	6.37	0.086	3.22	1.18	1.82	3.52	0.124	100.1
HR	148	797B	2H	3	138 140	6.83	60.4	0.746	16.2	6.19	0.070	3.15	1.23	1.79	3.38	0.121	100.0
HR	149	797B	2H	3	145 147	6.02	60.7	0.748	16.6	6.26	0.090	3.21	1.17	1.76	3.46	0.119	100.2
HR	150	797B	2H	4	2 4	8.78	57.3	0.671	15.6	7.70	0.073	3.11	1.10	1.72	3.24	0.140	99.5
HR	151	797B	2H	4	9 11	5.78	59.4	0.737	16.4	6.96	0.072	3.28	1.17	1.76	3.55	0.116	99.2
HR	152	797B	2H	4	16 18	6.42	58.8	0.708	15.9	7.62	0.075	3.25	1.17	1.76	3.43	0.121	99.3
HR	153	797B	2H	4	23 25	6.70	58.6	0.731	16.2	7.56	0.071	3.25	1.14	1.71	3.46	0.124	99.6
HR	154	797B	2H	4	32 34	5.49	60.0	0.759	16.5	6.50	0.083	3.28	1.26	1.79	3.52	0.125	99.2
HR	155	797B	2H	4	37 39	5.71	59.3	0.752	16.7	6.75	0.079	3.23	1.21	1.75	3.47	0.119	99.1
HR	156	797B	2H	4	46 47												
HR	157	797B	2H	4	51 53	7.27	58.0	0.722	16.1	7.42	0.076	3.12	1.13	1.69	3.39	0.129	99.0
HR	158	797B	2H	4	58 60	11.76	52.2	0.664	15.3	10.68	0.054	2.44	0.87	1.54	3.04	0.121	98.6
HR	159	797B	2H	4	65 67	5.61	59.8	0.747	16.8	6.17	0.084	3.25	1.33	1.77	3.52	0.165	99.3
HR	160	797B	2H	4	71 73	6.31	58.7	0.714	15.9	7.45	0.130	3.28	1.24	1.73	3.51	0.131	99.1
HR	161	797B	2H	4	79 81	7.16	58.0	0.731	16.6	6.84	0.078	3.13	1.17	1.74	3.50	0.123	99.1
HR	162	797B	2H	4	86 88	8.38	55.2	0.689	15.5	6.57	1.717	3.27	2.49	1.63	3.35	0.154	99.0
HR	163	797B	2H	4	93 95	7.62	56.8	0.701	16.1	6.76	0.358	3.33	1.81	1.67	3.47	0.125	98.8
HR	164	797B	2H	4	99 101	6.26	58.5	0.726	16.5	7.19	0.123	3.27	1.10	1.69	3.53	0.117	99.0
HR	165	797B	2H	4	107 109	6.27	58.5	0.748	17.0	6.40	0.123	3.30	1.14	1.71	3.58	0.119	98.8
HR	166	797B	2H	4	114 116	5.70	59.0	0.760	17.3	6.22	0.105	3.25	1.08	1.78	3.53	0.117	98.8
HR	167	797B	2H	4	121 123	7.10	55.1	0.698	15.5	10.78	0.089	2.94	0.99	1.64	3.31	0.111	98.2
HR	168	797B	2H	4	128 130	6.39	58.9	0.722	16.4	7.19	0.085	3.17	1.08	1.77	3.39	0.116	99.2
HR	169	797B	2H	4	132 134	8.07	58.1	0.740	16.5	5.90	0.080	3.09	1.15	1.87	3.32	0.120	98.9
HR	170	797B	2H	4	142 144	11.24	55.9	0.666	15.4	7.77	0.059	2.35	0.88	1.73	2.97	0.121	99.0

Table 2 (*continued*)

Type	No	Hole	Core	Sec	Interval		L.O.I.	SiO2	TiO2	Al2O3	Fe2O3	MnO	MgO	CaO	Na2O	K2O	P2O5	Total
HR	171	797B	2H	5	0	2	12.37	53.5	0.667	15.8	8.51	0.053	2.36	0.83	1.61	2.97	0.119	98.7
HR	172	797B	2H	5	7	9	6.05	59.3	0.751	17.1	5.82	0.109	3.34	1.23	1.77	3.50	0.122	99.0
HR	173	797B	2H	5	16	18	5.53	58.8	0.753	17.1	6.28	0.083	3.35	1.16	1.78	3.54	0.113	98.5
HR	174	797B	2H	5	21	23	5.39	58.7	0.749	17.0	6.99	0.081	3.37	1.14	1.70	3.52	0.113	98.8
HR	175	797B	2H	5	29	31	11.22	55.7	0.658	15.9	6.37	0.093	2.76	1.09	1.85	2.99	0.154	98.8
HR	176	797B	2H	5	35	37	6.63	58.9	0.721	17.1	6.23	0.092	3.09	1.08	1.86	3.35	0.114	99.1
HR	177	797B	2H	5	41	43	5.64	59.2	0.764	17.4	6.32	0.103	3.32	1.14	1.80	3.50	0.111	99.3
HR	178	797B	2H	5	49	51	6.88	58.3	0.687	16.6	6.45	0.117	2.94	1.06	1.91	3.26	0.110	98.3
HR	179	797B	2H	5	56	58	6.77	59.6	0.684	17.0	6.28	0.091	2.86	0.98	1.84	3.15	0.104	99.4
HR	180	797B	2H	5	62	64	6.71	59.9	0.696	17.3	5.83	0.077	2.78	1.02	1.89	3.18	0.114	99.5
LR	1	797B	1H	1	13	15	6.70	60.1	0.645	16.5	6.03	0.814	2.55	0.96	2.29	3.01	0.165	99.8
LR	2	797B	1H	1	44	46	7.50	57.7	0.627	15.3	9.17	0.625	2.73	1.01	2.14	2.85	0.265	99.9
LR	3	797B	1H	1	74	76	9.15	57.7	0.627	16.5	6.50	0.153	2.57	1.13	2.22	2.91	0.154	99.7
LR	4	797B	1H	1	134	136	9.00	52.9	0.652	14.4	7.39	0.110	2.71	5.25	1.79	2.82	0.132	97.1
LR	5	797B	1H	2	13	15	8.33	55.1	0.693	14.7	7.07	0.078	2.79	4.49	2.04	2.89	0.132	98.4
LR	6	797B	1H	2	44	46	8.78	54.3	0.679	15.3	8.02	0.060	2.90	3.44	1.88	3.02	0.125	98.5
LR	7	797B	1H	2	74	76	5.96	60.0	0.749	17.2	5.91	0.064	3.15	1.26	2.07	3.39	0.128	99.9
LR	8	797B	1H	2	104	106	6.68	58.6	0.693	15.9	7.93	0.064	3.28	1.26	1.91	3.32	0.142	99.8
LR	9	797B	1H	3	13	15	5.69	60.2	0.742	17.2	6.15	0.064	3.26	1.28	2.22	3.38	0.133	100.3
LR	10	797B	1H	3	44	46	7.68	58.6	0.705	16.5	6.64	0.067	3.08	1.21	2.05	3.23	0.138	99.9
LR	11	797B	1H	3	74	76	5.35	60.8	0.762	17.0	6.10	0.117	3.25	1.30	2.02	3.43	0.132	100.2
LR	12	797B	1H	3	104	106	19.04	51.6	0.646	14.7	5.13	0.083	2.73	1.08	1.86	2.92	0.113	99.9
LR	13	797B	1H	3	134	136	13.02	52.5	0.661	15.4	8.85	0.064	2.67	1.68	1.88	2.82	0.131	99.7
LR	14	797B	1H	4	13	15	15.16	52.5	0.637	15.0	7.88	0.059	2.60	1.12	1.91	2.71	0.134	99.7
LR	15	797B	1H	4	44	46	8.60	58.2	0.693	16.7	6.52	0.072	3.02	1.12	1.77	3.03	0.136	99.9
LR	16	797B	1H	4	71	73	12.13	55.1	0.586	14.8	8.49	0.084	2.78	1.02	1.84	2.70	0.136	99.7
LR	17	797B	1H	4	104	106	15.11	52.5	0.643	14.7	5.57	0.079	2.90	3.91	1.74	2.86	0.110	100.1
LR	18	797B	2H	1	14	16	6.82	58.7	0.727	17.0	6.68	0.089	3.15	1.20	2.14	3.27	0.124	99.9
LR	19	797B	2H	1	44	46	8.30	57.9	0.669	17.0	6.26	0.116	2.93	1.07	2.07	3.03	0.116	99.5
LR	20	797B	2H	1	102	104	14.58	43.0	0.461	10.9	6.96	0.089	1.98	11.70	1.57	2.01	0.108	93.4
LR	21	797B	2H	1	134	136	7.42	57.5	0.664	15.6	8.59	0.303	3.17	0.95	1.92	3.07	0.108	99.4
LR	22	797B	2H	2	14	16	6.33	60.7	0.643	16.3	6.29	0.455	2.95	0.98	2.09	3.15	0.106	100.0
LR	23	797B	2H	2	102	104	5.70	60.1	0.750	17.1	5.91	0.332	3.27	1.21	1.88	3.43	0.128	99.8
LR	24	797B	2H	2	134	136	10.28	56.2	0.671	15.1	7.32	0.131	2.63	1.38	2.42	3.20	0.120	99.5
LR	25	797B	2H	2	44	46	6.96	60.7	0.622	16.3	5.79	0.367	2.87	1.00	2.02	3.03	0.109	99.8
LR	26	797B	2H	2	74	76	5.84	60.2	0.670	17.4	6.81	0.136	2.87	0.88	2.23	3.10	0.108	100.2
LR	27	797B	2H	3	14	16	5.88	59.8	0.747	16.8	6.36	0.242	3.21	1.29	1.92	3.44	0.130	99.8
LR	28	797B	2H	3	44	46	5.13	60.9	0.753	17.0	6.05	0.125	3.25	1.12	1.86	3.55	0.128	99.8
LR	29	797B	2H	3	74	76	11.01	52.3	0.668	14.9	8.48	0.103	2.84	3.30	1.59	2.91	0.121	98.2
LR	30	797B	2H	3	102	104	6.59	59.4	0.744	16.0	7.12	0.100	3.06	1.40	1.86	3.26	0.124	99.6
LR	31	797B	2H	3	134	136	5.38	60.8	0.757	16.7	6.33	0.088	3.22	1.18	1.83	3.46	0.123	99.9
LR	32	797B	2H	4	14	16	6.16	59.7	0.739	16.8	6.51	0.080	3.21	1.19	1.78	3.42	0.125	99.8
LR	33	797B	2H	4	44	46	7.14	59.0	0.709	16.5	6.95	0.084	3.23	1.15	1.72	3.35	0.122	100.0
LR	34	797B	2H	4	74	76	6.37	59.2	0.709	16.0	7.64	0.084	3.31	1.21	1.67	3.39	0.126	99.7
LR	35	797B	2H	4	102	104	6.40	59.0	0.734	16.7	6.82	0.136	3.36	1.16	1.73	3.49	0.118	99.7
LR	36	797B	2H	4	134	136	7.65	59.6	0.719	15.8	6.39	0.085	2.90	1.31	1.93	3.15	0.127	99.7
LR	37	797B	2H	5	44	46	6.19	59.2	0.707	16.8	7.00	0.284	3.21	1.12	1.85	3.23	0.113	99.7
LR	38	797B	2H	5	74	76	6.54	60.4	0.663	17.1	5.71	0.072	2.77	0.96	1.91	3.16	0.107	99.4
LR	39	797B	2H	5	102	104	6.55	58.9	0.709	16.4	6.97	0.146	3.09	1.09	1.83	3.32	0.131	99.1
LR	40	797B	2H	5	134	136	6.08	61.0	0.712	16.9	5.62	0.087	2.87	0.94	1.89	3.28	0.107	99.5
LRA	1	797A	1H	1	14	16	6.09	60.6	0.732	17.2	6.50	0.068	3.18	1.30	1.99	3.50	0.133	101.3
LRA	5	797A	1H	1	134	136	5.57	59.8	0.744	16.7	6.51	0.092	3.20	1.31	1.82	3.49	0.125	99.3
LRA	8	797A	1H	2	74	76	9.53	57.6	0.674	15.3	5.75	0.071	2.85	2.09	1.85	3.11	0.134	99.0
LRA	16	797A	1H	4	14	16	7.01	59.7	0.669	16.5	5.63	0.225	3.00	1.01	1.86	3.22	0.111	98.9
LRA	19	797A	1H	4	104	106	6.09	59.2	0.670	17.3	6.87	0.181	2.87	0.93	1.92	3.17	0.112	99.2
LRA	20	797A	1H	4	134	136	5.99	59.6	0.739	17.2	5.99	0.193	3.28	1.21	1.78	3.51	0.126	99.6
LRA	23	797A	1H	5	74	76	9.05	55.4	0.682	15.5	8.27	0.125	3.00	1.28	2.04	3.22	0.126	98.8
LRA	24	797A	1H	5	104	106	8.48	56.1	0.666	15.9	6.49	0.093	2.95	2.29	2.31	3.39	0.123	98.7
LRA	30	797A	1H	6	134	136	5.96	59.2	0.732	16.7	7.16	0.095	3.27	1.05	1.77	3.54	0.121	99.7
LRA	32	797A	1H	7	44	46	8.82	55.7	0.687	15.9	8.75	0.097	2.97	1.10	1.70	3.20	0.115	99.1
					Max		19.04	67.5	0.780	17.8	11.45	5.014	7.15	17.31	5.77	4.94	2.251	
					Min		3.27	41.5	0.390	10.9	4.36	0.048	1.23	0.83	1.23	2.01	0.076	
					Average		7.74	57.9	0.680	16.1	6.83	0.247	2.94	1.70	1.87	3.24	0.136	
					Std. Dev.		2.55	3.4	0.069	1.0	1.18	0.629	0.45	1.76	0.35	0.30	0.146	

Table 3 Biogenic silica ($bioSiO_2$), organic carbon (Org-C), carbonate carbon (Carb-C), GRAPE density, dry bulk density (DBD), and content of detritus (Detritus%) of all analyzed samples from ODP Site 797.

Type	No	Hole	Core	Sec	Interval		bioSiO2	Org-C	Carb-C	GRAPE	DBD(g/cm3)	Detritus%
HR	1	797A	1H	1	23	25	10	0.47	0.13	1.42	0.53	83
HR	2	797A	1H	2	86	88	15	4.01	0.18	1.32	0.38	71
HR	3	797A	1H	2	93	95	12	1.87	0.28	1.30	0.35	78
HR	4	797A	1H	2	130	132	12	2.77	0.13	1.37	0.45	77
HR	5	797A	1H	2	137	139	14	3.67	1.30	1.38	0.46	66
HR	6	797A	1H	2	144	146	14	1.84	0.07	1.35	0.42	78
HR	7	797A	1H	3	1	3	14	1.41	0.07	1.36	0.44	78
HR	8	797A	1H	3	8	10	13	1.41	0.05	1.39	0.49	78
HR	9	797A	1H	3	18	20	14	1.40	0.07	1.36	0.45	78
HR	10	797A	1H	3	22	24	13	1.13	0.06	1.31	0.37	80
HR	11	797A	1H	3	29	31	11	1.24	0.09	1.32	0.37	82
HR	12	797A	1H	3	36	38	13	0.73	0.10	1.36	0.44	80
HR	13	797A	1H	3	71	73	10	1.30	0.08	1.36	0.44	82
HR	14	797A	1H	3	98	100	11	4.20	0.31	1.35	0.43	73
HR	15	797A	1H	3	108	110	8	0.62	0.12	1.44	0.56	85
HR	16	797B	1H	1	17	19	14	0.72	0.10	1.32	0.38	78
HR	17	797B	1H	1	23	25	14	0.66	0.08	1.26	0.29	79
HR	18	797B	1H	1	31	33	15	0.63	0.06	1.24	0.26	78
HR	19	797B	1H	1	38	40	11	0.53	0.07	1.24	0.26	81
HR	20	797B	1H	1	45	47	13	0.97	0.11	1.26	0.30	78
HR	21	797B	1H	1	54	56	13	2.33	0.09	1.26	0.29	77
HR	22	797B	1H	1	59	61	12	2.37	0.11	1.23	0.25	78
HR	23	797B	1H	1	66	68	12	1.28	0.07	1.22	0.22	81
HR	24	797B	1H	1	73	75	15	2.02	0.10	1.28	0.33	75
HR	25	797B	1H	1	80	82	10			1.29	0.33	
HR	26	797B	1H	1	87	89	10	2.22	0.15	1.34	0.41	80
HR	27	797B	1H	1	96	98	8	4.72	0.79	1.38	0.48	73
HR	28	797B	1H	1	101	103	5	0.97	0.91	1.38	0.47	81
HR	29	797B	1H	1	108	110	5	0.52	3.55	1.36	0.44	61
HR	30	797B	1H	1	117	119	5	0.53	0.93	1.38	0.47	82
HR	31	797B	1H	1	121	123	4	0.50	0.25	1.31	0.37	89
HR	32	797B	1H	1	131	133	5	0.50	0.08	1.47	0.61	89
HR	33	797B	1H	1	141	143	5	1.39	0.95	1.43	0.55	81
HR	34	797B	1H	1	146	148	5	1.26	1.08	1.45	0.58	81
HR	35	797B	1H	2	0	2	4	1.16	1.00	1.45	0.57	83
HR	36	797B	1H	2	6	8	4	1.20	0.75	1.44	0.56	84
HR	37	797B	1H	2	15	17	4	1.24	0.79	1.46	0.60	84
HR	38	797B	1H	2	21	23	4	1.27	0.73	1.46	0.59	83
HR	39	797B	1H	2	29	31	4	1.11	0.78	1.49	0.63	83
HR	40	797B	1H	2	35	37	3	0.81	0.61	1.57	0.75	86
HR	41	797B	1H	2	40	42	4	1.12	0.48	1.51	0.66	85
HR	42	797B	1H	2	49	51	3	0.95	0.24	1.53	0.69	87
HR	43	797B	1H	2	56	58	4	1.13	0.44	1.51	0.66	86
HR	44	797B	1H	2	66	68	5	1.49	0.36	1.49	0.63	84
HR	45	797B	1H	2	70	72	4	1.72	0.23	1.49	0.64	86
HR	46	797B	1H	2	79	81	4	0.32	0.14	1.48	0.62	89
HR	47	797B	1H	2	84	86	11	0.33	0.07	1.56	0.74	84
HR	48	797B	1H	2	91	93	4	1.04	0.14	1.55	0.73	90
HR	49	797B	1H	2	100	102	19	1.66	0.16	1.44	0.55	72
HR	50	797B	1H	2	106	108	4	1.66	0.19	1.33	0.39	86
HR	51	797B	1H	2	112	114	3	1.19	0.19	1.44	0.56	88
HR	52	797B	1H	2	119	121	4	0.49	0.19			89
HR	53	797B	1H	2	127	129	4	1.16	0.19			88
HR	54	797B	1H	2	132	134	4	0.55	0.18			85
HR	55	797B	1H	2	138	140	4	0.37	0.19			89
HR	56	797B	1H	3	0	2	6	0.62	0.13			87
HR	57	797B	1H	3	7	9	7	1.67	0.14	1.36	0.44	85
HR	58	797B	1H	3	21	23	7	1.30	0.13	1.38	0.47	85
HR	59	797B	1H	3	25	27	5	3.27	0.15	1.42	0.53	84

Table 3 (*continued*)

Type	No	Hole	Core	Sec	Interval		bioSiO2	Org-C	Carb-C	GRAPE	DBD(g/cm3)	Detritus%
HR	60	797B	1H	3	35	37	7	0.35	0.16	1.51	0.67	87
HR	61	797B	1H	3	40	42	4	0.42	0.14	1.44	0.56	90
HR	62	797B	1H	3	49	51	6	1.83	0.24	1.43	0.54	85
HR	63	797B	1H	3	56	58	5	0.84	0.16	1.42	0.53	87
HR	64	797B	1H	3	63	64	6			1.39	0.48	
HR	65	797B	1H	3	70	72	4	0.36	0.14	1.50	0.66	90
HR	66	797B	1H	3	78	80	5	0.32	0.22	1.50	0.65	88
HR	67	797B	1H	3	84	86	4	0.90	0.14	1.47	0.60	89
HR	68	797B	1H	3	91	93	4	0.34	0.15	1.49	0.63	90
HR	69	797B	1H	3	97	99	5	0.66	0.13	1.49	0.63	87
HR	70	797B	1H	3	105	107	4	0.39	0.17	1.50	0.65	92
HR	71	797B	1H	3	112	114	4	0.30	0.17	1.54	0.70	90
HR	72	797B	1H	3	120	121	4			1.42	0.53	
HR	73	797B	1H	3	126	128	5	0.33	0.13	1.46	0.59	89
HR	74	797B	1H	3	131	133	5	3.17	0.11	1.52	0.69	83
HR	75	797B	1H	3	140	142	4	0.71	0.18	1.42	0.53	89
HR	76	797B	1H	3	147	149	4	0.28	0.28	1.50	0.64	89
HR	77	797B	1H	4	4	6	5	0.34	0.14	1.46	0.59	88
HR	78	797B	1H	4	11	13	7	3.25	0.09	1.40	0.50	82
HR	79	797B	1H	4	18	20	7	4.16	0.27	1.42	0.53	77
HR	80	797B	1H	4	24	26	5	0.38	0.15	1.44	0.56	89
HR	81	797B	1H	4	32	34	7	0.49	0.11	1.35	0.43	87
HR	82	797B	1H	4	39	41	6	3.06	0.01	1.33	0.40	83
HR	83	797B	1H	4	49	51	8	2.37	0.00	1.37	0.46	83
HR	84	797B	1H	4	53	55	7	2.30	0.28	1.44	0.56	81
HR	85	797B	1H	4	60	62	7	2.18	0.18	1.43	0.55	82
HR	86	797B	1H	4	67	69	10	2.78	0.19	1.31	0.37	78
HR	87	797B	1H	4	88	90	7	0.39	0.34	1.41	0.52	85
HR	88	797B	1H	4	94	96	7	0.31	0.31	1.46	0.59	86
HR	89	797B	1H	4	102	104	6	0.41	0.53	1.46	0.59	85
HR	90	797B	1H	4	109	111	7	0.41	0.19	1.42	0.53	86
HR	91	797B	2H	1	17	19	7	1.47	0.08	1.03		85
HR	92	797B	2H	1	24	26	9	1.01	0.05	1.28		84
HR	93	797B	2H	1	32	34	7	1.72	0.05	1.42	0.53	85
HR	94	797B	2H	1	39	41	5	1.70	0.12	1.35	0.42	86
HR	95	797B	2H	1	53	55	7	0.44	0.14	1.47	0.61	
HR	96	797B	2H	1	60	62	7	0.59	0.10	1.43	0.54	86
HR	97	797B	2H	1	67	69	10	3.72	0.15	1.36	0.44	78
HR	98	797B	2H	1	88	90	9	0.41	0.09	1.42	0.54	85
HR	99	797B	2H	1	95	97	9	2.04	0.10	1.40	0.50	79
HR	100	797B	2H	1	104	106	8	5.01	2.30	1.44	0.56	64
HR	101	797B	2H	1	109	111	9	1.43	0.47	1.53	0.69	81
HR	102	797B	2H	1	115	117	8	2.04	1.53	1.45	0.57	73
HR	103	797B	2H	1	123	125	9	1.08	0.34	1.43	0.55	81
HR	104	797B	2H	1	130	132	10	0.89	0.08	1.43	0.55	83
HR	105	797B	2H	1	137	139	8	1.05	0.10	1.36	0.44	84
HR	106	797B	2H	1	144	146	8	0.52	0.13	1.36	0.44	77
HR	107	797B	2H	2	1	3	9	0.43	0.15	1.39	0.48	84
HR	108	797B	2H	2	8	10	11	0.42	0.11	1.41	0.52	82
HR	109	797B	2H	2	17	19	14	0.38	0.19	1.34	0.41	79
HR	110	797B	2H	2	22	24	15	0.47	0.81	1.31	0.36	73
HR	111	797B	2H	2	30	32	12	0.34	0.00	1.39	0.48	84
HR	112	797B	2H	2	36	38	13	0.75	0.15	1.33	0.40	80
HR	113	797B	2H	2	42	44	13	0.66	1.03	1.34	0.41	72
HR	114	797B	2H	2	50	52	14	0.57	0.92	1.35	0.43	73
HR	115	797B	2H	2	57	59	10	0.56	0.00	1.37	0.45	84
HR	116	797B	2H	2	64	66	10	0.45	0.09	1.35	0.43	84
HR	117	797B	2H	2	71	73	9	0.40	0.02	1.37	0.46	85
HR	118	797B	2H	2	79	81	9	0.52	0.03	1.43	0.54	85

Table 3 (*continued*)

Type	No	Hole	Core	Sec	Interval		bioSiO2	Org-C	Carb-C	GRAPE	DBD(g/cm3)	Detritus%
HR	119	797B	2H	2	84	86	9	0.44	0.01	1.35	0.43	85
HR	120	797B	2H	2	92	94	5	0.57	0.31	1.47	0.61	87
HR	121	797B	2H	2	98	100	5	0.46	0.24	1.45	0.57	88
HR	122	797B	2H	2	106	108	5	0.35	0.14	1.54	0.70	89
HR	123	797B	2H	2	113	115	7	0.30	0.14	1.48	0.62	87
HR	124	797B	2H	2	121	123	5	0.27	0.06	1.48	0.62	89
HR	125	797B	2H	2	127	129	6	0.35	0.09	1.49	0.63	88
HR	126	797B	2H	2	136	138	5	1.23	0.06	1.56	0.74	87
HR	127	797B	2H	2	141	143	5	1.19	0.09	1.47	0.61	88
HR	128	797B	2H	2	148	150	4	1.02	0.04	1.63	0.85	89
HR	129	797B	2H	3	5	7	5	0.41	0.14	1.56	0.74	89
HR	130	797B	2H	3	11	13	5	0.44	0.14	1.53	0.69	88
HR	131	797B	2H	3	19	21	5	0.41	0.11	1.52	0.68	89
HR	132	797B	2H	3	24	26	4	0.43	0.00	1.56	0.75	90
HR	133	797B	2H	3	33	35	2	0.32	0.09	1.59	0.78	92
HR	134	797B	2H	3	40	42	3	0.30	0.02	1.57	0.75	92
HR	135	797B	2H	3	48	50	3	0.95	0.00	1.55	0.72	91
HR	136	797B	2H	3	54	56	3	1.06	0.05	1.60	0.79	87
HR	137	797B	2H	3	64	66	2	1.15	0.07	1.56	0.74	89
HR	138	797B	2H	3	71	73	2	1.11	0.08	1.59	0.78	89
HR	139	797B	2H	3	79	81	2	1.24	0.00	1.53	0.69	90
HR	140	797B	2H	3	82	84	3	1.22	0.14	1.57	0.75	89
HR	141	797B	2H	3	92	94	3	1.85	0.00	1.50	0.65	88
HR	142	797B	2H	3	96	98	2	0.87	0.13	1.64	0.85	90
HR	143	797B	2H	3	103	105	5	0.62	0.07	1.53	0.70	88
HR	144	797B	2H	3	108	110	2	0.51	0.10	1.54	0.71	92
HR	145	797B	2H	3	116	117	2			1.53	0.69	
HR	146	797B	2H	3	126	128	3	0.33	0.14	1.59	0.78	92
HR	147	797B	2H	3	131	133	2	0.36	0.07	1.55	0.72	92
HR	148	797B	2H	3	138	140	3	1.23	0.09	1.58	0.76	89
HR	149	797B	2H	3	145	147	3	0.75	0.11	1.49	0.64	91
HR	150	797B	2H	4	2	4	3	2.38	0.05	1.39	0.48	88
HR	151	797B	2H	4	9	11	3	0.56	0.10	1.53	0.70	91
HR	152	797B	2H	4	16	18	3	0.92	0.11	1.46	0.59	90
HR	153	797B	2H	4	23	25	4	1.15	0.08	1.44	0.56	89
HR	154	797B	2H	4	32	34	3	0.47	0.13	1.52	0.68	91
HR	155	797B	2H	4	37	39	2	0.41	0.09	1.46	0.58	91
HR	156	797B	2H	4	46	47	3			1.50	0.65	
HR	157	797B	2H	4	51	53	3	1.46	0.03	1.48	0.61	90
HR	158	797B	2H	4	58	60	3	2.96	0.00	1.52	0.67	85
HR	159	797B	2H	4	65	67	3	0.56	0.12	1.53	0.69	91
HR	160	797B	2H	4	71	73	3	0.88	0.10	1.54	0.70	90
HR	161	797B	2H	4	79	81	3	1.34	0.10	1.52	0.68	90
HR	162	797B	2H	4	86	88	3	1.22	0.65	1.50	0.65	85
HR	163	797B	2H	4	93	95	3	1.39	0.26	1.46	0.59	88
HR	164	797B	2H	4	99	101	4	0.88	0.04	1.48	0.61	90
HR	165	797B	2H	4	107	109	3	0.87	0.04	1.46	0.58	91
HR	166	797B	2H	4	114	116	3	0.55	0.00	1.51	0.67	91
HR	167	797B	2H	4	121	123	6	0.46	0.00	1.48	0.62	87
HR	168	797B	2H	4	128	130	4	0.91	0.00	1.57	0.76	90
HR	169	797B	2H	4	132	134	3	1.91	0.04	1.45	0.58	88
HR	170	797B	2H	4	142	144	4	3.09	0.00	1.45	0.58	84
HR	171	797B	2H	5	0	2	4	3.51	0.01	1.46	0.59	83
HR	172	797B	2H	5	7	9	3	0.69	0.08	1.54	0.71	90
HR	173	797B	2H	5	16	18	3	0.40	0.08	1.52	0.68	91
HR	174	797B	2H	5	21	23	3	0.38	0.07	1.46	0.58	91
HR	175	797B	2H	5	29	31	6	3.94	0.01	1.38	0.48	83
HR	176	797B	2H	5	35	37	4	1.13	0.02	1.45	0.58	90
HR	177	797B	2H	5	41	43	4	0.46	0.02	1.53	0.69	91

Table 3 (*continued*)

Type	No	Hole	Core	Sec	Interval		bioSiO2	Org-C	Carb-C	GRAPE	DBD(g/cm3)	Detritus%
HR	178	797B	2H	5	49	51	5	1.32	0.04	1.38	0.47	88
HR	179	797B	2H	5	56	58	6	1.24	0.00	1.37	0.46	87
HR	180	797B	2H	5	62	64	6	1.22	0.00	1.41	0.51	87
LR	1	797B	1H	1	13	15	12	0.78	0.07	1.34	0.40	81
LR	2	797B	1H	1	44	46	14	1.10	0.08	1.26	0.30	78
LR	3	797B	1H	1	74	76	10	2.08	0.09	1.28	0.33	81
LR	4	797B	1H	1	134	136	4	1.46	1.10	1.43	0.55	82
LR	5	797B	1H	2	13	15	3	1.12	0.89	1.52	0.68	84
LR	6	797B	1H	2	44	46	4	1.06	0.66	1.57	0.76	84
LR	7	797B	1H	2	74	76	4	0.53	0.18	1.48	0.62	89
LR	8	797B	1H	2	104	106	5	0.96	0.18	1.44	0.55	87
LR	9	797B	1H	3	13	15	4	0.49	0.19	1.44	0.57	89
LR	10	797B	1H	3	44	46	5	1.60	0.15	1.41	0.52	87
LR	11	797B	1H	3	74	76	4	0.35	0.17	1.57	0.76	90
LR	12	797B	1H	3	104	106	4	0.51	0.16	1.46	0.59	76
LR	13	797B	1H	3	134	136	5	3.37	0.25	1.49	0.64	80
LR	14	797B	1H	4	13	15	7	4.32	0.12	1.40	0.50	77
LR	15	797B	1H	4	44	46	7	1.82	0.09	1.38	0.47	84
LR	16	797B	1H	4	71	73	9	3.43	0.10	1.33	0.40	79
LR	17	797B	1H	4	104	106	5	0.38	0.77	1.40	0.49	76
LR	18	797B	2H	1	14	16	5	0.76	0.14	0.90		87
LR	19	797B	2H	1	44	46	7	1.75	0.08	1.42	0.53	84
LR	20	797B	2H	1	102	104	11	4.08	2.38	1.44	0.56	64
LR	21	797B	2H	1	134	136	8	0.81	0.03	1.42	0.52	84
LR	22	797B	2H	2	14	16	12	0.42	0.10	1.38	0.47	82
LR	23	797B	2H	2	102	104	4	0.38	0.20	1.47	0.61	89
LR	24	797B	2H	2	134	136	5	1.47	0.20	1.50	0.64	84
LR	25	797B	2H	2	44	46	13	0.84	0.08	1.37	0.46	80
LR	26	797B	2H	2	74	76	7	0.40	0.00	1.33	0.40	87
LR	27	797B	2H	3	14	16	4	0.49	0.18	1.53	0.70	89
LR	28	797B	2H	3	44	46	4	0.28	0.13	1.60	0.80	90
LR	29	797B	2H	3	74	76	3	1.31	0.62	1.62	0.83	83
LR	30	797B	2H	3	102	104	3	0.66	0.19	1.53	0.70	89
LR	31	797B	2H	3	134	136	4	0.42	0.13	1.48	0.62	91
LR	32	797B	2H	4	14	16	4	0.73	0.11	1.49	0.64	90
LR	33	797B	2H	4	44	46	4	1.33	0.10	1.47	0.61	89
LR	34	797B	2H	4	74	76	4	0.76	0.15	1.55	0.72	89
LR	35	797B	2H	4	102	104	4	0.79	0.12	1.38	0.47	89
LR	36	797B	2H	4	134	136	5	1.43	0.14	1.52	0.69	87
LR	37	797B	2H	5	44	46	7	0.49	0.10	1.51	0.66	87
LR	38	797B	2H	5	74	76	9	0.95	0.00	1.44	0.56	85
LR	39	797B	2H	5	102	104	6	0.70	0.11	1.51	0.67	87
LR	40	797B	2H	5	134	136	8	0.79	0.00	1.46	0.59	86
LRA	1	797A	1H	1	14	16	3	0.67	0.12	1.27		90
LRA	5	797A	1H	1	134	136	3	0.33	0.02	1.52	0.67	91
LRA	8	797A	1H	2	74	76	6	2.29	0.35	1.42	0.53	83
LRA	16	797A	1H	4	14	16	9	0.91	0.08	1.39	0.49	83
LRA	19	797A	1H	4	104	106	6	0.40	0.00	1.40	0.51	88
LRA	20	797A	1H	4	134	136	3	0.39	0.13	1.46	0.59	90
LRA	23	797A	1H	5	74	76	4	1.21	0.00	1.54	0.71	87
LRA	24	797A	1H	5	104	106	4	1.14	0.34	1.47	0.60	86
LRA	30	797A	1H	6	134	136	3	0.50	0.04	1.57	0.75	91
LRA	32	797A	1H	7	44	46	3	1.43	0.10	1.51	0.66	87
					Max		19	5.01	3.55	1.64	0.85	92
					Min		2	0.27	0.00	0.90	0.22	61
					Average		6	1.17	0.23	1.44	0.56	85
					Std. Dev.		4	0.96	0.39	0.10	0.13	6

Table 4 Mineral composition of all analyzed samples from ODP Site 797. Total = total sum of mineral contents described + bioSiO_2 + Org-C. Detrital mineral total is sum of contents of smectite through detrital amorphous.

Type	No	Hole	Core	Sec	Interval	Smectite	Illiae	Chlorite + Kaolinite	Amphiboles	Quartz	Feldspars	Detrital Amorphous	Rhodochrosite	Calcite	Pyrite	Total	Detrital Mineral Total	Remarks
HR	1	797A	1H	1	23 25	18	16	3.5	0	18	5	23	0.0	0	0.8	94	82	
HR	2	797A	1H	2	86 88	21	14	3.2	0	9	3	25	0.0	0	2.0	96	75	
HR	3	797A	1H	2	93 95	20	19	4.1	2	12	4	12	0.0	0	1.6	88	73	
HR	4	797A	1H	2	130 132	22	17	3.7	0	12	4	24	0.0	0	0.6	98	82	
HR	5	797A	1H	2	137 139	17	16	3.5	2	12	4	15	0.0	10	3.6	100	68	
HR	6	797A	1H	2	144 146	19	18	3.8	0	13	6	19	0.0	0	1.5	96	79	
HR	7	797A	1H	3	1 3	22	17	4.0	2	14	5	17	0.0	0	0.9	98	82	
HR	8	797A	1H	3	8 10	19	16	3.5	0	12	4	29	0.0	0	2.3	99	82	
HR	9	797A	1H	3	18 20	21	17	4.1	0	14	4	27	0.0	0	0.7	103	88	
HR	10	797A	1H	3	22 24	18	16	3.6	0	15	5	24	0.0	0	0.5	96	82	
HR	11	797A	1H	3	29 31	19	16	3.4	0	15	4	27	0.0	0	0.8	98	84	
HR	12	797A	1H	3	36 38	20	15	3.4	0	16	4	28	0.0	0	0.8	101	87	
HR	13	797A	1H	3	71 73	20	15	3.5	2	16	5	31	0.0	0	0.0	104	92	
HR	14	797A	1H	3	98 100	16	14	3.2	0	11	3	38	0.0	0	6.2	106	85	Gypsum
HR	15	797A	1H	3	108 110	17	15	3.4	2	19	5	26	0.0	0	1.2	98	88	
HR	16	797B	1H	1	17 19	18	15	3.3	0	14	4	30	0.0	0	0.5	99	84	
HR	17	797B	1H	1	23 25	19	15	3.2	0	13	4	30	0.0	0	0.5	98	83	
HR	18	797B	1H	1	31 33	19	14	3.2	0	13	3	32	0.0	0	0.0	101	85	
HR	19	797B	1H	1	38 40	16	15	3.2	0	13	3	33	0.0	0	0.0	95	84	
HR	20	797B	1H	1	45 47	18	14	3.1	0	9	2	26	0.0	0	0.0	87	73	
HR	21	797B	1H	1	54 56	19	14	3.1	0	13	4	34	0.0	0	0.0	103	88	
HR	22	797B	1H	1	59 61	19	14	3.2	1	14	4	32	0.0	0	0.0	102	87	
HR	23	797B	1H	1	66 68	18	14	3.1	0	8	5	41	0.0	0	0.0	103	89	K-Feldspar
HR	24	797B	1H	1	73 75	19	14	3.2	0	12	3	33	0.0	0	0.0	102	85	
HR	25	797B	1H	1	80 82													
HR	26	797B	1H	1	87 89	20	14	3.3	0	12	3	33	0.0	0	0.8	99	86	
HR	27	797B	1H	1	96 98	19	15	3.3	0	12	3	42	0.0	6	0.7	114	95	
HR	28	797B	1H	1	101 103	16	15	3.3	0	15	4	32	0.0	7	0.5	100	86	
HR	29	797B	1H	1	108 110	17	15	3.3	2	10	3	14	0.0	34	0.0	102	63	
HR	30	797B	1H	1	117 119	17	15	3.2	2	16	4	29	0.0	9	0.0	99	85	
HR	31	797B	1H	1	121 123	19	15	3.5	0	18	5	26	0.0	0	0.5	92	87	Gypsum
HR	32	797B	1H	1	131 133	18	16	3.5	0	20	5	28	0.0	0	0.0	94	89	
HR	33	797B	1H	1	141 143	16	15	3.4	1	15	4	25	0.0	7	3.1	97	80	Gypsum
HR	34	797B	1H	1	146 148	17	16	3.5	2	17	5	29	0.0	8	3.8	106	89	Gypsum
HR	35	797B	1H	2	0 2	16	15	3.4	0	17	4	24	0.0	7	3.2	96	80	Gypsum
HR	36	797B	1H	2	6 8	18	15	3.5	2	15	5	27	0.0	4	4.5	99	85	Gypsum
HR	37	797B	1H	2	15 17	17	16	3.6	2	16	4	25	0.0	4	4.6	98	84	Gypsum
HR	38	797B	1H	2	21 23	17	15	3.4	1	16	4	25	0.0	5	5.3	97	82	Gypsum
HR	39	797B	1H	2	29 31	17	15	3.5	1	18	5	28	0.0	5	2.3	100	88	Gypsum
HR	40	797B	1H	2	35 37	17	16	3.5	2	17	5	27	0.0	3	4.6	99	87	Gypsum
HR	41	797B	1H	2	40 42	17	15	3.6	0	17	4	25	0.0	2	5.2	94	80	Gypsum
HR	42	797B	1H	2	49 51	16	15	3.4	2	17	4	28	0.0	0	5.1	94	85	Gypsum
HR	43	797B	1H	2	56 58	18	16	3.6	2	17	5	29	0.0	0	3.7	100	90	
HR	44	797B	1H	2	66 68	16	15	3.6	1	16	4	24	0.0	0	6.1	94	81	
HR	45	797B	1H	2	70 72	18	15	3.6	2	18	4	27	0.0	0	3.7	97	88	
HR	46	797B	1H	2	79 81	18	15	3.4	2	18	5	30	0.0	0	0.0	97	92	
HR	47	797B	1H	2	84 86	17	14	3.2	0	11	3	61	0.0	0	0.0	120	109	
HR	48	797B	1H	2	91 93	18	15	3.6	0	16	4	28	0.0	0	6.1	96	85	
HR	49	797B	1H	2	100 102	18	16	3.6	0	15	5	13	0.0	0	0.9	91	70	
HR	50	797B	1H	2	106 108	18	15	3.5	0	17	3	33	0.0	0	1.8	98	90	
HR	51	797B	1H	2	112 114	17	15	3.6	0	18	5	32	0.0	0	0.7	97	92	
HR	52	797B	1H	2	119 121	17	15	3.4	3	20	4	32	0.0	0	0.9	99	94	
HR	53	797B	1H	2	127 129	19	15	3.5	0	17	4	27	0.0	0	1.0	91	85	
HR	54	797B	1H	2	132 134	18	16	3.5	0	20	5	32	0.0	0	0.9	99	93	
HR	55	797B	1H	2	138 140	18	16	3.6	1	17	6	27	0.0	0	0.9	94	89	
HR	56	797B	1H	3	0 2	18	15	3.3	0	20	5	33	0.0	0	0.0	100	93	
HR	57	797B	1H	3	7 9	18	15	3.4	0	17	4	30	0.0	0	0.0	97	89	
HR	58	797B	1H	3	21 23	17	14	3.2	2	18	4	34	0.0	0	0.0	101	93	
HR	59	797B	1H	3	25 27	19	15	3.4	2	16	4	30	0.0	0	0.8	98	89	
HR	60	797B	1H	3	35 37	18	16	3.5	0	18	5	25	0.0	0	1.3	93	84	
HR	61	797B	1H	3	40 42	19	16	3.5	3	18	5	28	0.0	0	0.6	98	93	
HR	62	797B	1H	3	49 51	21	18	3.9	1	15	6	22	0.0	0	0.6	96	88	
HR	63	797B	1H	3	56 58	17	17	3.6	3	17	5	21	0.0	0	0.3	90	84	
HR	64	797B	1H	3	63 64													
HR	65	797B	1H	3	70 72	17	17	3.5	2	21	5	22	0.0	0	0.6	92	87	
HR	66	797B	1H	3	78 80	18	16	3.6	1	17	5	22	0.0	0	0.7	90	84	
HR	67	797B	1H	3	84 86	18	17	3.9	2	19	6	24	0.0	0	0.3	96	91	
HR	68	797B	1H	3	91 93	18	17	3.8	1	19	6	24	0.0	0	0.5	93	88	
HR	69	797B	1H	3	97 99	18	17	3.8	1	18	6	21	0.0	0	0.3	91	86	
HR	70	797B	1H	3	105 107	18	17	3.7	2	18	7	22	0.0	0	0.0	93	88	
HR	71	797B	1H	3	112 114	18	15	3.5	1	20	6	19	0.0	0	0.0	87	83	
HR	72	797B	1H	3	120 121													
HR	73	797B	1H	3	126 128	17	15	3.4	2	19	5	25	0.0	0	0.7	92	86	
HR	74	797B	1H	3	131 133	17	16	3.6	2	14	5	22	0.0	0	4.1	92	80	
HR	75	797B	1H	3	140 142	17	17	3.9	2	17	6	23	0.0	0	1.5	93	87	
HR	76	797B	1H	3	147 149	16	17	3.6	2	19	7	22	0.0	0	1.1	91	86	
HR	77	797B	1H	4	4 6	17	16	3.5	1	18	5	26	0.0	0	1.1	93	86	
HR	78	797B	1H	4	11 13	17	16	3.5	0	14	4	33	0.0	0	1.2	100	88	
HR	79	797B	1H	4	18 20	17	15	3.3	2	12	4	24	0.0	0	7.0	96	78	
HR	80	797B	1H	4	24 26	20	17	3.7	1	18	5	22	0.0	0	0.7	94	87	
HR	81	797B	1H	4	32 34	19	16	3.5	1	15	4	24	0.0	0	0.9	91	83	Anorthitic
HR	82	797B	1H	4	39 41	19	15	3.3	2	13	4	30	0.0	0	1.5	98	87	
HR	83	797B	1H	4	49 51	19	15	3.3	2	14	4	30	0.0	0	1.1	99	88	
HR	84	797B	1H	4	53 55	18	15	3.3	0	11	3	33	0.0	0	2.5	97	84	
HR	85	797B	1H	4	60 62	19	15	3.3	1	14	4	22	0.0	0	0.9	88	78	
HR	86	797B	1H	4	67 69	19	15	3.3	1	12	4	30	0.0	0	2.2	99	84	Anorthitic
HR	87	797B	1H	4	88 90	17	17	3.7	2	17	5	27	0.0	0	0.4	97	89	
HR	88	797B	1H	4	94 96	17	16	3.7	2	18	5	25	0.0	0	0.0	95	87	
HR	89	797B	1H	4	102 104	17	17	3.6	1	17	5	24	0.0	3	0.6	95	85	
HR	90	797B	1H	4	109 111	19	16	3.5	3	19	5	22	0.0	0	0.5	94	86	
HR	91	797B	2H	1	17 19	18	15	3.5	2	17	5	27	0.0	0	1.6	98	88	
HR	92	797B	2H	1	24 26	17	15	3.2	2	11	3	38	0.0	0	2.4	101	89	
HR	93	797B	2H	1	32 34	18	15	3.3	2	13	4	38	0.0	0	1.0	103	93	
HR	94	797B	2H	1	39 41	19	15	3.3	2	14	5	36	0.0	0	0.9	101	93	
HR	95	797B	2H	1	53 55	16	15	3.5	3	16	5	26	0.0	0	0.7	92	84	
HR	96	797B	2H	1	60 62	17	15	3.2	1	13	3	37	0.0	0	1.4	99	90	
HR	97	797B	2H	1	67 69	18	15	3.3	1	14	4	33	0.0	0	1.0	103	89	Anothitic
HR	98	797B	2H	1	88 90	18	15	3.4	0	15	4	24	0.0	0	0.8	91	81	Anothitic
HR	99	797B	2H	1	95 97	19	15	3.3	0	13	4	30	0.0	0	1.3	97	84	
HR	100	797B	2H	1	104 106	16	14	3.2	1	9	2	23	0.0	17	4.2	103	69	
HR	101	797B	2H	1	109 111	17	16	3.5	1	15	5	30	0.0	4	0.7	101	87	
HR	102	797B	2H	1	115 117	18	15	3.2	1	10	3	27	3.7	6	1.4	97	76	

Table 4 (*continued*)

Type	No	Hole	Core	Sec	Interval	Smectite	Illite	Chlorite + Kaolinite	Amphiboles	Quartz	Feldspars	Detrital Amorphous	Rhodochrosite	Calcite	Pyrite	Total	Detrital Mineral Total	Remarks
HR	103	797B	2H	1	123–125	18	15	3.3	1	13	4	25	2.0	0	1.2	93	79	Anorthitic
HR	104	797B	2H	1	130–132	19	16	3.4	2	13	4	32	0.0	0	0.5	100	89	
HR	105	797B	2H	1	137–139	20	15	3.2	1	13	6	30	0.0	0	1.8	98	87	Anorthitic
HR	106	797B	2H	1	144–146	18	16	3.4	1	15	4	30	0.0	0	0.0	97	88	
HR	107	797B	2H	2	1–3	19	15	3.3	2	14	5	28	0.0	0	0.0	96	87	
HR	108	797B	2H	2	8–10	19	15	3.4	0	13	4	26	0.0	0	0.5	93	81	
HR	109	797B	2H	2	17–19	20	15	3.2	1	11	4	29	0.0	0	0.6	97	82	
HR	110	797B	2H	2	22–24	17	14	3.1	1	7	7	23	6.2	0	0.0	95	73	K-Feldspar
HR	111	797B	2H	2	30–32	15	14	3.0	2	3	10	46	0.0	0	0.4	107	94	Anorthitic
HR	112	797B	2H	2	36–38	17	15	3.3	1	13	4	34	0.0	0	0.2	100	87	
HR	113	797B	2H	2	42–44	17	14	3.2	0	9	3	22	9.5	0	0.1	92	69	
HR	114	797B	2H	2	50–52	17	14	3.1	1	10	3	28	7.1	0	0.1	97	75	Anorthitic
HR	115	797B	2H	2	57–59	19	15	3.2	1	14	4	32	0.0	0	0.2	99	86	Anorthitic
HR	116	797B	2H	2	64–66	18	15	3.2	2	13	4	27	0.0	0	0.4	92	82	
HR	117	797B	2H	2	71–73	19	15	3.2	0	14	4	30	0.0	0	0.2	95	85	Anorthitic
HR	118	797B	2H	2	79–81	18	15	3.2	2	14	4	31	0.0	0	0.0	97	87	
HR	119	797B	2H	2	84–86	17	14	3.2	0	11	4	27	0.0	0	0.4	86	77	K-Feldspar
HR	120	797B	2H	2	92–94	19	15	3.4	1	18	4	26	3.5	0	0.0	96	87	
HR	121	797B	2H	2	98–100	18	16	3.7	0	17	5	31	2.6	0	0.3	99	91	
HR	122	797B	2H	2	106–108	20	16	3.5	2	18	5	17	0.0	0	0.3	86	81	
HR	123	797B	2H	2	113–115	19	15	3.5	0	17	4	25	0.0	0	0.4	93	85	
HR	124	797B	2H	2	121–123	18	15	3.5	2	18	5	24	0.0	0	0.5	92	86	
HR	125	797B	2H	2	127–129	18	16	3.5	2	17	5	28	0.0	0	0.5	97	90	
HR	126	797B	2H	2	136–138	17	16	3.5	2	17	5	25	0.0	0	2.2	94	85	
HR	127	797B	2H	2	141–143	18	16	3.7	0	18	5	24	0.0	0	2.6	94	85	
HR	128	797B	2H	2	148–150	18	15	3.6	1	19	5	24	0.0	0	2.1	94	87	
HR	129	797B	2H	3	5–7	19	15	3.5	1	18	5	26	0.0	0	0.8	94	88	
HR	130	797B	2H	3	11–13	17	15	3.4	1	20	5	27	0.0	0	1.0	95	88	
HR	131	797B	2H	3	19–21	16	16	3.5	1	20	6	28	0.0	0	0.0	97	91	
HR	132	797B	2H	3	24–26	17	15	3.4	2	17	4	24	0.0	0	0.7	89	84	
HR	133	797B	2H	3	33–35	19	16	3.5	2	19	5	30	0.0	0	0.0	97	94	
HR	134	797B	2H	3	40–42	18	15	3.4	2	20	5	28	0.0	0	0.2	95	92	
HR	135	797B	2H	3	48–50	17	16	3.5	1	18	5	37	0.0	0	1.4	102	97	Anorthitic
HR	136	797B	2H	3	54–56	17	16	3.7	2	14	4	26	0.0	0	6.3	94	83	Gypsum
HR	137	797B	2H	3	64–66	18	16	3.6	2	16	5	24	0.0	0	5.2	93	85	Gypsum
HR	138	797B	2H	3	71–73	17	17	3.6	2	17	5	28	0.0	0	4.4	96	89	Gypsum
HR	139	797B	2H	3	79–81	18	15	3.4	1	17	4	32	0.0	0	3.3	98	91	Gypsum
HR	140	797B	2H	3	82–84	17	15	3.4	1	17	5	33	0.0	0	2.2	98	91	Gypsum
HR	141	797B	2H	3	92–94	16	14	3.3	0	13	4	36	0.0	2	3.8	97	87	Gypsum Anorthitic
HR	142	797B	2H	3	96–98	18	15	3.5	1	19	5	27	0.0	0	2.5	94	88	
HR	143	797B	2H	3	103–105	18	15	3.4	2	17	5	21	0.0	0	2.8	89	81	
HR	144	797B	2H	3	108–110	18	15	3.3	1	20	5	28	0.0	0	0.2	93	90	
HR	145	797B	2H	3	116–117													
HR	146	797B	2H	3	126–128	17	15	3.4	2	21	5	24	0.0	0	0.3	91	88	
HR	147	797B	2H	3	131–133	16	15	3.3	2	20	6	29	0.0	0	0.7	94	91	
HR	148	797B	2H	3	138–140	18	16	3.5	1	20	4	27	0.0	0	0.7	94	89	
HR	149	797B	2H	3	145–147	15	15	3.5	2	19	5	28	0.0	0	0.0	92	89	
HR	150	797B	2H	4	2–4	18	15	3.4	0	14	4	33	0.0	0	0.5	93	87	
HR	151	797B	2H	4	9–11	18	15	3.4	1	18	5	29	0.0	0	0.5	93	89	
HR	152	797B	2H	4	16–18	18	15	3.4	1	18	5	27	0.0	0	0.5	91	87	
HR	153	797B	2H	4	23–25	18	15	3.4	1	16	4	27	0.0	0	0.8	91	85	
HR	154	797B	2H	4	32–34	17	15	3.5	2	18	5	27	0.0	0	0.1	91	87	
HR	155	797B	2H	4	37–39	18	15	3.4	0	20	4	29	0.0	0	0.6	93	89	
HR	156	797B	2H	4	46–47													
HR	157	797B	2H	4	51–53	18	16	3.5	1	17	4	31	0.0	0	1.5	97	91	
HR	158	797B	2H	4	58–60	17	15	3.3	1	14	4	25	0.0	0	6.7	91	78	
HR	159	797B	2H	4	65–67	17	16	3.6	3	20	6	34	0.0	0	0.2	102	99	
HR	160	797B	2H	4	71–73	18	15	3.5	2	19	4	26	0.0	0	0.7	93	88	
HR	161	797B	2H	4	79–81	18	15	3.3	1	17	4	33	0.0	0	1.4	96	91	
HR	162	797B	2H	4	86–88	17	15	3.3	2	16	4	28	4.5	0	0.6	94	85	Anorthitic
HR	163	797B	2H	4	93–95	19	15	3.4	1	17	4	32	0.0	0	0.6	96	91	
HR	164	797B	2H	4	99–101	18	15	3.3	2	17	4	27	0.0	0	1.2	92	87	
HR	165	797B	2H	4	107–109	17	15	3.3	1	17	4	32	0.0	0	0.0	94	90	
HR	166	797B	2H	4	114–116	17	15	3.2	1	14	4	32	0.0	0	0.7	90	86	
HR	167	797B	2H	4	121–123	18	15	3.3	2	14	4	19	0.0	0	4.8	87	75	
HR	168	797B	2H	4	128–130	18	15	3.3	1	17	4	25	0.0	0	1.1	90	84	
HR	169	797B	2H	4	132–134	18	15	3.3	2	17	5	27	0.0	0	0.8	93	87	Anorthitic
HR	170	797B	2H	4	142–144	17	15	3.4	1	15	5	34	0.0	0	3.8	102	91	
HR	171	797B	2H	5	0–2	17	15	3.3	0	14	2	35	0.0	0	4.4	98	86	
HR	172	797B	2H	5	7–9	18	16	3.7	1	18	5	24	0.0	0	0.3	90	86	
HR	173	797B	2H	5	16–18	18	16	3.6	1	17	5	24	0.0	0	1.1	88	84	
HR	174	797B	2H	5	21–23	19	15	3.5	2	16	4	22	0.0	0	0.8	87	82	
HR	175	797B	2H	5	29–31	18	15	3.4	1	14	4	31	0.0	0	0.9	98	87	
HR	176	797B	2H	5	35–37	19	16	3.6	2	15	4	28	0.0	0	0.7	94	88	
HR	177	797B	2H	5	41–43	18	15	3.4	1	18	4	23	0.0	0	1.0	87	82	
HR	178	797B	2H	5	49–51	19	15	3.3	1	15	4	35	0.0	0	0.2	100	93	Anorthitic
HR	179	797B	2H	5	56–58	19	15	3.2	2	14	4	37	0.0	0	0.5	102	93	
HR	180	797B	2H	5	62–64	19	14	3.2	1	13	4	36	0.0	0	0.7	98	90	
LR	1	797B	1H	1	13–15	19	15	3.3	1	12	4	29	0.0	0	0.6	97	83	
LR	2	797B	1H	1	44–46	20	14	3.2	2	12	3	35	0.0	0	0.5	106	90	
LR	3	797B	1H	1	74–76	19	14	3.2	1	12	3	29	0.0	0	0.4	94	81	
LR	4	797B	1H	1	134–136	16	17	3.7	2	15	5	18	0.0	8	4.6	93	76	
LR	5	797B	1H	2	13–15	16	16	3.4	2	17	5	22	0.0	5	4.2	96	82	
LR	6	797B	1H	2	44–46	17	18	3.6	2	13	5	21	0.0	4	4.7	93	79	
LR	7	797B	1H	2	74–76	19	16	3.7	1	18	6	21	0.0	0	0.8	90	84	
LR	8	797B	1H	2	104–106	19	15	3.5	1	18	4	26	0.0	0	0.6	93	86	
LR	9	797B	1H	3	13–15	18	15	3.4	1	19	5	24	0.0	0	0.3	91	86	
LR	10	797B	1H	3	44–46	17	15	3.3	1	17	4	29	0.0	0	0.4	94	87	
LR	11	797B	1H	3	74–76	18	15	3.5	2	21	5	22	0.0	0	0.3	89	85	
LR	12	797B	1H	3	104–106	17	15	3.4	2	18	5	28	0.0	0	0.4	93	88	
LR	13	797B	1H	3	134–136	16	15	3.4	2	13	4	26	0.0	0	7.0	96	80	
LR	14	797B	1H	4	13–15	15	14	3.3	2	14	3	32	0.0	0	4.7	99	83	
LR	15	797B	1H	4	44–46	17	15	3.4	1	15	5	32	0.0	0	1.4	97	88	
LR	16	797B	1H	4	73–73	19	14	3.2	2	11	3	25	0.0	0	3.3	92	76	Anorthitic
LR	17	797B	1H	4	104–106	18	15	3.4	2	16	4	18	0.0	6	0.7	89	77	
LR	18	797B	2H	1	14–16	17	15	3.3	1	16	4	30	0.0	0	1.6	93	85	
LR	19	797B	2H	1	44–46	18	15	3.2	2	12	4	30	0.0	0	1.0	94	84	Anorthitic
LR	20	797B	2H	1	102–104	15	14	3.1	0	8	2	19	0.0	19	5.5	102	62	Anorthitic
LR	21	797B	2H	1	134–136	18	14	3.2	1	12	3	26	0.0	0	2.9	90	79	
LR	22	797B	2H	2	14–16	19	14	3.2	0	12	3	32	0.0	0	0.7	95	83	
LR	23	797B	2H	2	102–104	19	15	3.5	2	19	4	24	0.0	0	0.3	92	87	
LR	24	797B	2H	2	134–136	16	14	3.2	2	15	3	38	0.0	0	3.1	101	92	

Table 4 (*continued*)

Type	No	Hole	Core	Sec	Interval	Smectite	Illite	Chlorite + Kaolinite	Amphiboles	Quartz	Feldspars	Detrital Amorphous	Rhodochrosite	Calcite	Pyrite	Total	Detrital Mineral Total	Remarks
LR	25	797B	2H	2	44 46	18	14	3.2	0	12	3	34	0.0	0	0.6	98	84	Anorthitic
LR	26	797B	2H	2	74 76	19	14	3.2	1	13	3	34	0.0	0	0.5	96	88	Anorthitic
LR	27	797B	2H	3	14 16	18	15	3.4	1	19	5	26	0.0	0	1.1	93	88	
LR	28	797B	2H	3	44 46	18	15	3.5	1	20	5	22	0.0	0	0.0	88	84	
LR	29	797B	2H	3	74 76	16	15	3.3	1	15	4	22	0.0	4	6.3	91	76	
LR	30	797B	2H	3	102 104	16	15	3.4	2	19	5	23	0.0	0	3.2	91	84	
LR	31	797B	2H	3	134 136	17	15	3.4	0	20	5	27	0.0	0	0.5	92	88	
LR	32	797B	2H	4	14 16	18	15	3.3	1	17	5	32	0.0	0	0.5	96	91	
LR	33	797B	2H	4	44 46	18	15	3.3	1	17	4	29	0.0	0	0.7	94	88	
LR	34	797B	2H	4	74 76	20	15	3.4	2	17	5	26	0.0	0	1.3	93	87	
LR	35	797B	2H	4	102 104	19	15	3.3	1	17	4	24	0.0	0	0.8	89	83	
LR	36	797B	2H	4	134 136	18	16	3.3	1	17	5	28	0.0	0	2.5	97	89	
LR	37	797B	2H	5	44 46	17	15	3.3	1	16	4	28	0.0	0	1.2	93	85	
LR	38	797B	2H	5	74 76	19	14	3.2	1	14	4	38	0.0	0	0.5	103	93	Anorthitic
LR	39	797B	2H	5	102 104	16	15	3.4	2	16	4	30	0.0	0	1.8	95	86	Anorthitic
LR	40	797B	2H	5	134 136	19	15	3.3	1	15	4	31	0.0	0	0.0	97	88	Anorthitic
LRA	1	797A	1H	1	14 16	17	15	3.4	1	19	4	28	0.0	0	0.8	92	87	
LRA	5	797A	1H	1	134 136	18	15	3.4	2	20	5	24	0.0	0	0.5	91	87	
LRA	8	797A	1H	2	74 76	15	15	3.4	1	17	4	36	0.0	0	1.4	101	92	
LRA	16	797A	1H	4	14 16	18	14	3.2	2	14	4	29	0.0	0	0.4	94	83	
LRA	19	797A	1H	4	104 106	19	14	3.2	1	13	3	37	0.0	0	0.5	97	91	Anorthitic
LRA	20	797A	1H	4	134 136	16	15	3.3	1	18	4	34	0.0	0	0.0	95	91	
LRA	23	797A	1H	5	74 76	17	15	3.3	2	15	4	28	0.0	0	4.8	93	83	
LRA	24	797A	1H	5	104 106	16	14	3.3	2	17	3	32	0.0	2	2.7	97	87	
LRA	30	797A	1H	6	134 136	19	15	3.3	1	16	4	32	0.0	0	0.8	94	90	
LRA	32	797A	1H	7	44 46	17	15	3.5	0	14	4	27	0.0	0	3.7	89	80	
					Max	22	19	4.1	3	21	10	61	9.5	34	7.0	120	109	
					Min	15	14	3.0	0	3	2	12	0.0	0	0.0	86	62	
					Average	18	15	3.4	1	16	4	28	0.2	1	1.4	96	86	
					Std. Dev	1	1	0.2	1	3	1	6	1.0	3	1.7	5	6	

Table 5 Grain size compostion of bulk sample and biogenic silica contents ($bioSiO_2$) and major elements composition of silt and clay fraction of selected 10 samples from ODP Site 797.

Type	No	Hole	Core	Sec	Interval	Sand%	Silt%	Clay%	bioSiO2	L.O.I.	SiO2	TiO2	Al2O3	Fe2O3	MnO	MgO	CaO	Na2O	K2O	P2O5	Total
Bulk Grain Size Composition																					
LRA	1	797A	1H	1	14 16	2	40	58													
LRA	5	797A	1H	1	134 136	2	38	61													
LRA	8	797A	1H	2	74 76	2	38	60													
LRA	16	797A	1H	4	14 16	1	28	71													
LRA	19	797A	1H	4	104 106	0	24	76													
LRA	20	797A	1H	4	134 136	1	34	66													
LRA	23	797A	1H	5	74 76	3	34	62													
LRA	24	797A	1H	5	104 106	1	41	58													
LRA	30	797A	1H	6	134 136	1	32	67													
LRA	32	797A	1H	7	44 46	11	32	56													
Silt Fraction																					
LRA	1	797A	1H	1	14 16				3	3.17	68.0	0.731	13.2	4.22	0.060	2.04	1.76	3.08	2.98	0.292	99.6
LRA	5	797A	1H	1	134 136				0	2.81	69.0	0.808	13.0	3.84	0.051	2.11	1.90	2.83	2.65	0.359	99.4
LRA	8	797A	1H	2	74 76				4	4.16	67.8	0.706	12.5	4.04	0.054	1.87	2.47	2.89	2.69	0.333	99.4
LRA	16	797A	1H	4	14 16				4	3.02	69.3	0.747	13.6	3.53	0.057	1.77	1.69	3.01	2.61	0.356	99.7
LRA	19	797A	1H	4	104 106				3	2.61	68.5	0.764	14.0	3.78	0.057	1.44	1.62	3.24	2.78	0.509	99.2
LRA	20	797A	1H	4	134 136				1	3.08	69.6	0.792	12.9	3.42	0.052	2.24	1.86	2.65	2.65	0.359	99.6
LRA	23	797A	1H	5	74 76				1	3.14	69.5	0.789	13.3	3.92	0.044	1.63	1.20	2.75	2.85	0.340	99.5
LRA	24	797A	1H	5	104 106				6	3.47	66.3	0.626	14.1	4.57	0.077	1.68	1.42	3.72	3.19	0.234	99.5
LRA	30	797A	1H	6	134 136				1	2.67	70.0	0.796	13.1	3.51	0.046	1.88	1.75	2.87	2.68	0.309	99.6
LRA	32	797A	1H	7	44 46				2	7.42	63.6	0.648	11.4	12.34	0.099	1.37	1.21	2.55	2.29	0.324	103.3
Clay Fraction																					
LRA	1	797A	1H	1	14 16				5	6.89	56.2	0.733	20.0	7.88	0.072	3.49	0.67	2.17	3.78	0.320	102.2
LRA	5	797A	1H	1	134 136				3	6.16	54.6	0.738	19.0	7.75	0.096	3.42	0.69	2.27	3.79	0.560	99.1
LRA	8	797A	1H	2	74 76				6	10.84	52.5	0.679	17.7	7.12	0.071	3.10	0.87	2.42	3.26	0.508	99.1
LRA	16	797A	1H	4	14 16				10	7.56	57.1	0.652	17.8	6.57	0.225	3.15	0.55	2.47	3.23	0.319	99.6
LRA	19	797A	1H	4	104 106				6	6.62	56.5	0.636	18.4	7.69	0.210	2.99	0.56	2.47	3.10	0.330	99.5
LRA	20	797A	1H	4	134 136				5	6.60	55.1	0.729	19.3	7.25	0.156	3.47	0.63	2.17	3.69	0.368	99.5
LRA	23	797A	1H	5	74 76				5	11.33	49.6	0.654	16.9	10.47	0.056	2.41	0.40	2.40	3.64	0.690	98.5
LRA	24	797A	1H	5	104 106				3	8.91	51.8	0.677	18.1	8.95	0.078	3.00	0.67	2.43	3.63	0.518	98.7
LRA	30	797A	1H	6	134 136				3	6.40	55.5	0.741	18.7	7.71	0.104	3.49	0.60	2.26	3.78	0.355	99.6
LRA	32	797A	1H	7	44 46				5	8.65	53.7	0.704	18.5	7.95	0.072	3.06	0.50	2.33	3.42	0.485	99.4

Table 6 Mineral composition of silt and clay fraction of selected 10 samples from ODP Site 797.

Type	No	Hole	Core	Sec	Interval	Smectite	Illite	Chlorite + Kaolinite	Amphiboles	Quartz	Feldspars	Detrital Amorphous	Rhodochrosite	Calcite	Pyrite	Remarks	
Silt Fraction																	
LRA	1	797A	1H	1	14 16	14	15	3.6	1.8	33	6.4	20	0.0	0.0	0.0		
LRA	5	797A	1H	1	134 136	14	16	3.5	2.0	40	8.0	10	0.0	0.0	0.0		
LRA	8	797A	1H	2	74 76	14	15	3.3	3.6	33	6.7	23	0.0	0.0	1.8		
LRA	16	797A	1H	4	14 16	16	15	3.5	1.5	33	8.1	13	0.0	0.0	0.0		
LRA	19	797A	1H	4	104 106	14	15	3.3	0.7	31	8.5	17	0.0	0.0	2.4		Anorthitic
LRA	20	797A	1H	4	134 136	14	15	3.6	2.0	41	8.5	12	0.0	0.0	0.0		
LRA	23	797A	1H	5	74 76	14	16	3.4	2.1	38	8.1	15	0.0	0.0	0.0		
LRA	24	797A	1H	5	104 106	14	15	3.3	2.4	32	6.9	22	0.0	0.0	1.5		
LRA	30	797A	1H	6	134 136	14	16	3.5	1.7	41	9.8	4	0.0	0.0	1.1		
LRA	32	797A	1H	7	44 46	16	14	3.3	2.4	24	5.0	17	0.0	0.0	9.4		
Clay Fraction																	
LRA	1	797A	1H	1	14 16	21	16	3.5	1.3	9	3.1	25	0.0	0.0	0.0		Anorthitic
LRA	5	797A	1H	1	134 136	20	15	3.4	0.8	9	2.8	30	0.0	0.0	0.9		
LRA	8	797A	1H	2	74 76	20	15	3.3	1.2	8	2.4	36	0.0	0.0	1.1		
LRA	16	797A	1H	4	14 16	21	15	3.3	0.0	8	2.4	31	0.0	0.0	0.0		Anorthitic
LRA	19	797A	1H	4	104 106	24	15	3.2	1.2	8	2.4	28	0.0	0.0	0.5		Anorthitic
LRA	20	797A	1H	4	134 136	23	15	3.4	0.0	9	2.9	27	0.0	0.0	0.0		
LRA	23	797A	1H	5	74 76	18	14	3.2	1.4	7	1.2	25	0.0	0.0	2.7	Jarosite	Anorthitic
LRA	24	797A	1H	5	104 106	21	14	3.2	0.0	8	1.9	35	0.0	0.0	1.7		
LRA	30	797A	1H	6	134 136	23	15	3.3	1.0	10	2.6	29	0.0	0.0	0.0		Anorthitic
LRA	32	797A	1H	7	44 46	22	14	3.2	1.0	9	2.2	28	0.0	0.0	1.4		Anorthitic

Table 7 Composition scores of factors calculated by Q-mode factor analysis for all analyzed samples using all elements with varimax rotation, and multi-regression coefficients calculated by multi-regression analysis of mineral composition to the composition loadings.

	Factor A	Factor B	Factor C	Factor D	Factor E	Sample Average (wt%)
Varimax Compostion Loading						
LOI	-12.3	25.3	11.0	11.5	5.3	**8.0**
SiO2	77.3	38.8	68.7	50.0	52.8	**58.0**
TiO2	1.47	0.54	0.01	0.57	0.42	**0.68**
Al2O3	25.4	11.8	15.0	12.4	12.2	**16.1**
Fe2O3	-0.68	3.20	3.02	26.49	4.46	**6.89**
MnO	-2.62	-0.63	-0.98	-0.65	13.73	**0.26**
MgO	6.71	2.54	-1.05	1.99	3.32	**2.95**
CaO	-1.46	15.45	-3.27	-7.42	3.00	**1.82**
Na2O	1.10	1.08	3.93	1.95	1.98	**1.87**
K2O	5.11	1.82	3.50	2.76	2.45	**3.24**
P2O5	-0.11	0.11	0.04	0.46	0.39	**0.14**
Multi-regression Coefficient						
Smectite	20	16	18	19	17	**18**
Illite	20	15	12	14	12	**15**
Chlorite (+ Kaolinite)	4	3	3	3	3	**3**
Amphiboles	4	1	-1	1	-1	**1**
Quartz	45	12	-2	4	-1	**16**
Feldspars	9	3	4	2	2	**4**
detAmorphous	12	20	60	31	17	**27**
Calcite	-4	24	-4	-16	-3	**1**
Pyrite	-9	3	3	15	-5	**1**
Rhodochrosite	-7	-4	-5	-5	24	**0**
Org-C	-5.19	4.56	3.43	5.30	-2.47	**1.18**
bioSiO2	-14.5	6.0	24.5	9.0	28.7	**6.8**

Table 8 Varimax composition scores and possible ranges of chemical composition for each detrital subcomponent calculated by Q-mode factor analysis for 213 selected samples with 6 detrital elements with oblique rotation. Left and right side of the ranges correspond to non-negative score limit and non-negative loading limit, respectively.

	Factor 1	Factor 2	Factor 3	Factor 4
Varimax Score				
SiO2/Al2O3	3.9	1.9	3.9	2.7
TiO2/Al2O3	0.051	0.032	0.039	0.056
MgO/Al2O3	0.24	0.15	0.16	-0.03
Na2O/Al2O3	0.08	0.13	0.17	0.05
K2O/Al2O3	0.24	0.16	0.19	0.14
Possible Range				
SiO2/Al2O3	5.7-4.5	0.0-1.2	8.2-4.3	2.7-3.1
TiO2/Al2O3	0.071-0.058	0.018-0.027	0.019-0.038	0.054-0.045
MgO/Al2O3	0.38-0.29	0.10-0.13	0.00-0.14	0.00-0.15
Na2O/Al2O3	0.00-0.05	0.16-0.14	0.49-0.20	0.07-0.10
K2O/Al2O3	0.34-0.28	0.10-0.14	0.12-0.18	0.15-0.19

Table 9 Mineral composition ranges of each detrital subcomponent calculated by multi-regression analysis of detrital mineral composition and composition loadings. Left and right side of the ranges correspond to mineral composition for non-negative score limit and non-negative loading limit, respectively, of each factor.

(% in detritus)	Factor 1	Factor 2	Factor 3	Factor 4
Smectite	12 - 15	93 - 45	10 - 17	11 - 19
Illite	14 - 15	55 - 30	5 - 13	20 - 18
Chlorite + Kaolinite	3 - 4	12 - 7	1 - 3	4 - 4
Amphiboles	3 - 2	-9 - -2	3 - 2	3 - 2
Quartz	34 - 28	-45 - -2	5 - 13	27 - 20
Feldspars	8 - 7	-3 - 2	-2 - 3	9 - 6
Detrital Amorphous	-3 - 9	105 - 56	101 - 58	36 - 33

Table 10 Summary of chemical and mineral compositions, the silt / clay ratio of each detrital subcomponent, and their probable origin. See also Table 11 for grain size data.

	Factor 1	Factor 2	Factor 3	Factor 4
Chemical Composition				
SiO2/Al2O3	5.7	1.2	8.2	2.7
TiO2/Al2O3	0.071	0.027	0.019	0.054
MgO/Al2O3	0.38	0.13	0.00	0.00
Na2O/Al2O3	0.00	0.14	0.49	0.07
K2O/Al2O3	0.34	0.14	0.12	0.15
Mineral Composition (% in detritus)				
Smectite	12	45	10	11
Illite	14	30	5	20
Chlorite (+ Kaolinite)	3	7	1	4
Amphiboles	3	-2	3	3
Quartz	34	-2	5	27
Feldspars	8	2	-2	9
Detrital Amorphous	-3	56	101	36
Silt/Clay Ratio	0.42	0.19	1.2	3.5
Origin	Fine Kosa	Fine arc-derived detritus	Coarse arc-derived detritus	Coarse Kosa

Table 11 Grain size of selected samples, chemical composition of silt and clay fractions of selected samples, and silt / clay ratio of each detrital subcomponents calculated for each sample.

Type	No.	Hole	Core	Sec	Interval		Silt Fraction					Clay Fraction					Silt / Clay ratio				
							detSiO2/Al2O3	TiO2/Al2O3	MgO/Al2O3	Na2O/Al2O3	K2O/Al2O3	detSiO2/Al2O3	TiO2/Al2O3	MgO/Al2O3	Na2O/Al2O3	K2O/Al2O3	Bulk	Factor1	Factor2	Factor3	Factor4
LRA	1	797A	1H	1	14	16	4.9	0.055	0.15	0.23	0.23	2.6	0.037	0.17	0.11	0.19	0.70	0.50	0.28	3.11	3.07
LRA	5	797A	1H	1	134	136	5.3	0.062	0.16	0.22	0.20	2.7	0.039	0.18	0.12	0.20	0.62	0.49	0.19	2.17	2.66
LRA	8	797A	1H	2	74	76	5.1	0.057	0.15	0.23	0.22	2.6	0.038	0.17	0.14	0.18	0.64	0.55	0.23	1.62	2.24
LRA	16	797A	1H	4	14	16	4.8	0.055	0.13	0.22	0.19	2.6	0.037	0.18	0.14	0.18	0.40	0.30	0.13	0.88	5.55
LRA	19	797A	1H	4	104	106	4.7	0.055	0.10	0.23	0.20	2.7	0.035	0.16	0.13	0.17	0.31	0.21	0.12	0.50	2.80
LRA	20	797A	1H	4	134	136	5.3	0.061	0.17	0.21	0.21	2.6	0.038	0.18	0.11	0.19	0.51	0.43	0.13	2.20	2.49
LRA	23	797A	1H	5	74	76	5.1	0.059	0.12	0.21	0.21	2.6	0.039	0.14	0.14	0.21	0.55	0.55	0.13	1.47	1.04
LRA	24	797A	1H	5	104	106	4.3	0.044	0.12	0.26	0.23	2.7	0.037	0.17	0.13	0.20	0.71	0.42	0.43	1.99	1.63
LRA	30	797A	1H	6	134	136	5.3	0.061	0.14	0.22	0.20	2.8	0.040	0.19	0.12	0.20	0.48	0.34	0.14	1.52	2.74
LRA	32	797A	1H	7	44	46	5.4	0.057	0.12	0.22	0.20	2.6	0.038	0.17	0.13	0.18	0.58	0.45	0.12	1.78	1.60
					Max		**5.4**	**0.062**	**0.17**	**0.26**	**0.23**	**2.8**	**0.040**	**0.19**	**0.14**	**0.21**	**0.71**	**0.55**	**0.43**	**3.11**	**5.55**
					Min		**4.3**	**0.044**	**0.10**	**0.21**	**0.19**	**2.6**	**0.035**	**0.14**	**0.11**	**0.17**	**0.31**	**0.21**	**0.12**	**0.50**	**1.04**
					Average		**5.0**	**0.057**	**0.14**	**0.23**	**0.21**	**2.7**	**0.038**	**0.17**	**0.13**	**0.19**	**0.55**	**0.42**	**0.19**	**1.72**	**2.58**
					Std Dev		**0.4**	**0.005**	**0.02**	**0.02**	**0.01**	**0.1**	**0.001**	**0.01**	**0.01**	**0.01**	**0.13**	**0.11**	**0.10**	**0.72**	**1.22**

Table 12 Chemical composition of possible source materials. The data included in Kosa category are Kosa collected in Japan (n=21) [*Inoue and Naruse*, 1987, *Kanamori et al.*, 1991], and air-suspended dust from Gobi (n=3) [*Parungo et al.*, 1995], whereas the data included in arc-derived detritus category are neritic mudstones of the Japan Sea side (n=195) [*Irino*, 1992MS, *Sakamoto*, unpublished data]. Data for various Quaternary tephra (n=8) is from *Machida and Arai* [1992].

Category	Sample	SiO2/Al2O3	TiO2/Al2O3	MgO/Al2O3	Na2O/Al2O3	K2O/Al2O3	Data Source
Kosa	Asahikawa1	4.3	0.056	0.22	0.16	0.12	Inoue and Naruse (1987)
Kosa	Hachimutai2	3.7	0.063	0.14	0.17	0.14	Inoue and Naruse (1987)
Kosa	Morioka3	3.1	0.036	0.22	0.12	0.15	Inoue and Naruse (1987)
Kosa	Takada4	3.2	0.053	0.18	0.12	0.15	Inoue and Naruse (1987)
Kosa	Osaka5	3.6	0.037	0.12	0.12	0.14	Inoue and Naruse (1987)
Kosa	Yashiro6-2	4.1	0.076	0.09	0.09	0.13	Inoue and Naruse (1987)
Kosa	Yashiro6-4	3.8	0.055	0.08	0.09	0.12	Inoue and Naruse (1987)
Kosa	Yashiro6-12	6.7	0.033	0.12	0.08	0.18	Inoue and Naruse (1987)
Kosa	Yashiro6-21	4.3	0.037	0.09	0.16	0.16	Inoue and Naruse (1987)
Kosa	Asahikawa55	4.3	0.056	0.22	0.16	0.13	Kanamori et al. (1991)
Kosa	Morioka77	3.1	0.036	0.22	0.12	0.15	Kanamori et al. (1991)
Kosa	Takada67	3.2	0.053	0.18	0.12	0.15	Kanamori et al. (1991)
Kosa	Osaka73		0.058		0.14	0.27	Kanamori et al. (1991)
Kosa	Osaka77		0.054		0.17	0.22	Kanamori et al. (1991)
Kosa	Nagoya87			0.32	0.43	0.38	Kanamori et al. (1991)
Kosa	Wajima88		0.050	0.19	0.12	0.23	Kanamori et al. (1991)
Kosa	Kanazawa88		0.046	0.20	0.06	0.22	Kanamori et al. (1991)
Kosa	Nagasaki88		0.041	0.22	0.09	0.22	Kanamori et al. (1991)
Kosa	Fukuejima88		0.045	0.24	0.02	0.22	Kanamori et al. (1991)
Kosa	Yakushima88washed		0.040	0.24	0.07	0.16	Kanamori et al. (1991)
Kosa	Yulin92	2.0	0.061	0.07	0.16	0.27	Parungo et al. (1992)
Kosa	Beijing92	2.7	0.058	0.17	0.17	0.26	Parungo et al. (1992)
Kosa	Lin'an92	2.7	0.046	0.17	0.10	0.20	Parungo et al. (1992)
Arc-derived detritus	SH30		0.030	0.10	0.19	0.14	Irino (1992MS)
Arc-derived detritus	SH31		0.032	0.12	0.16	0.14	Irino (1992MS)
Arc-derived detritus	SH32		0.028	0.10	0.19	0.15	Irino (1992MS)
Arc-derived detritus	SH33a		0.026	0.08	0.21	0.15	Irino (1992MS)
Arc-derived detritus	SH34		0.032	0.11	0.19	0.16	Irino (1992MS)
Arc-derived detritus	SH35a		0.029	0.11	0.20	0.14	Irino (1992MS)
Arc-derived detritus	SH36		0.035	0.17	0.18	0.14	Irino (1992MS)
Arc-derived detritus	SH37		0.034	0.14	0.16	0.14	Irino (1992MS)
Arc-derived detritus	SH38		0.035	0.13	0.17	0.14	Irino (1992MS)
Arc-derived detritus	SH39		0.032	0.11	0.18	0.15	Irino (1992MS)
Arc-derived detritus	SH40		0.034	0.11	0.18	0.14	Irino (1992MS)
Arc-derived detritus	SH41a		0.034	0.11	0.18	0.14	Irino (1992MS)
Arc-derived detritus	SH49		0.038	0.11	0.17	0.16	Irino (1992MS)
Arc-derived detritus	SH71		0.037	0.13	0.16	0.15	Irino (1992MS)
Arc-derived detritus	sh-9m		0.034	0.11	0.14	0.15	Irino (1992MS)
Arc-derived detritus	sh1		0.034	0.09	0.18	0.14	Irino (1992MS)
Arc-derived detritus	sh6		0.035	0.10	0.17	0.15	Irino (1992MS)
Arc-derived detritus	sh10m		0.035	0.09	0.17	0.14	Irino (1992MS)
Arc-derived detritus	MUIII3		0.035	0.14	0.11	0.14	Irino (1992MS)
Arc-derived detritus	MA1		0.037	0.11	0.13	0.14	Irino (1992MS)
Arc-derived detritus	MA2		0.037	0.13	0.13	0.15	Irino (1992MS)
Arc-derived detritus	MA3		0.037	0.13	0.13	0.14	Irino (1992MS)
Arc-derived detritus	MA4		0.037	0.12	0.14	0.15	Irino (1992MS)
Arc-derived detritus	MA5		0.038	0.13	0.18	0.15	Irino (1992MS)
Arc-derived detritus	MA6		0.035	0.12	0.26	0.16	Irino (1992MS)
Arc-derived detritus	MA7		0.036	0.12	0.14	0.15	Irino (1992MS)
Arc-derived detritus	MA8		0.037	0.13	0.16	0.16	Irino (1992MS)
Arc-derived detritus	MA9		0.036	0.13	0.16	0.16	Irino (1992MS)
Arc-derived detritus	MA10		0.036	0.12	0.20	0.16	Irino (1992MS)
Arc-derived detritus	MA11		0.036	0.14	0.26	0.17	Irino (1992MS)
Arc-derived detritus	MA12		0.036	0.14	0.26	0.18	Irino (1992MS)
Arc-derived detritus	MA13		0.030	0.11	0.24	0.21	Irino (1992MS)
Arc-derived detritus	MA14		0.037	0.14	0.29	0.17	Irino (1992MS)
Arc-derived detritus	MA15		0.036	0.15	0.26	0.16	Irino (1992MS)
Arc-derived detritus	MA16		0.036	0.13	0.20	0.16	Irino (1992MS)
Arc-derived detritus	MA17		0.037	0.15	0.25	0.17	Irino (1992MS)
Arc-derived detritus	MA18		0.037	0.13	0.25	0.16	Irino (1992MS)
Arc-derived detritus	MA19		0.038	0.14	0.20	0.17	Irino (1992MS)
Arc-derived detritus	MA20		0.038	0.13	0.25	0.17	Irino (1992MS)
Arc-derived detritus	MA21		0.040	0.14	0.20	0.16	Irino (1992MS)
Arc-derived detritus	MA22		0.037	0.13	0.22	0.17	Irino (1992MS)
Arc-derived detritus	MA23		0.037	0.15	0.22	0.17	Irino (1992MS)
Arc-derived detritus	MA24		0.036	0.15	0.22	0.17	Irino (1992MS)
Arc-derived detritus	MA25		0.035	0.15	0.20	0.17	Irino (1992MS)
Arc-derived detritus	MA26		0.037	0.17	0.27	0.17	Irino (1992MS)
Arc-derived detritus	MA27		0.034	0.16	0.31	0.18	Irino (1992MS)
Arc-derived detritus	MA34		0.034	0.12	0.28	0.18	Irino (1992MS)
Arc-derived detritus	MA47		0.037	0.14	0.12	0.14	Irino (1992MS)
Arc-derived detritus	MA48		0.037	0.15	0.13	0.15	Irino (1992MS)
Arc-derived detritus	MA49		0.037	0.15	0.12	0.14	Irino (1992MS)
Arc-derived detritus	MA50		0.038	0.13	0.18	0.15	Irino (1992MS)
Arc-derived detritus	MA51		0.036	0.13	0.20	0.16	Irino (1992MS)
Arc-derived detritus	MA52		0.035	0.12	0.26	0.18	Irino (1992MS)
Arc-derived detritus	MA53		0.036	0.13	0.41	0.18	Irino (1992MS)
Arc-derived detritus	MA55		0.037	0.14	0.23	0.16	Irino (1992MS)
Arc-derived detritus	MA56		0.037	0.14	0.22	0.16	Irino (1992MS)
Arc-derived detritus	MA57		0.037	0.15	0.22	0.16	Irino (1992MS)
Arc-derived detritus	MA58		0.036	0.14	0.25	0.17	Irino (1992MS)
Arc-derived detritus	MA59		0.036	0.13	0.25	0.17	Irino (1992MS)
Arc-derived detritus	MA60		0.035	0.12	0.28	0.18	Irino (1992MS)
Arc-derived detritus	MA61		0.032	0.10	0.24	0.20	Irino (1992MS)
Arc-derived detritus	MA62		0.035	0.11	0.21	0.16	Irino (1992MS)

Table 12 (*continued*)

Category	Sample	SiO2/Al2O3	TiO2/Al2O3	MgO/Al2O3	Na2O/Al2O3	K2O/Al2O3	Data Source
Arc-derived detritus	MA63		0.038	0.14	0.21	0.16	Irino (1992MS)
Arc-derived detritus	MA64		0.037	0.14	0.20	0.16	Irino (1992MS)
Arc-derived detritus	MA65		0.038	0.15	0.17	0.16	Irino (1992MS)
Arc-derived detritus	MA66		0.037	0.15	0.18	0.16	Irino (1992MS)
Arc-derived detritus	MA67		0.038	0.14	0.22	0.16	Irino (1992MS)
Arc-derived detritus	MA68		0.036	0.14	0.28	0.17	Irino (1992MS)
Arc-derived detritus	MA69		0.038	0.14	0.26	0.17	Irino (1992MS)
Arc-derived detritus	MA70		0.035	0.13	0.29	0.18	Irino (1992MS)
Arc-derived detritus	MA72		0.038	0.14	0.24	0.18	Irino (1992MS)
Arc-derived detritus	MA73		0.037	0.13	0.24	0.18	Irino (1992MS)
Arc-derived detritus	MA74		0.040	0.14	0.28	0.18	Irino (1992MS)
Arc-derived detritus	MA75		0.039	0.14	0.26	0.17	Irino (1992MS)
Arc-derived detritus	MA76		0.035	0.15	0.19	0.18	Irino (1992MS)
Arc-derived detritus	MA77		0.039	0.15	0.20	0.15	Irino (1992MS)
Arc-derived detritus	MA78		0.041	0.15	0.17	0.14	Irino (1992MS)
Arc-derived detritus	MA79		0.037	0.13	0.18	0.16	Irino (1992MS)
Arc-derived detritus	MA80		0.036	0.11	0.23	0.17	Irino (1992MS)
Arc-derived detritus	MA92		0.022	0.07	0.21	0.29	Irino (1992MS)
Arc-derived detritus	MA148		0.039	0.14	0.16	0.13	Irino (1992MS)
Arc-derived detritus	MA158		0.037	0.14	0.20	0.16	Irino (1992MS)
Arc-derived detritus	HIII1		0.037	0.11	0.14	0.15	Irino (1992MS)
Arc-derived detritus	MZI1b		0.036	0.12	0.16	0.16	Irino (1992MS)
Arc-derived detritus	MZI3		0.038	0.14	0.14	0.16	Irino (1992MS)
Arc-derived detritus	MZI15		0.033	0.09	0.17	0.20	Irino (1992MS)
Arc-derived detritus	YIII3		0.037	0.06	0.13	0.15	Irino (1992MS)
Arc-derived detritus	YIII1		0.039	0.06	0.15	0.15	Irino (1992MS)
Arc-derived detritus	MZII-1m		0.018	0.05	0.20	0.31	Irino (1992MS)
Arc-derived detritus	MZII0.3m		0.033	0.09	0.14	0.15	Irino (1992MS)
Arc-derived detritus	MZII1m		0.040	0.11	0.15	0.15	Irino (1992MS)
Arc-derived detritus	MZII2m		0.037	0.12	0.14	0.16	Irino (1992MS)
Arc-derived detritus	MZII3m		0.038	0.13	0.15	0.15	Irino (1992MS)
Arc-derived detritus	MZII4m		0.036	0.12	0.15	0.15	Irino (1992MS)
Arc-derived detritus	MZII5m		0.037	0.16	0.12	0.15	Irino (1992MS)
Arc-derived detritus	MZII6m		0.039	0.14	0.15	0.16	Irino (1992MS)
Arc-derived detritus	MZII7m		0.042	0.11	0.15	0.14	Irino (1992MS)
Arc-derived detritus	MZII8m		0.038	0.11	0.16	0.16	Irino (1992MS)
Arc-derived detritus	MZII9m		0.040	0.10	0.16	0.17	Irino (1992MS)
Arc-derived detritus	MZII10m		0.037	0.12	0.15	0.15	Irino (1992MS)
Arc-derived detritus	MZII11m		0.037	0.10	0.15	0.15	Irino (1992MS)
Arc-derived detritus	MZII12m		0.034	0.12	0.15	0.18	Irino (1992MS)
Arc-derived detritus	MZII13m		0.040	0.14	0.14	0.15	Irino (1992MS)
Arc-derived detritus	MZII 1		0.038	0.14	0.14	0.16	Irino (1992MS)
Arc-derived detritus	MZII14m		0.038	0.12	0.15	0.15	Irino (1992MS)
Arc-derived detritus	MZII15m		0.041	0.13	0.14	0.17	Irino (1992MS)
Arc-derived detritus	MZII16m		0.038	0.10	0.16	0.16	Irino (1992MS)
Arc-derived detritus	MZII17m		0.036	0.12	0.14	0.16	Irino (1992MS)
Arc-derived detritus	MZII18m		0.034	0.12	0.13	0.17	Irino (1992MS)
Arc-derived detritus	MZII 8		0.049	0.09	0.15	0.15	Irino (1992MS)
Arc-derived detritus	MZII19m		0.039	0.13	0.12	0.14	Irino (1992MS)
Arc-derived detritus	MZII20m		0.037	0.16	0.10	0.14	Irino (1992MS)
Arc-derived detritus	MZII21m		0.037	0.15	0.10	0.15	Irino (1992MS)
Arc-derived detritus	MZII22m		0.037	0.14	0.11	0.14	Irino (1992MS)
Arc-derived detritus	MZII 13		0.037	0.14	0.11	0.13	Irino (1992MS)
Arc-derived detritus	MZII23m		0.036	0.14	0.11	0.14	Irino (1992MS)
Arc-derived detritus	MZII24m		0.037	0.12	0.15	0.14	Irino (1992MS)
Arc-derived detritus	MZIII25m		0.034	0.15	0.11	0.14	Irino (1992MS)
Arc-derived detritus	MZIII26m		0.035	0.15	0.09	0.14	Irino (1992MS)
Arc-derived detritus	MZIII27m		0.032	0.13	0.11	0.16	Irino (1992MS)
Arc-derived detritus	MZIII28m		0.039	0.14	0.12	0.14	Irino (1992MS)
Arc-derived detritus	MZIII29m		0.038	0.15	0.12	0.14	Irino (1992MS)
Arc-derived detritus	MZIII30m		0.033	0.10	0.15	0.15	Irino (1992MS)
Arc-derived detritus	MZIII31m		0.032	0.14	0.14	0.19	Irino (1992MS)
Arc-derived detritus	MZIII32m		0.029	0.13	0.14	0.19	Irino (1992MS)
Arc-derived detritus	MZIII33m		0.039	0.14	0.13	0.16	Irino (1992MS)
Arc-derived detritus	MZIII34m		0.038	0.16	0.11	0.14	Irino (1992MS)
Arc-derived detritus	MZIII35m		0.038	0.15	0.10	0.14	Irino (1992MS)
Arc-derived detritus	MZIII36m		0.043	0.11	0.11	0.15	Irino (1992MS)
Arc-derived detritus	MZIII37m		0.040	0.08	0.13	0.13	Irino (1992MS)
Arc-derived detritus	MZIII38m		0.040	0.12	0.10	0.13	Irino (1992MS)
Arc-derived detritus	MZIII39m		0.036	0.14	0.10	0.13	Irino (1992MS)
Arc-derived detritus	MZIII40m		0.037	0.12	0.07	0.11	Irino (1992MS)
Arc-derived detritus	MZIII41m		0.037	0.15	0.07	0.11	Irino (1992MS)
Arc-derived detritus	MZIII42m		0.040	0.15	0.09	0.12	Irino (1992MS)
Arc-derived detritus	MZIII43m		0.040	0.14	0.09	0.12	Irino (1992MS)
Arc-derived detritus	MZIII44m		0.037	0.12	0.07	0.12	Irino (1992MS)
Arc-derived detritus	MZIII45m		0.045	0.12	0.08	0.11	Irino (1992MS)
Arc-derived detritus	MZIII46m		0.038	0.11	0.08	0.11	Irino (1992MS)
Arc-derived detritus	MZIII47m		0.040	0.13	0.10	0.13	Irino (1992MS)
Arc-derived detritus	MZIII48m		0.038	0.15	0.08	0.12	Irino (1992MS)
Arc-derived detritus	MZIII49m		0.039	0.15	0.09	0.12	Irino (1992MS)
Arc-derived detritus	WK102		0.038	0.13	0.12	0.18	Sakamoto (1994MS)
Arc-derived detritus	WK101		0.040	0.12	0.07	0.16	Sakamoto (1994MS)
Arc-derived detritus	WK97		0.037	0.11	0.07	0.14	Sakamoto (1994MS)
Arc-derived detritus	WK94		0.037	0.11	0.07	0.13	Sakamoto (1994MS)
Arc-derived detritus	WK92		0.037	0.15	0.10	0.19	Sakamoto (1994MS)

Table 12 (*continued*)

Category	Sample	SiO2/Al2O3	TiO2/Al2O3	MgO/Al2O3	Na2O/Al2O3	K2O/Al2O3	Data Source
Arc-derived detritus	WK90		0.038	0.13	0.07	0.14	Sakamoto (1994MS)
Arc-derived detritus	WK88		0.038	0.11	0.06	0.14	Sakamoto (1994MS)
Arc-derived detritus	WK86		0.033	0.08	0.07	0.14	Sakamoto (1994MS)
Arc-derived detritus	WK84		0.040	0.09	0.05	0.13	Sakamoto (1994MS)
Arc-derived detritus	WK82		0.036	0.10	0.06	0.13	Sakamoto (1994MS)
Arc-derived detritus	WK80		0.037	0.11	0.05	0.12	Sakamoto (1994MS)
Arc-derived detritus	WK78		0.038	0.15	0.06	0.14	Sakamoto (1994MS)
Arc-derived detritus	WK74		0.032	0.10	0.08	0.15	Sakamoto (1994MS)
Arc-derived detritus	WK72		0.039	0.08	0.07	0.14	Sakamoto (1994MS)
Arc-derived detritus	WK70		0.041	0.10	0.07	0.16	Sakamoto (1994MS)
Arc-derived detritus	WK68		0.041	0.09	0.07	0.15	Sakamoto (1994MS)
Arc-derived detritus	WK66		0.035	0.09	0.05	0.11	Sakamoto (1994MS)
Arc-derived detritus	WK63		0.038	0.09	0.06	0.13	Sakamoto (1994MS)
Arc-derived detritus	WK59		0.037	0.12	0.06	0.14	Sakamoto (1994MS)
Arc-derived detritus	WK57		0.039	0.09	0.06	0.14	Sakamoto (1994MS)
Arc-derived detritus	WK55		0.037	0.09	0.06	0.13	Sakamoto (1994MS)
Arc-derived detritus	WK53		0.035	0.10	0.05	0.11	Sakamoto (1994MS)
Arc-derived detritus	WK51		0.039	0.11	0.06	0.14	Sakamoto (1994MS)
Arc-derived detritus	WK49		0.036	0.16	0.07	0.14	Sakamoto (1994MS)
Arc-derived detritus	WK47		0.036	0.15	0.06	0.14	Sakamoto (1994MS)
Arc-derived detritus	WK45		0.037	0.10	0.06	0.14	Sakamoto (1994MS)
Arc-derived detritus	WK43		0.038	0.13	0.07	0.15	Sakamoto (1994MS)
Arc-derived detritus	WK41		0.040	0.10	0.05	0.12	Sakamoto (1994MS)
Arc-derived detritus	WK35		0.038	0.11	0.06	0.14	Sakamoto (1994MS)
Arc-derived detritus	WK33		0.038	0.10	0.06	0.13	Sakamoto (1994MS)
Arc-derived detritus	WK31		0.036	0.13	0.07	0.14	Sakamoto (1994MS)
Arc-derived detritus	WK28		0.036	0.16	0.07	0.13	Sakamoto (1994MS)
Arc-derived detritus	WK26		0.040	0.12	0.08	0.15	Sakamoto (1994MS)
Arc-derived detritus	WK24		0.037	0.15	0.08	0.13	Sakamoto (1994MS)
Arc-derived detritus	WK22		0.036	0.14	0.07	0.13	Sakamoto (1994MS)
Arc-derived detritus	WK20		0.038	0.19	0.09	0.15	Sakamoto (1994MS)
Arc-derived detritus	WK18		0.039	0.14	0.07	0.14	Sakamoto (1994MS)
Arc-derived detritus	WK16		0.040	0.13	0.07	0.15	Sakamoto (1994MS)
Arc-derived detritus	WK14		0.038	0.13	0.08	0.14	Sakamoto (1994MS)
Arc-derived detritus	WK12		0.035	0.14	0.08	0.13	Sakamoto (1994MS)
Arc-derived detritus	WK10		0.037	0.14	0.10	0.13	Sakamoto (1994MS)
Arc-derived detritus	WK8		0.038	0.14	0.10	0.14	Sakamoto (1994MS)
Arc-derived detritus	WK4		0.038	0.15	0.09	0.14	Sakamoto (1994MS)
Arc-derived detritus	WK2		0.038	0.14	0.08	0.13	Sakamoto (1994MS)
Arc-derived detritus	WKS18		0.037	0.10	0.05	0.11	Sakamoto (1994MS)
Arc-derived detritus	WKS19		0.037	0.10	0.07	0.12	Sakamoto (1994MS)
Arc-derived detritus	WKS20		0.041	0.13	0.06	0.15	Sakamoto (1994MS)
Arc-derived detritus	WKS21		0.041	0.10	0.08	0.13	Sakamoto (1994MS)
Arc-derived detritus	WKS22		0.040	0.14	0.06	0.14	Sakamoto (1994MS)
Arc-derived detritus	WKS23		0.036	0.10	0.07	0.13	Sakamoto (1994MS)
Arc-derived detritus	WKS24		0.036	0.13	0.03	0.10	Sakamoto (1994MS)
Arc-derived detritus	WKS25		0.043	0.11	0.05	0.13	Sakamoto (1994MS)
Tephra	K-Ah	5.8	0.042	0.04	0.25	0.23	Machida & Arai (1992)
Tephra	AT	6.4	0.011	0.01	0.30	0.29	Machida & Arai (1992)
Tephra	Ata	5.8	0.037	0.04	0.29	0.20	Machida & Arai (1992)
Tephra	Toya	6.2	0.004	0.00	0.34	0.20	Machida & Arai (1992)
Tephra	Aso-3	4.7	0.043	0.04	0.30	0.27	Machida & Arai (1992)
Tephra	Kc-Hb	6.6	0.029	0.03	0.37	0.16	Machida & Arai (1992)
Tephra	U-Oki	3.0	0.014	0.01	0.38	0.26	Machida & Arai (1992)
Tephra	B-Tm	6.9	0.023	0.00	0.42	0.43	Machida & Arai (1992)

Table 13 Composition loadings of each detrital subcomponent, Kosa fraction, Kosa grain size index (KGI), and arc-derived detritus grain size index (AGI) for each sample.

Type	No.	Hole	Core	Sec	Interval	Depth (cmbsf)	Age (ka)	Fine Kosa (% in detritus)	Coarse Kosa (% in detritus)	Fine arc-derived detritus (% in detritus)	Coarse arc-derived detritus (% in detritus)	Kosa Fraction (% in detritus)	KGI	AGI
LR	1	797B	1H	1	13 15	13	0.0	32	9	27	32	41	0.21	0.55
HR	16	797B	1H	1	17 19	17	0.0	37	10	28	24	47	0.21	0.46
HR	17	797B	1H	1	23 25	23	0.8	38	11	30	22	49	0.22	0.42
HR	18	797B	1H	1	31 33	30	1.8	37	11	30	21	48	0.23	0.42
HR	19	797B	1H	1	38 40	37	2.9	42	9	26	22	51	0.17	0.46
LR	2	797B	1H	1	44 46	43	3.8	38	6	30	26	44	0.13	0.46
HR	20	797B	1H	1	45 47	44	4.0	42	4	29	25	46	0.08	0.46
HR	21	797B	1H	1	54 56	52	5.2	38	10	30	23	48	0.21	0.43
HR	22	797B	1H	1	59 61	57	6.0	38	11	30	20	50	0.23	0.40
HR	23	797B	1H	1	66 68	64	7.1							
HR	24	797B	1H	1	73 75	70	8.0	37	10	36	18	47	0.21	0.33
LR	3	797B	1H	1	74 76	71	8.2	32	8	26	34	40	0.19	0.56
HR	25	797B	1H	1	80 82	77	9.1							
HR	26	797B	1H	1	87 89	84	10.2	39	6	27	28	45	0.13	0.51
HR	27	797B	1H	1	96 98	92	11.4	41	7	27	24	49	0.15	0.47
HR	28	797B	1H	1	101 103	97	12.3	47	8	22	23	55	0.14	0.52
HR	29	797B	1H	1	108 110	104	13.5	50	6	24	20	57	0.11	0.46
HR	30	797B	1H	1	117 119	112	15.0	50	6	22	22	57	0.11	0.50
HR	31	797B	1H	1	121 123	116	15.7	51	6	22	21	57	0.10	0.49
HR	32	797B	1H	1	131 133	126	17.4	52	5	20	23	57	0.09	0.54
LR	4	797B	1H	1	134 136	128	17.7	44	8	20	28	52	0.16	0.58
HR	33	797B	1H	1	141 143	135	18.5							
HR	34	797B	1H	1	146 148	140	19.1	46	9	20	26	54	0.16	0.56
HR	35	797B	1H	2	0 2	144	19.5	45	11	18	25	57	0.20	0.58
HR	36	797B	1H	2	6 8	149	20.1	47	10	21	23	57	0.18	0.53
LR	5	797B	1H	2	13 15	156	20.9	41	8	19	31	50	0.17	0.61
HR	37	797B	1H	2	15 17	158	21.1	47	11	21	21	58	0.18	0.50
HR	38	797B	1H	2	21 23	164	21.8	47	11	20	23	58	0.19	0.54
HR	39	797B	1H	2	29 31	171	22.6	48	10	20	22	58	0.18	0.53
HR	40	797B	1H	2	35 37	177	23.3	48	9	20	23	57	0.16	0.54
HR	41	797B	1H	2	40 42	182	23.9							
LR	6	797B	1H	2	44 46	186	24.3	45	7	21	26	52	0.14	0.55
HR	42	797B	1H	2	49 51	190	24.8							
HR	43	797B	1H	2	56 58	197	25.6	48	2	17	33	50	0.03	0.65
HR	44	797B	1H	2	66 68	206	26.5	53	4	23	20	57	0.08	0.47
HR	45	797B	1H	2	70 72	210	27.0	49	5	23	23	54	0.09	0.50
LR	7	797B	1H	2	74 76	214	27.4	45	8	22	26	53	0.15	0.54
HR	46	797B	1H	2	79 81	219	28.0	52	6	23	19	58	0.11	0.46
HR	47	797B	1H	2	84 86	224	28.5							
HR	48	797B	1H	2	91 93	230	29.8							
HR	49	797B	1H	2	100 102	239	31.8	52	4	40	4	56	0.06	0.09
LR	8	797B	1H	2	104 106	243	32.6	50	3	22	25	53	0.06	0.54
HR	50	797B	1H	2	106 108	245	33.1	51	4	21	24	55	0.07	0.52
HR	51	797B	1H	2	112 114	250	34.2	52	5	21	22	57	0.09	0.51
HR	52	797B	1H	2	119 121	257	35.7	51	6	22	20	58	0.11	0.48
HR	53	797B	1H	2	127 129	265	37.4	54	2	20	24	56	0.03	0.54
HR	54	797B	1H	2	132 134	269	38.3	51	7	21	20	58	0.12	0.49
HR	55	797B	1H	2	138 140	275	39.6	52	6	21	21	58	0.11	0.51
HR	56	797B	1H	3	0 2	286	42.0	49	6	19	26	55	0.11	0.58
LRA	1	797A	1H	1	14 16	291	43.1	49	9	27	16	57	0.15	0.37
HR	57	797B	1H	3	7 9	293	43.5	44	5	24	27	49	0.11	0.53
HR	1	797A	1H	1	23 25	297	44.4	51	7	27	14	58	0.12	0.34
LR	9	797B	1H	3	13 15	299	44.8	44	6	22	28	49	0.12	0.56
HR	58	797B	1H	3	21 23	306	46.3	45	8	22	25	53	0.15	0.54
HR	59	797B	1H	3	25 27	310	47.2	52	4	21	23	57	0.08	0.53
HR	60	797B	1H	3	35 37	320	49.4	51	8	21	20	59	0.13	0.49
HR	61	797B	1H	3	40 42	324	50.2	44	6	13	36	50	0.13	0.73
LR	10	797B	1H	3	44 46	328	51.1	44	6	22	28	50	0.12	0.57
HR	62	797B	1H	3	49 51	333	52.2	50	5	21	24	55	0.10	0.53
HR	63	797B	1H	3	56 58	340	53.7	52	6	22	20	58	0.10	0.48
HR	64	797B	1H	3	63 64	345	54.8							
HR	65	797B	1H	3	70 72	353	56.5	49	8	20	23	57	0.14	0.54
LR	11	797B	1H	3	74 76	357	57.4	47	7	20	26	54	0.14	0.56
HR	66	797B	1H	3	78 80	361	58.3	52	7	22	20	58	0.12	0.48
HR	67	797B	1H	3	84 86	366	59.4	48	9	21	22	56	0.15	0.52
HR	68	797B	1H	3	91 93	373	60.9	50	9	21	21	59	0.15	0.50
HR	69	797B	1H	3	97 99	379	62.2	52	7	22	20	59	0.11	0.48
LR	12	797B	1H	3	104 106	385	63.5	44	7	23	26	51	0.15	0.54
HR	70	797B	1H	3	105 107	386	63.7	48	8	21	22	56	0.14	0.51
HR	71	797B	1H	3	112 114	393	65.2	49	8	21	22	57	0.15	0.51
HR	72	797B	1H	3	120 121	400	66.8							
LRA	5	797A	1H	1	134 136	405	67.8	51	10	26	13	61	0.17	0.33
HR	73	797B	1H	3	126 128	406	68.1	49	8	21	22	57	0.14	0.52
HR	74	797B	1H	3	131 133	411	69.2	41	14	22	23	55	0.26	0.52
LR	13	797B	1H	3	134 136	414	69.8	41	10	23	26	51	0.19	0.52
HR	75	797B	1H	3	140 142	420	71.1	48	10	20	22	58	0.18	0.52
HR	76	797B	1H	3	147 149	426	72.4	49	9	21	21	58	0.15	0.50
HR	77	797B	1H	4	4 6	433	73.9	50	9	21	20	59	0.15	0.48
HR	78	797B	1H	4	11 13	440	75.0	41	11	22	25	53	0.22	0.53
LR	14	797B	1H	4	13 15	441	75.2	40	9	25	27	49	0.19	0.52
HR	79	797B	1H	4	18 20	446	75.9	40	15	24	20	56	0.28	0.46
HR	80	797B	1H	4	24 26	452	76.9	48	7	21	24	55	0.13	0.54
HR	81	797B	1H	4	32 34	460	78.1	46	7	21	25	53	0.13	0.54
HR	82	797B	1H	4	39 41	466	79.1	49	9	24	18	59	0.16	0.43
LR	15	797B	1H	4	44 46	471	79.8	47	8	22	23	55	0.14	0.51
HR	83	797B	1H	4	49 51	476	80.6	48	7	25	21	54	0.12	0.46
HR	84	797B	1H	4	53 55	480	81.3	45	6	25	25	51	0.11	0.50
HR	85	797B	1H	4	60 62	486	82.2	46	6	23	25	52	0.12	0.52
LRA	8	797A	1H	2	74 76	489	82.7	47	10	27	16	57	0.18	0.37
HR	86	797B	1H	4	67 69	493	83.3	40	6	26	27	47	0.13	0.51
LR	16	797B	1H	4	71 73	497	83.9	43	3	24	31	46	0.06	0.57

Table 13 (*continued*)

Type	No.	Hole	Core	Sec	Interval		Depth (cmbsf)	Age (ka)	Fine Kosa (% in detritus)	Coarse Kosa (% in detritus)	Fine arc-derived detritus (% in detritus)	Coarse arc-derived detritus (% in detritus)	Kosa Fraction (% in detritus)	KG1	AG1
HR	2	797A	1H	2	86	88	499	84.2	51	9	29	15	53	0.08	0.34
HR	3	797A	1H	2	93	95	505	85.2	48	6	28	17	55	0.11	0.38
HR	87	797B	1H	4	88	90	513	86.4	45	7	21	27	52	0.14	0.56
HR	88	797B	1H	4	94	96	519	87.3	47	7	23	23	54	0.14	0.51
HR	89	797B	1H	4	102	104	526	88.4	50	6	24	20	56	0.10	0.46
LR	17	797B	1H	4	104	106	528	88.8	48	6	22	24	53	0.10	0.52
HR	90	797B	1H	4	109	111	533	89.5	51	7	24	18	58	0.12	0.43
HR	4	797A	1H	2	130	132	542	90.9	51	6	30	13	57	0.10	0.31
HR	5	797A	1H	2	137	139	549	92.1	46	6	37	11	53	0.12	0.23
HR	6	797A	1H	2	144	146	556	93.2	48	8	31	13	56	0.14	0.29
HR	7	797A	1H	3	1	3	563	94.3	49	9	31	11	57	0.15	0.27
HR	8	797A	1H	3	8	10	570	95.4	42	5	26	27	46	0.10	0.51
HR	9	797A	1H	3	18	20	579	96.8	47	9	31	13	56	0.17	0.30
HR	10	797A	1H	3	22	24	584	97.6	45	10	29	16	55	0.19	0.35
HR	11	797A	1H	3	29	31	592	98.8	49	6	25	20	55	0.10	0.44
HR	12	797A	1H	3	36	38	600	100.1	46	8	30	16	54	0.15	0.35
LR	18	797B	2H	1	14	16	604	100.7	43	7	23	27	50	0.13	0.53
HR	91	797B	2H	1	17	19	607	101.2	45	8	20	27	52	0.14	0.57
HR	92	797B	2H	1	24	26	614	102.3							
HR	93	797B	2H	1	32	34	622	103.5	43	8	24	25	51	0.16	0.51
HR	94	797B	2H	1	39	41	629	104.7	48	4	22	26	52	0.08	0.54
LR	19	797B	2H	1	44	46	633	105.3	40	6	25	28	46	0.14	0.53
HR	13	797A	1H	3	71	73	634	105.4	44	9	28	19	53	0.17	0.40
HR	95	797B	2H	1	53	55	642	106.7							
HR	96	797B	2H	1	60	62	649	107.8	40	5	21	35	44	0.10	0.63
HR	97	797B	2H	1	67	69	656	108.9	39	9	28	24	48	0.19	0.46
HR	14	797A	1H	3	98	100	659	109.4	35	19	26	19	55	0.35	0.42
HR	15	797A	1H	3	108	110	668	110.8	52	8	24	16	59	0.13	0.40
HR	98	797B	2H	1	88	90	676	111.7	43	7	26	25	50	0.14	0.49
HR	99	797B	2H	1	95	97	683	112.6	49	5	25	21	54	0.08	0.46
LR	20	797B	2H	1	102	104	689	113.3	38	6	28	28	44	0.15	0.50
HR	100	797B	2H	1	104	106	691	113.5	43	9	26	23	52	0.18	0.47
HR	101	797B	2H	1	109	111	696	114.1	47	8	23	22	55	0.15	0.49
HR	102	797B	2H	1	115	117	702	114.8	52	2	25	21	54	0.03	0.46
HR	103	797B	2H	1	123	125	710	115.7	51	5	25	20	55	0.08	0.44
HR	104	797B	2H	1	130	132	716	116.4	45	8	24	23	53	0.15	0.48
LR	21	797B	2H	1	134	136	720	116.9	48	3	25	24	51	0.06	0.49
HR	105	797B	2H	1	137	139	723	117.3	48	5	22	24	54	0.09	0.52
LRA	16	797A	1H	4	14	16	723	117.3	47	8	32	13	55	0.14	0.29
HR	106	797B	2H	1	144	146	730	118.1	45	8	23	24	53	0.15	0.51
HR	107	797B	2H	2	1	3	737	118.9	49	8	25	18	57	0.14	0.43
HR	108	797B	2H	2	8	10	743	119.6	47	8	27	18	56	0.15	0.40
LR	22	797B	2H	2	14	16	749	120.3	42	4	27	28	46	0.08	0.51
HR	109	797B	2H	2	17	19	752	120.7	45	2	29	24	47	0.03	0.46
HR	110	797B	2H	2	22	24	757	121.3							
HR	111	797B	2H	2	30	32	765	122.2							
HR	112	797B	2H	2	36	38	771	122.9	44	5	27	24	49	0.10	0.48
HR	113	797B	2H	2	42	44	776	123.5	47	0	30	23	47	0.00	0.43
LR	25	797B	2H	2	44	46	778	123.7	41	3	27	28	45	0.08	0.51
HR	114	797B	2H	2	50	52	784	124.4	45	0	29	26	45	0.00	0.48
HR	115	797B	2H	2	57	59	791	125.3	43	8	28	21	51	0.17	0.43
HR	116	797B	2H	2	64	66	798	126.1	45	9	27	19	54	0.17	0.41
HR	117	797B	2H	2	71	73	804	126.8	41	9	26	24	50	0.17	0.47
LRA	19	797A	1H	4	104	106	804	126.8	44	10	29	17	54	0.19	0.37
LR	26	797B	2H	2	74	76	807	127.1	37	6	24	33	43	0.15	0.58
HR	118	797B	2H	2	79	81	812	127.7	39	11	26	25	49	0.21	0.50
HR	119	797B	2H	2	84	86	817	128.3							
HR	120	797B	2H	2	92	94	825	129.3	51	8	22	19	59	0.13	0.46
HR	121	797B	2H	2	98	100	830	129.8	51	7	22	19	58	0.12	0.46
LRA	20	797A	1H	4	134	136	832	130.1	52	9	26	12	61	0.15	0.31
LR	23	797B	2H	2	102	104	834	130.3	49	7	21	22	56	0.13	0.52
HR	122	797B	2H	2	106	108	838	130.8	53	7	22	19	59	0.11	0.47
HR	123	797B	2H	2	113	115	845	131.7	48	8	24	20	56	0.14	0.46
HR	124	797B	2H	2	121	123	853	132.6	52	7	21	20	59	0.12	0.49
HR	125	797B	2H	2	127	129	858	133.2	49	6	21	24	55	0.11	0.52
LR	24	797B	2H	2	134	136	865	134.1	36	7	23	34	43	0.17	0.60
HR	126	797B	2H	2	136	138	867	134.3	40	12	20	28	52	0.23	0.58
HR	127	797B	2H	2	141	143	872	134.9	50	11	19	20	61	0.18	0.51
HR	128	797B	2H	2	148	150	879	135.8	47	12	18	22	60	0.20	0.55
HR	129	797B	2H	3	5	7	885	136.5	53	9	21	17	62	0.15	0.45
HR	130	797B	2H	3	11	13	891	137.2	51	8	20	20	60	0.14	0.50
LR	27	797B	2H	3	14	16	894	137.6	48	7	21	23	56	0.13	0.53
HR	131	797B	2H	3	19	21	899	138.2	54	7	22	17	61	0.12	0.44
HR	132	797B	2H	3	24	26	904	138.8	54	5	20	21	60	0.09	0.51
HR	133	797B	2H	3	33	35	912	139.7	51	8	18	22	59	0.14	0.55
HR	134	797B	2H	3	40	42	919	140.6	51	9	18	22	60	0.15	0.56
LR	28	797B	2H	3	44	46	923	141.1	50	7	20	22	58	0.13	0.53
HR	135	797B	2H	3	48	50	927	141.6	45	8	15	33	52	0.15	0.69
LRA	23	797A	1H	5	74	76	930	141.9	46	7	30	16	54	0.14	0.34
HR	136	797B	2H	3	54	56	933	142.3	44	14	17	26	58	0.24	0.60
HR	137	797B	2H	3	64	66	942	144.4	47	12	16	24	59	0.21	0.60
HR	138	797B	2H	3	71	73	949	146.1	48	11	16	25	59	0.19	0.60
LR	29	797B	2H	3	74	76	952	146.8	49	9	20	22	58	0.15	0.52
HR	139	797B	2H	3	79	81	957	147.9	47	12	16	25	59	0.20	0.61
LRA	24	797A	1H	5	104	106	959	148.4	43	6	33	18	48	0.11	0.35
HR	140	797B	2H	3	82	84	960	148.6	41	7	19	32	48	0.15	0.62
HR	141	797B	2H	3	92	94	969	150.8							
HR	142	797B	2H	3	96	98	973	151.7	51	8	18	23	59	0.13	0.56
LR	30	797B	2H	3	102	104	979	153.1	47	9	18	26	56	0.16	0.59
HR	143	797B	2H	3	103	105	980	153.4	47	8	20	25	55	0.14	0.56
HR	144	797B	2H	3	108	110	985	154.5	48	8	17	26	57	0.15	0.60

Table 13 (*continued*)

Type	No.	Hole	Core	Sec	Interval		Depth (cmbsf)	Age (ka)	Fine Kosa (% in detritus)	Coarse Kosa (% in detritus)	Fine arc-derived detritus (% in detritus)	Coarse arc-derived detritus (% in detritus)	Kosa Fraction (% in detritus)	KGI	AGI
HR	145	797B	2H	3	116	117	992	156.2							
HR	146	797B	2H	3	126	128	1002	158.6	47	10	17	26	57	0.17	0.61
HR	147	797B	2H	3	131	133	1006	159.5	50	8	17	24	58	0.14	0.58
LR	31	797B	2H	3	134	136	1009	160.2	50	8	19	23	58	0.14	0.56
HR	148	797B	2H	3	138	140	1014	161.4	50	8	18	24	58	0.14	0.58
HR	149	797B	2H	3	145	147	1021	163.0	51	8	17	24	59	0.13	0.58
HR	150	797B	2H	4	2	4	1027	164.4	51	4	18	27	55	0.07	0.59
HR	151	797B	2H	4	9	11	1034	166.1	53	6	19	22	59	0.10	0.54
LR	32	797B	2H	4	14	16	1039	167.3	51	7	20	23	58	0.13	0.53
HR	152	797B	2H	4	16	18	1041	167.8	53	4	19	24	57	0.08	0.56
HR	153	797B	2H	4	23	25	1048	169.4	53	6	20	20	60	0.11	0.51
HR	154	797B	2H	4	32	34	1056	171.3	52	7	19	21	59	0.13	0.53
HR	155	797B	2H	4	37	39	1061	172.5	52	8	19	22	59	0.13	0.54
LR	33	797B	2H	4	44	46	1068	174.1	52	5	20	23	57	0.09	0.54
HR	156	797B	2H	4	46	47	1069	174.4							
HR	157	797B	2H	4	51	53	1075	175.6	52	7	19	22	59	0.13	0.54
HR	158	797B	2H	4	58	60	1081	176.8	45	15	19	21	60	0.25	0.53
HR	159	797B	2H	4	65	67	1088	178.1	52	7	19	22	59	0.12	0.53
HR	160	797B	2H	4	71	73	1094	179.2	54	4	19	23	58	0.08	0.54
LR	34	797B	2H	4	74	76	1097	179.8	55	4	19	22	59	0.07	0.54
HR	161	797B	2H	4	79	81	1102	180.7	51	8	20	21	59	0.13	0.51
HR	162	797B	2H	4	86	88	1108	181.9	56	4	22	18	60	0.06	0.46
HR	163	797B	2H	4	93	95	1115	183.2	56	3	22	19	60	0.06	0.47
HR	164	797B	2H	4	99	101	1121	184.3	55	6	21	19	60	0.10	0.48
LR	35	797B	2H	4	102	104	1124	184.9	54	5	21	19	60	0.09	0.47
HR	165	797B	2H	4	107	109	1129	185.8	54	7	21	17	61	0.12	0.45
HR	166	797B	2H	4	114	116	1135	187.0	52	9	21	19	60	0.14	0.47
LRA	30	797A	1H	6	134	136	1139	187.7	53	8	26	13	61	0.13	0.33
HR	167	797B	2H	4	121	123	1142	188.3	52	9	23	15	61	0.15	0.39
HR	168	797B	2H	4	128	130	1149	189.6	51	7	20	23	58	0.12	0.53
HR	169	797B	2H	4	132	134	1153	190.2	47	9	20	24	56	0.16	0.54
LR	36	797B	2H	4	134	136	1155	190.5	44	9	18	29	53	0.17	0.61
HR	170	797B	2H	4	142	144	1162	191.5	39	15	16	30	54	0.27	0.64
HR	171	797B	2H	5	0	2	1170	192.6	41	17	19	24	58	0.29	0.56
HR	172	797B	2H	5	7	9	1177	193.6	53	7	21	20	59	0.11	0.49
HR	173	797B	2H	5	16	18	1186	194.9	53	7	21	19	60	0.11	0.47
HR	174	797B	2H	5	21	23	1190	195.5	55	6	21	18	61	0.11	0.45
HR	175	797B	2H	5	29	31	1198	196.6	43	8	22	27	51	0.16	0.55
LRA	32	797A	1H	7	44	46	1203	197.3	50	10	26	13	61	0.17	0.33
HR	176	797B	2H	5	35	37	1204	197.5	47	8	21	24	55	0.14	0.54
HR	177	797B	2H	5	41	43	1210	198.3	52	8	22	19	60	0.13	0.46
LR	37	797B	2H	5	44	46	1213	198.8	49	6	23	22	55	0.10	0.49
HR	178	797B	2H	5	49	51	1217	199.3	45	7	22	26	52	0.14	0.55
HR	179	797B	2H	5	56	58	1224	200.3	43	9	21	27	52	0.17	0.57
HR	180	797B	2H	5	62	64	1230	201.2	41	11	20	28	52	0.21	0.58
LR	38	797B	2H	5	74	76	1242	202.9	41	8	23	28	49	0.17	0.54
LR	39	797B	2H	5	102	104	1269	206.8	49	7	22	22	56	0.13	0.50
LR	40	797B	2H	5	134	136	1299	211.1	44	10	22	24	54	0.19	0.53
								Max	**56**	**19**	**40**	**36**	**62**	**0.35**	**0.73**
								Min	**32**	**0**	**13**	**4**	**40**	**0.00**	**0.09**
								Average	**47**	**8**	**23**	**23**	**55**	**0.14**	**0.50**
								Std Dev	**5**	**3**	**4**	**5**	**5**	**0.05**	**0.08**

Table 14 Average linear sedimentation rate (LSR), dry bulk density (DBD), content of detritus (Detritus%), and mass accumulation rates (MARs) of Kosa and arc-derived detritus between 12 datums. Age controlling datums are cited from *Tada et al.*, [1996].

Datum	Depth (cmbsf)	AMS14C Age (ka)	Calender Age (ka)	LSR (cm/ky)	DBD (g/cm3)	Detritus%	Kosa MAR (g/cm2/ky)	Arc-derived detritus MAR (g/cm2/ky)
Top	18		0.0					
				6.50	0.320	78.9	0.8	0.9
TL1	92	9.9±0.2	11.4					
				5.62	0.472	80.3	1.2	0.9
Top TL2	127	14.9±0.2	17.6					
				8.75	0.629	83.3	2.5	2.1
Bottom TL2	190	21.0±0.2	24.8					
				9.16	0.652	86.1	2.7	2.3
A-T	224	24.3±0.2	28.5					
				4.60	0.584	86.4	1.3	1.0
Stage 5.0	433		73.91					
				6.40	0.480	81.1	1.4	1.2
Stage 5.2	542		90.95					
				6.35	0.459	80.7	1.2	1.1
Stage 5.4	668		110.79					
				8.50	0.491	79.8	1.7	1.7
Stage 6.0	830		129.84					
				8.28	0.706	88.5	3.0	2.2
Stage 6.3	933		142.28					
				4.24	0.684	89.3	1.5	1.1
Stage 6.5	1072		175.05					
				5.29	0.646	88.6	1.8	1.2
Stage 7.0	1149		189.61					

Appendix

I. Determination of Major Elements Composition of Fine Grained Sediments using X-ray Fluorescence Analysis

Introduction

X-ray fluorescence analysis is conducted on fused glass bead which contain the particular fraction of sample. Sample - flux ratio of glass bead is adopted to be 0.1000 which result in the almost constant mass absorption effect in spite of the compositional variation of samples [*Goto and Tatsumi*, 1991]. However, sediment samples have much wider compositional variation than igneous rocks used by *Goto and Tatsumi* because marine sediment often contains siliceous and / or calcareous fossils and diagenetic products such as carbonate and phosphate which are rich in calcium, magnesium, manganese, and phosphorous. Thus the calibration method which is effective for wide range of element composition should be established to analyze sediment samples. In addition, sediments usually contains a lot of volatiles such as structural water of minerals, carbonate, and organic carbon. So special care is needed for sample preparation.

Sample Preparation

Analyzed samples are recommended to be desalted and powdered.

As the first step, sample is dried and ignited in order to remove volatiles to prevent concentration change of sample during glass bead fusion. Approximately 0.6 g of powdered sample is put in a ceramic crucible whose weight is exactly known. Sample in crucible is covered and dried in an oven set at 50 °C overnight. After dried, sample in crucible is put in a desiccator immediately after taking out of the oven and is cooled to room temperature. After cooling, sample is weighed with ceramic crucible. Then sample in crucible is covered and

dried in an oven at 110 °C longer than 4 hours. After dried, sample in crucible is put in a desiccator immediately after taking out of the oven and is cooled to room temperature. After cooling, sample is weighed with ceramic crucible.

Sample in crucible is covered and ignited in an oven at 1000 °C for 6 hours. Ignition longer than 6 hours does not result in the further weight loss and, in many case, sample is sintered. Thus 6 hours ignition is best. After ignition, sample in crucible is put in a desiccator immediately after taking out of the oven and the desiccator is vacuumed using vacuum pump in order to prevent rehydration and recarbonatization of lime (CaO) in calcareous sample. Sample is cooled to room temperature. After cooling, sample is weighed with ceramic crucible. Loss on ignition (LOI) is defined here as,

LOI = {(110 °C dried sample + crucible weight) - (1000 °C ignited sample + crucible weight)} / {(110 °C dried sample + crucible weight) - (crucible weight)} * 100.

If sample is sintered, sample is powdered using back of spoon or agate mortar which depends on the hardness of sintering.

Bead Sampling

Approximately 0.4 g of powdered ignited sample is mixed with $Li_2B_4O_7$ flux in exact ratio of 0.1000 : 1.000. $Li_2B_4O_7$ flux was dried at 110 °C for longer than 48 hours and cooled down to room temperature in a desiccator. Ignited sample and flux are well-mixed in platinum crucible and then three drops of 2 % LiBr solution are added to sample - flux mixture in order to easily rip up glass bead from platinum crucible after fusion.

Sample - flux mixture in platinum crucible is fused approximately at 1150 °C using a radio-frequency induction furnace. Ignition time is 7 minutes and sample - flux mixture in platinum crucible is agitated during last 3 minutes in order to remove bubble in the fused glass. Cooled glass bead is used for XRF analysis and the side which faced to the bottom of platinum crucible is used for measurement. So the bottom of platinum crucible should be clean and polished up.

The glass bead is weighed to check the ignition loss of flux and it should be approximately 0.5 %. Sample identification is described on the side which is not used for measurement and glass bead is kept in sealed small bag.

Calibration Method

Reference materials

Geochemical reference samples provided by Geological Survey of Japan, US Geological Survey and National Bureau of Standards and their mixtures were used as calibration standards. In addition, pure silica, pure calcium carbonate, and pure manganese carbonate are mixed with a geochemical reference sample (JB-1a) and used as calibration standards to verify a wide compositional range. All used standards (n = 40) and their composition are listed in Table I-1. All composition values are cited from *Potts et al.* [1992] and recalculated as dry base values for igneous rock standards and ignited base values for sedimentary rock standards. Fe content is calculated to total ferric form (Fe_2O_3).

Glass bead sampling of reference materials

Geochemical standards used here include various igneous rocks and sedimentary rocks. To make glass bead of them, pre-treatments fitted for each standard was conducted.

For igneous rocks, standard samples were not pre-ignited at 1000 °C because all divalent iron (FeO) was not oxidized to trivalent iron (Fe_2O_3), which makes it impossible to estimate appropriate loss on ignition. They are only dried at 110 °C and used for bead sampling.

For sedimentary rock standards except for phosphate standard (NBS-120c), the same pre-treatment including pre-ignition described above was conducted. Carbonate fluoro-apatite contained in NBS-120c is not decomposed at 1000 °C, which makes it impossible to estimate appropriate loss on ignition of this sample. Thus NBS-120c was used for bead sampling after dried at 110 °C.

Measurement condition

Rigaku 3270 X-ray Spectrometer of Ocean Research Institute was used for measurement. It is equipped with Rh tube and acceleration voltage 50 kV and current 50 mA was adopted. Measurement condition for each element was determined. Adopted condition is listed in Table I-2. Under these condition, 40 reference samples are measured and the intensity of characteristic X-ray of each element for each sample was collected.

Calibration curve

Calibration which convert the intensity of characteristic X-ray of each element to weight % of oxide form of the element was conducted by best fit linear or quadratic equation. Because mass absorption by Ca could not neglected for TiO_2, Fe_2O_3, and MnO, calibration which is proportional to the Ca X-ray intensity of each sample was conducted (matrix calibration). Matrix calibration of element i for element j is calculated as

(Calibrated intensity of i)
$= (\text{Raw intensity of i}) \times [1 + (\text{Matrix calibration coefficient for j}) \times (\text{Raw intensity of j})]$

Calibration for mass absorption by other elements was not necessary. All calibration coefficient are listed in Table I-3.

SiO_2 and P_2O_5 calibration were conducted by quadratic equation (Figures I-a, n, o). One quadratic calibration equation can be used for 0 to 35 wt% P_2O_5 (Figure I-n), which is shown in Figure I-o as good fitness of curve with in the 0 to 0.5 wt% P_2O_5 range.

Calibration for Al_2O_3, MgO, CaO, Na_2O, and K_2O were conducted by simple linear equation (Figures I-d, j, k, l, m).

Calibration for TiO_2, Fe_2O_3, and MnO were conducted by linear equation (Figures I-c, f, h). Because the intensity of these elements were systematically low for mass absorption

effect for Ca (Figures I-b, e, g), matrix calibration for Ca was conducted. Within the range of 1 to 6 wt% MnO, intensity of prepared samples were systematically lower than general trend of other samples (Figure I-i). The author prepared high Mn sample as mixture of JB-1a and pure manganese carbonate. When manganese carbonate was heated at temperature higher than 110 °C, Mn was oxidized to unknown oxidized form. Thus the author used pure manganese carbonate without drying. This may have resulted in the lower intensity of Mn for mixture standards by loss of adsorbed water. Although these high Mn standards could not be used for calibration, Figure I-i shows that the linearity between intensity and content of Mn is guaranteed approximately to 5 wt% MnO.

Calibration of measurement condition

One glass bead of JB-1a which was named CALIB is measured to check and calibrate the measurement condition every time when unknown sample is measured. To prevent counting error, measurement time of CALIB for each element is set as twice as described in Table I-2. Collected intensity of CALIB for each element are used to calculate the correction factor to the intensity when calibration curve were made. Correction factor for element i is defined as

$$\text{Correction factor} = \frac{\text{Intensity of i for CALIB measured when calibration curve was made}}{\text{Intensity of i for CALIB measured when unknown sample is measured}}.$$

The intensity of i for unknown sample is used after being multiplied by the correction factor.

When correction factor become larger than 1.02 or smaller than 0.98, calibration curve should be revised. Na and P in sweat of people easily pollute the surface of glass beads. When the correction factors for Na and P calculated using CALIB become systematically larger, pollution of glass bead surface by people's sweat is probable. In this case, measurement surface of CALIB is polished using less than 1μm diamond paste and CALIB is measured

again. Only when the intensity of Na and P cannot be better, calibration curve should be revised.

Precision of Measurement

Analytical errors of measurement are estimated by 9 times repetition of glass bead making and their measurement by the spectrometer using the geological standard JB-1a of the Geological Survey of Japan.

The reproducibility (95 % reliability) of measurement is 52.4±0.3 % for SiO_2, 1.32±0.01 % for TiO_2, 14.2±0.1 % for Al_2O_3, 9.16±0.06 % for Fe_2O_3, 0.144±0.002 % for MnO, 7.85±0.08 % for MgO, 9.34±0.07 % for CaO, 2.56±0.04 % for Na_2O, 1.41±0.01 % for K_2O, and 0.244±0.003 % for P_2O_5. They correspond to relative error of ±0.6% for SiO_2, ±0.8% for TiO_2, ±0.7% for Al_2O_3, ±0.7% for Fe_2O_3, ±1.4% for MnO, ±1.0% for MgO, ±0.8% for CaO, ±1.6% for Na_2O, ±0.7% for K_2O, and ±1.2% for P_2O_5, respectively.

References

Goto, A. and Tatsumi, Y., Quantitative analysis of rock sample using X-ray fluorescence analyzer, *The Rigaku-Denki Journal, 22*, 28-44, 1991.

Potts, P. J., Tindle, A. G., and Webb, P. C., *Geochemical Reference Material Compositions: Rocks, Minerals, Sediments, Soils, Carbonates, Refractories and Ores in Research and Industry*, 313 pp., Whittles Publishing, U. K., 1992.

Table I-1 Composition values of reference standards used for calibration curve. All composition values are cited from *Potts et al.* [1992] and recalculated as dry base values for igneous rock standards and ignited base values for sedimentary rock standards. Fe content is calculated to total ferric form (Fe_2O_3).

Standard ID	SiO2	TiO2	Al2O3	Fe2O3	MnO	MgO	CaO	Na2O	K2O	P2O5	Remarks
G-2	69.1	0.492	15.2	2.68	0.034	0.76	1.97	4.07	4.49	0.140	USGS standard (Igneous rock)
AGV-1	59.9	1.071	17.3	6.83	0.097	1.55	4.99	4.29	2.90	0.485	USGS standard (Igneous rock)
JG-2	77.1	0.040	12.4	0.94	0.015	0.04	0.80	3.55	4.72	0.002	GSJ standard (Igneous rock)
JG-3	67.2	0.481	15.6	3.74	0.072	1.79	3.77	4.04	2.63	0.120	GSJ standard (Igneous rock)
JR-1	75.5	0.100	12.9	0.96	0.100	0.09	0.63	4.11	4.41	0.020	GSJ standard (Igneous rock)
JR-2	75.8	0.090	12.8	0.86	0.110	0.05	0.45	4.04	4.45	0.010	GSJ standard (Igneous rock)
JR-3	72.7	0.211	12.1	4.77	0.085	0.05	0.09	4.70	4.33	0.009	GSJ standard (Igneous rock)
JB-1a	52.6	1.311	14.6	9.18	0.151	7.82	9.31	2.76	1.42	0.262	GSJ standard (Igneous rock)
JB-2	53.2	1.191	14.7	14.35	0.200	4.66	9.90	2.03	0.42	0.100	GSJ standard (Igneous rock)
JB-3	51.1	1.450	16.9	11.88	0.160	5.20	9.86	2.82	0.78	0.290	GSJ standard (Igneous rock)
JGb-1	43.5	1.621	17.7	15.16	0.170	7.83	11.98	1.23	0.24	0.050	GSJ standard (Igneous rock)
JP-1	42.6	0.010	0.6	8.37	0.120	44.90	0.56	0.02	0.00	0.000	GSJ standard (Igneous rock)
JA-1	64.2	0.872	15.0	6.97	0.150	1.61	5.69	3.87	0.78	0.160	GSJ standard (Igneous rock)
JA-3	62.4	0.681	15.6	6.60	0.106	3.66	6.29	3.18	1.41	0.110	GSJ standard (Sedimentary rock)
JDo-1	0.4	0.008	0.0	0.04	0.012	35.19	63.77	0.02	0.00	0.069	GSJ standard (Sedimentary rock)
JSd-3	79.1	0.441	10.6	4.61	0.151	1.24	0.56	0.46	2.01	0.094	GSJ standard (Sedimentary rock)
JSl-2	62.9	0.796	19.1	7.03	0.090	2.58	2.05	1.48	2.93	0.180	GSJ standard (Sedimentary rock)
JCh-1	98.4	0.030	0.7	0.38	0.018	0.08	0.04	0.03	0.22	0.010	GSJ standard (Sedimentary rock)
NBS120c	5.5	0.103	1.3	1.08	0.027	0.32	48.02	0.52	0.15	33.340	NBS standard (Phosphate rock)
Si93.3	93.5	0.179	2.0	1.25	0.021	1.07	1.27	0.38	0.19	0.036	JB-1a mixed with pure silica
Si88.7	88.7	0.314	3.5	2.20	0.036	1.87	2.23	0.66	0.34	0.063	JB-1a mixed with pure silica
Si83.8	83.8	0.449	5.0	3.14	0.052	2.67	3.19	0.95	0.49	0.090	JB-1a mixed with pure silica
Ca7.3	62.2	1.045	11.7	7.31	0.121	6.23	7.42	2.20	1.13	0.209	JB-1a mixed with pure silica
Mg28.4	13.4	0.332	3.7	2.31	0.046	28.38	50.22	0.70	0.35	0.117	JB-1a mixed with JDo-1
Mg21.6	26.4	0.657	7.3	4.59	0.081	21.56	36.65	1.38	0.71	0.165	JB-1a mixed with JDo-2
Mg14.6	39.6	0.987	11.0	6.90	0.117	14.63	22.87	2.08	1.07	0.214	JB-1a mixed with JDo-3
Ca42	33.7	0.840	9.4	5.88	0.097	5.01	41.93	1.77	0.91	0.168	JB-1a mixed with pure calcium carbonate
Ca30	40.6	1.013	11.3	7.09	0.117	6.04	29.93	2.14	1.10	0.203	JB-1a mixed with pure calcium carbonate
Ca17	48.2	1.201	13.4	8.41	0.139	7.16	16.90	2.53	1.30	0.240	JB-1a mixed with pure calcium carbonate
Mn6	49.5	1.235	13.8	8.64	5.992	7.36	8.77	2.60	1.34	0.247	JB-1a mixed with pure manganese carbonate
Mn5	50.1	1.248	13.9	8.73	4.991	7.44	8.86	2.63	1.35	0.250	JB-1a mixed with pure manganese carbonate
Mn4	50.6	1.261	14.1	8.82	4.004	7.52	8.95	2.66	1.37	0.252	JB-1a mixed with pure manganese carbonate
Mn3	51.1	1.274	14.2	8.91	3.002	7.59	9.04	2.68	1.38	0.255	JB-1a mixed with pure manganese carbonate
Mn2	51.6	1.287	14.4	9.01	2.001	7.67	9.14	2.71	1.39	0.257	JB-1a mixed with pure manganese carbonate
Mn1	52.2	1.300	14.5	9.10	0.999	7.75	9.23	2.74	1.41	0.260	JB-1a mixed with pure manganese carbonate
P27.5	13.8	0.316	3.7	2.51	0.049	1.64	41.18	0.92	0.37	27.496	JB-1a mixed with NBS-120c
P22	21.7	0.517	5.9	3.86	0.070	2.89	34.75	1.29	0.58	22.000	JB-1a mixed with NBS-120c
P16.5	29.5	0.718	8.1	5.20	0.090	4.13	28.33	1.66	0.79	16.516	JB-1a mixed with NBS-120c
P11	37.3	0.919	10.3	6.54	0.111	5.38	21.89	2.03	1.01	11.013	JB-1a mixed with NBS-120c
P5.5	45.1	1.120	12.5	7.89	0.132	6.63	15.45	2.41	1.22	5.505	JB-1a mixed with NBS-120c
Maximum	98.4	1.621	19.1	15.16	5.992	44.90	63.77	4.70	4.72	33.340	
Minimum	0.4	0.008	0.0	0.04	0.012	0.04	0.04	0.02	0.00	0.000	

Table I-2 Measurement condition for each element.

Element	Filter	Diafrum	Attainator	Slit	Crystal	Detector	PHA	Background1		Peak		Background2	
								2theta (degree)	Time (second)	2theta (degree)	Time (second)	2theta (degree)	Time (second)
SiO2	out	30mm	none	coarse	PET	PC	100-300	107.00	25	109.04	50	111.00	25
TiO2	out	30mm	none	coarse	LiF	SC	100-300	85.00	50	86.14	100	88.00	50
Al2O3	out	30mm	none	coarse	PET	PC	100-300	141.00	25	144.78	50		
Fe2O3	out	30mm	none	coarse	LiF	SC	100-300	56.50	25	57.50	50	58.50	25
MnO	out	30mm	none	coarse	LiF	SC	100-300	61.50	25	62.95	50	64.50	25
MgO	out	30mm	none	coarse	TAP	PC	100-300	42.93	50	45.19	100	47.45	50
CaO	out	30mm	none	coarse	TAP	SC	100-300	111.50	25	113.09	50	114.50	25
Na2O	out	30mm	none	coarse	TAP	PC	100-300	52.50	50	55.15	100	58.50	50
K2O	out	30mm	none	coarse	PET	PC	100-300	49.00	25	50.59	50	51.84	25
P2O5	out	30mm	none	coarse	Ge	PC	100-300	139.50	40	141.03	80	143.20	40

PC=Proportional Counter SC=Scintilation Counter

Table I-3 Coefficients for calibration equations and matrix calibration.

Element	Coefficient (Intensity=X)			Accuracy	Matrix calibration coefficient	
	X^2	X^1	X^0		Element	Coefficient
SiO2	-0.0016165	1.3889	-1.2171	0.4598		
TiO2		0.7552	0.0025	0.0085	Ca	0.0071828
Al2O3		1.2812	0.0197	0.1805		
Fe2O3		0.0862	-0.0478	0.1125	Ca	0.0074968
MnO		0.1097	0.0017	0.0057	Ca	0.0096351
MgO		3.7592	0.0570	0.1098		
CaO		1.1252	0.0380	0.0814		
Na2O		10.4530	0.0313	0.0518		
K2O		0.3830	-0.0243	0.0392		
P2O5	-0.0005976	0.4664	0.0004	0.0123		

Matrix calibration of element i for element j is calculated as
(Calibrated intensity of i) = (Raw intensity of i) * {1 + (Matrix calibration coefficient for j) * (Raw intensity of j)}

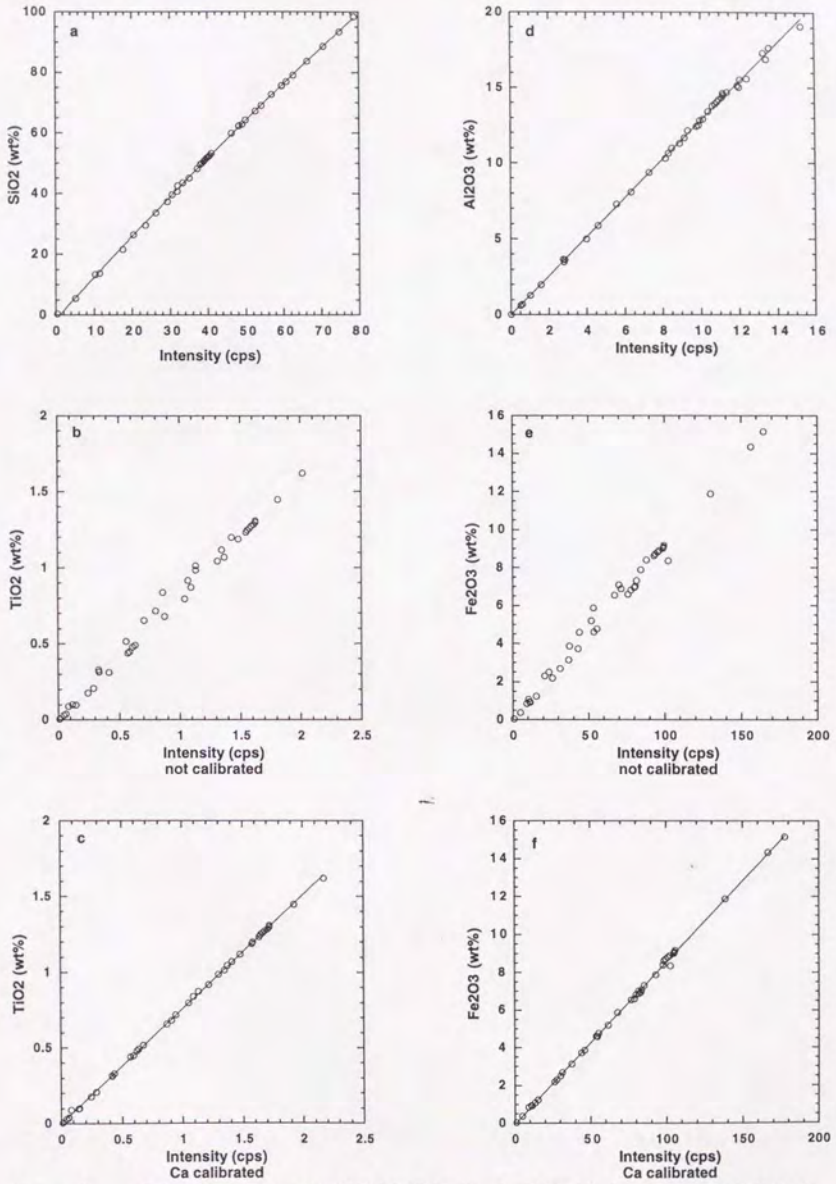

Figure I Calibration curves for SiO_2(a), TiO_2 (b, c), Al_2O_3 (d), Fe_2O_3 (e, f), MnO (g, h, i), MgO (j), CaO (k), Na_2O (l), K_2O(m), and P_2O_5 (n, o).

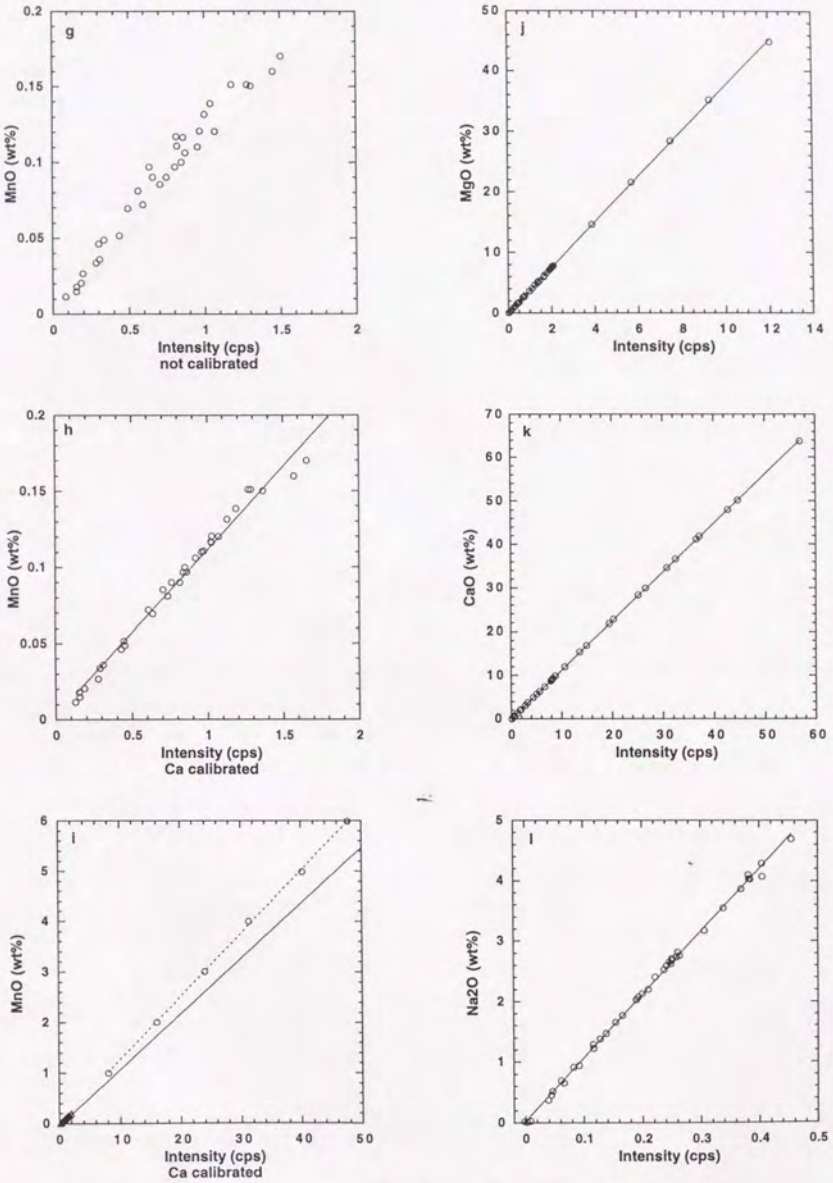

Figure I (*continued*)

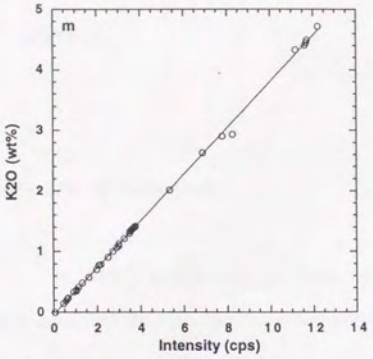

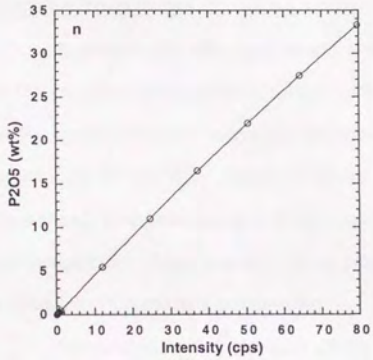

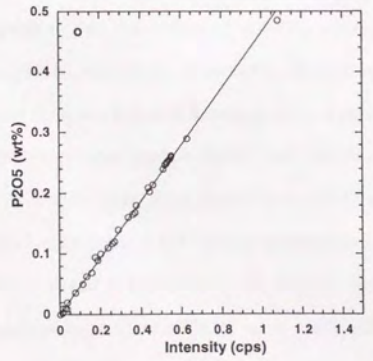

Figure I (*continued*)

II. Determination of Biogenic Silica Content using Alkali Extraction Method

Manual for Measurement

In order to establish the procedure for determination of biogenic opal content, the author modified the procedure described in *Mortlock and Froerich* [1989].

Pre-treatment of samples

Approximately 100 mg of sample is desalted with 50 ml of doubly distilled water (DDW) in a 75 ml polypropylene tube and sample with DDW in the tube is centrifuged at 3500 rpm for 1 to 2 hours until supernatant becomes clear. Clear supernatant is decanted and sample is dried at 50 °C overnight. Sample is moved to small glass crucible and dried at 110 °C for longer than 2 hours and sample in glass crucible is moved to desiccator to be cooled down to room temperature. Approximately 50 mg of desalted and 110 °C dried sample is exactly weighed into 75 ml polypropylene tube.

Approximately 5 ml (10 ml if sample is organic rich) of 10 % H_2O_2 solution (1 : 2 solution of first grade 30 % H_2O_2 and DDW) is added to sample in 75 ml tube to remove organic matter, the tube is capped with a polypropylene cap with a small hall to allow gas expansion, and left for 30 minutes. Then sample with H_2O_2 in the tube is moved to 50 °C water bath and left until babbling stop. Approximately 10 ml of 1N HCl solution (1 : 9 solution of super grade 10N HCl and DDW) is added to sample to remove carbonates and sample with the solution in tube is sonified for 30 minutes. Approximately 20 ml of DDW is added and sample is left for approximately 1 hour until babbling stop. Then sample in the tube is centrifuged at 3500 rpm for 30 minutes. Supernatant is decanted. Sample is rinsed with approximately 50 ml of DDW again and centrifuged at 3500 rpm for 1 to 2 hours until

supernatant become clear. Supernatant is decanted and sample in the tube is dried at 50 °C overnight.

Alkali extraction

Alkali extraction is time consuming and busy work. If all work is done by one person, he can treat maximum 24 samples per day. If there is one more helper, he can treat 48 samples per day. Procedure described below is the manual for one person.

Exactly 50 ml of 2M Na_2CO_3 solution is added to sample in 75 ml tube, capped with polypropylene cap with a small hole. Sample with alkali solution in the tube is swirled and then sonified for 5.5 minutes in supersonic vibrator with 85 °C water. This step is repeated every 1 minute for analyzed samples. After sonified, sample in the tube is moved to 85 °C water bath. Sample is swirled every 1 hour.

After n, (n+1), (n+2), ···· hours since 2M Na_2CO_3 solution was added to first sample, 0.500 ml of alkaline supernatant which contains Si from sample is sampled using micropipette and moved to small plastic cell. This step is also repeated every 1 minute for analyzed samples.

After n (also (n+1), (n+2), ····) hours 25 minutes since 2M Na_2CO_3 solution was added to first sample, preparation for Si determination by molybdate-blue spectrophotometry starts. This step should be finished within 35 minutes. The procedure is described later.

Calibration standards

The author used commercially sold silica standard solution (1000 ppm (= 35.606 mM Si) in 0.4N Na_2CO_3) as calibration standard. In order to check the quality, two kinds of standards (produced by Wako Chemical Co. Ltd. and Junsei Chemical Co. Ltd.) are used every time. 3M Na_2CO_3 solution is also prepared to adjust the matrix solution of calibration standards.

In order to make standard silica solution of various concentration, commercial silica solution, 3M Na_2CO_3 solution, and DDW are mixed in ratios below;

7.01 mM Si standard	1.97 ml : 6.54 ml : 1.49 ml
4.98 mM Si standard	1.40 ml : 6.57 ml : 2.03 ml
2.99 mM Si standard	0.84 ml : 6.61 ml : 2.55 ml
1.00 mM Si standard	0.28 ml : 6.65 ml : 3.07 ml
0.00 mM Si standard	2M Na_2CO_3 solution for alkali extraction was used.

Preparation of reagents

Preparation of reagents should be finished until the day before alkali extraction. All reagents are adjusted using DDW and stored in plastic bottle.

Molybdate reagent: 16.731 g of super grade $(NH_4)6Mo_7O_{24}\cdot 4H_2O$ is dissolved in DDW and adjusted to 1000 ml into mesflask.

Hydrochloric acid reagent: 48 ml of super grade 10N HCl is added to approximately 900 ml of DDW in a plastic beaker. The solution is cooled down to room temperature, moved to mesflask and adjusted to 1000 ml.

Metol-sulfite reagent: 12.000 g of super grade Na_2SO_3 is dissolved in DDW and adjusted to 1000 ml of mesflask. The solution is moved to plastic beaker, 20 g of metol (paramethylaminophenl sulfate) is added and stirred well. This solution is filtered using no.1 filter paper and stored in brown bottle.

Oxalic acid reagent: 60 g of super grade $(COOH)_2\cdot 2H_2O$ is dissolved in DDW and adjusted to 1000 ml of mesflask.

Sulfuric acid reagent: 30 ml of super grade H_2SO_4 is added to approximately 700 ml of DDW in a plastic beaker. The solution is cooled down to room temperature, moved to mesflask and adjusted to 1000 ml.

Adjustment of working solution

Adjustment of working solution should be conducted during the waiting time of alkali extraction procedure which is from 2 to 3 hours after addition of alkali solution to first sample. Working solutions can be stored approximately 6 hours.

Molybdate working solution: Molybdate reagent, hydrochloric acid reagent, and DDW are mixed exactly in a ratio of 1 : 1: 5.

Reducing working solution: Metol-sulfite reagent, oxalic acid reagent, and sulfuric acid reagent are mixed exactly in a ratio of 1 : 1 : 1.

Measurement of Si in alkali solution

Si in alkali solution extracted from sample is measured by molybdate-blue photospectrometry. Blue coloring process should conducted during wating time of alkali extraction.

Exactly 14.00 ml of molybdate working solution is dipensed in a clean dried 30 ml polypropylene tube. This should be done before first sampling of sample Si solution. Exactly 0.100 ml of sample Si solution is pippeted to prepared molybdate working solution, the 30 ml tube is capped with polypropylene cap and the solution is swirled. This step is repeated every 30 seconds for all analyzed sample. Exactly after 20 minutes, 6.00 ml of reducing working solution is dispenced to the mixture of sample solution and molybdate working solution, the 30 ml tube is capped with polypropylene cap and the solution is swirled. This step is also repeated every 30 seconds for all analyzed sample. Blue coloring takes longer than 12 hours. Prepared Si standards are reacted with working solutions using this procedure before sampling of sample Si solution.

On next day, colored solution is measured by spectrophotometer. The solution is put in a 1 cm cell, and the absorbance at 812 nm is measured. The absorbance at 812 nm of DDW is set to zero.

First, Si standards of are measured and calibration curve is calculated. The absorbance of 0 mM Si standard should be less than 0.004. Correlation coefficient of respctive set of Si standards of the two should be larger than 0.99 and correlation coefficient calculated using both sets should also be larger than 0.99.

After calculation of calibration curve, sample solutions are measured with same condition.

Dissolution of Silica from Sediment Samples as a Function of Time

The author checked the mode of dissolution of silica from sediment samples as a finction of time using 2 samples from the pelagic sediment core KH92-1, 5bPC (Euaripik Rise; 3° 31.94'N, 141° 51.40'E). Samples are Sec1-2 and Sec1-22 of the core. Extracted silica from samples at 2, 4, 6, 8, 10, and 12 hours since alkali extraction started were measured in duplicate, which also enabled the estimation of reproducibility of extraction procedure.

Figure II-1 shows the extracted SiO_2 wt% from samples as a fuction of time. During first 6 hours, silica dessolved to alkali solution rapidly. Whereas after 8 hours, silica dissolved slowly at a constant rate. Smear slide observation of dissolution residue showed that radioralian fragments could not be noted after 8 hours. This suggests that biogenic opal dissolution was finished during first 8 hours and dissolved silica after 8 hours originated from detrital fraction in the sediments [*DeMaster*, 1981].

Figure II-2 shows the x-y plots of dissolved silica for one aliquot vursus the other of duplication. 1 : 1 line shown in Figure II-2 indicate perfect agreement between two aliquots. Deviation around 1 : 1 line can be used as reproducibility of alkali extraction procedure. The result shows that the reproducibility of the procedure is ± 0.2 wt%SiO_2.

Determination of Time Needed for Biogenic Opal Dissolution for ODP Site 797 Sediments

To determine the reaction time required to perfect dissolution of biogenic silica for ODP Site 797 sediments, a smear slides of alkali treated samples for 0.5, 1, 2, 4, 6 hours are observed by optical microscope at the magnification of 40 powers. Diatom remains are observed in the samples treated for 0.5, 1, and 2 hours and no silica remains are noticed in those treated for 4 and 6 hours. Thus 4 hours alkali treatment are enough for dissolution of biogenic opal for the Japan Sea hemipelagic sediments.

Determination of Detrital Silica Dissolution Rate for ODP Site 797 Sediments

To check the dissolution rates of soluble detrital silicate minerals plus volcanic glass, dissolved silica extracted from samples after 5, 6, 7, 8, and 9 hours treatment were determined for 40 selected samples. As a result, 25 samples show that the correlation coefficient between dissolved SiO_2 vursus time was larger than 0.95 (Figure II-3). Although after perfect dissolution of biogenic silica, Figure II-3 shows that extracted silica increased linearly as the function of time which are caused by the dissolution of soluble detrital silicate minerals plus volcanic glass [*DeMaster*, 1981]. For these 25 samples, frequency of silica dissolution rate was examined (Figure II-4). Figure II-4 shows that silica dissolution rate of Site 797 sediments are deviated around 0.2 wt%SiO_2/hr and the 2σ is 0.1 wt%SiO_2/hr. Thus the author considers that average dissolution rate of silica from detritus is 0.2 ± 0.1 wt%SiO_2/hr for Site 797 sediments.

Simplified method

According to the results above, dissolution rate of silica from samples are constant at around 7 hours from starting of alkali treatment. Thus 7 hours alkali extraction of silica and the correction of 1.4 wt% (= 0.2 wt%/hr x 7 hours) for silica extracted from silicates could give a reasonable value for biogenic silica content of other samples. In this case, the error of estimation is within ±0.7 wt% (0.1 wt%/hr x 7 hours).

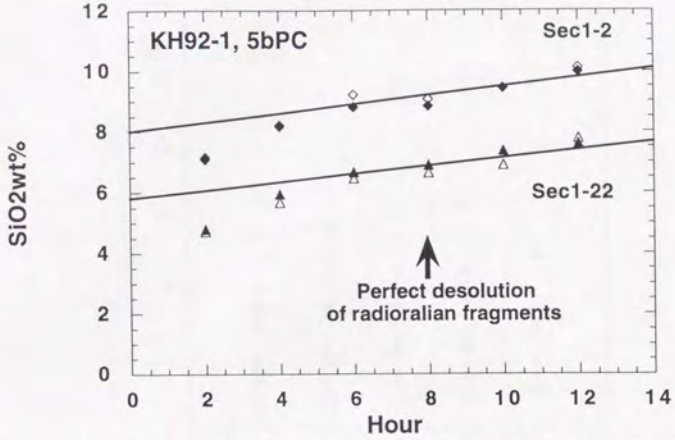

Figure II-1 Dissolved silica from sediment samples (KH92-1, 5bPC, Sec1-2 and 22) as a function of time.

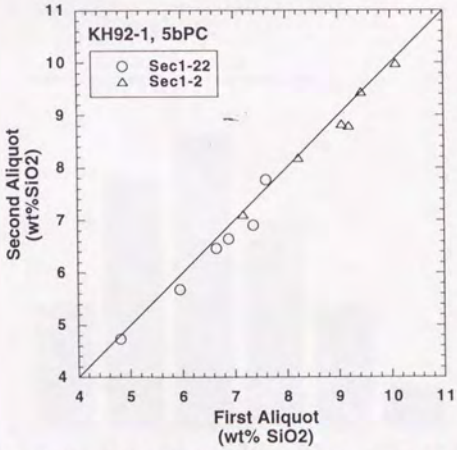

Figure II-2 Reproducibility of dissolved silica during the procedure of alkali extraction. Data are same as Figure II-1. 1 : 1 line indicates the perfect agreement between first aliquot and second of duplication.

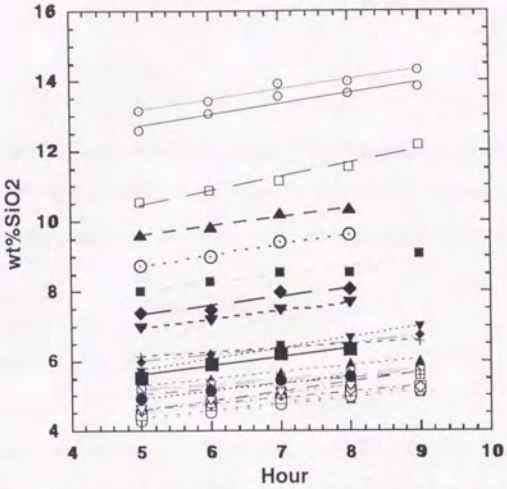

Figure II-3 Dissolved silica from selected sediment samples from ODP Site 797 as a function of time.

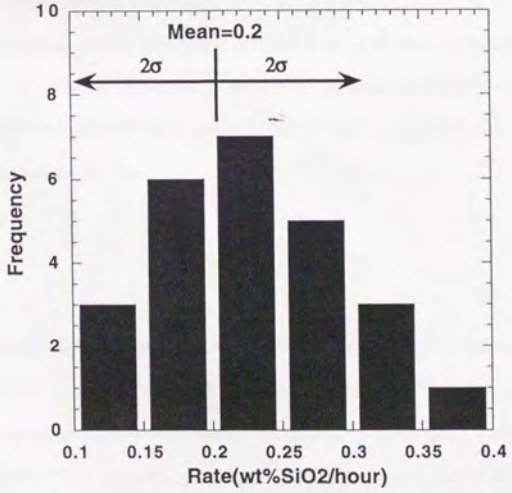

Figure II-4 Frequency distribution of dissolution rate of silica from detrital fraction of ODP Site 797 Sediments.

III. Determination of Mineral Composition using X-ray Diffraction Analysis

Introduction

In order to quantify the contens of minerals of ODP Site 797 sediments, X-ray diffraction analysis (XRD) was conducted. Diffraction intensity of minerals are calibrated to weight percent within the sample by calibration curve established using reference pure minerals.

Measurement Condition

Measurement was conducted by a MAC Science MXP-3 X-ray diffractometer (XRD) equipped with CuKα tube and monochrometer. Tube voltage and current are 40 kV and 20 mA, respectively. Scattering slit and divergent slit system is automatically controled as to obtain 25 mm beam width on the sample. Recieving slit is 0.15mm. Scanning speed is 4 °2θ/min and data sampling step is 0.02 °2θ.

Desalted powdered sample was finely ground in an agate mortar with approximately 5 ml of ethyl alchol for 5 minutes. Then, finely powdered sample is randomly mounted on a glass holder which has a circle deprresion with 25 mm diameter and 0.5 mm depth. Mounted sample is X-rayed from 2 to 40 °2θ.

Data processing

Before reading out the position and height of each reflection, two steps of data processing were applied.

As a first step, original data were smoothed by 5 points averaging which is equivalent to a window width of 0.2 °2θ. Smoothing calculation include noise removal by adaptive

smoothing followed by quadratic polynomial fitting. Noise level coefficient for adaptive smoothing is 1. This process minimize the error caused by noise.

As a second step, a background including amorphous hump is estimated by the background evaluation program using Sonneveld method which uses a wider smoothing window with 30 points (equivalent to 6 °2θ) between 2 and 40 °2θ. Because the peak width of smectite is approximately 6 °2θ, a smoothing window of 100 points (equivalent to 20 °θ) was used between 2 and 10 °2θ.

The background profile which is calculated using 30 points smoothing window is subtracted from the 5 points smoothed intensities to obtain the net peak intensities of crystalline minerals other than smectite. The background profile which is calculated using 100 points smoothing window is subtracted for smectite.

Diffraction Peak Identification

Identification of minerals are based on the following diagnostic peaks; 7.2 ° for smectite, 8.8 ° for illite, 10.4 ° for amphiboles, 11.5 ° for gypsum, 12.1 ° for chlorite + kaolinite, 26.6 ° for quartz, 27.8 ° for feldspars, 29.3 ° for calcite, 30.1 ° for rhodochrosite, and 32.9 ° for pyrite. The 7 Å and 14 Å peaks are considered as mainly contributed by chlorite because the peak ratios between 4.8 Å, 7 Å and 14 Å, which are diagnostic of chlorite are nearly constant (Figure III-1). The intensity of diagnostic peak (I) for each mineral was used to estimate the content of each mineral. Because 26.6 ° peak of illite overlaps the main peak of quartz, the quartz peak height at 26.6 ° was corrected for illite based on subtraction of twice of peak intensity of illite at 8.8 ° from the peak height at 26.6 °.

Background area from 16° to 32.5° is used as measure for amorphous materials. Background of sample profile is considered to be contributed by volcanic glass and / or its altered products, biogenic opal, and the background of other crystalline minerals. The author especially estimated the contribution from volcanic glass and / or its altered products by the method described later.

Standard Materials

As reference minerals for calibration of diffraction intensity to weight percent, montmorillonite (smectite) and serisite (illite) standards provided by Clay Mineral Society of Japan, chlorite, hornblende, and albite provided by University Museum of University of Tokyo, commercial quartz sand, andesitic volcanic glass from Pliocene section in the northeast Japan collected by the author, and biogenic opal extracted from diatomite of the Monterey Fromation provided by Associate Professor Ryuji Tada were used. Dignostic peak intensity and background intensity of these minerals were measured. The results are listed in Table III.

Calibration Curve

The peak intensities of the minerals (I) were transformed to their contents (wt%) using linear calibration equations for each mineral which were determined from meaurements of mixtures of pure reference minerals in various ratios. Calibration for calcite, pyrite, and rhodochrosite were performed by comparison between the peak intensity of these minerals and carbonate carbon content and total sulfur content.

The content of detrital amorphous material is estimated from the area of amorphous hump (A_{tot}) between 16 and 32.5 ° based on the following procedure. In order to evaluate the aerial contribution of detrital amorphous materials (A_{det}), the background area was corrected for biogenic opal of which content was determined by alkali extraction method as well as for the background of crystalline minerals as follows;

$$A_{det} = A_{tot} - \frac{1.1 \times bioSiO_2(wt\%) \times A_{opal(100)}}{100} - \sum_i \left(\frac{I_i}{I_{i(100)}} \times A_{i(100)} \right)$$

where I_i and A_i are peak intensity and background area of mineral *i* in the sample, respectively, whereas $I_{i(100)}$, $A_{i(100)}$, and $A_{opal(100)}$ are peak intensity and background areas of pure reference mineral *i* and opal, respectively. The water content of biogenic opal is assumed as 10% [*Mortlock and Froelich*, 1989]. Background area of pure andesitic volcanic glass from Pliocene section in the northeast Japan was used for a calibration standard for transformation of A_{det} to weight% because the detrital amorphous material in the samples are dominantly composed of altered volcanic glass.

Resulted calibration curves and equations are shown in Figure III-2.

Estimation Error

The reproducibility of measurement are within ±20% for smectite, ±30% for illite, ±30% for chlorite + kaolinite, ±60% for amphiboles, ±7% for quartz, ±15% for feldspars, ±10% for detrital amorphous, ±20% for calcite, and ±20% for pyrite, respectively.

Table III Intensities of main peak and background of reference minerals.

Mineral	Main Peak (cps)	Background (counts)	BG/Peak
Montmorillonite (Smectite)	375	15595	42
Serisite (Illite)	861	7784	9.0
Chlorite	3728	8874	2.4
Hornblende	901	6547	7.3
Quartz	10547	3096	0.3
Albite	8324	5851	0.7
Pumice		29304	
Opal		37332	

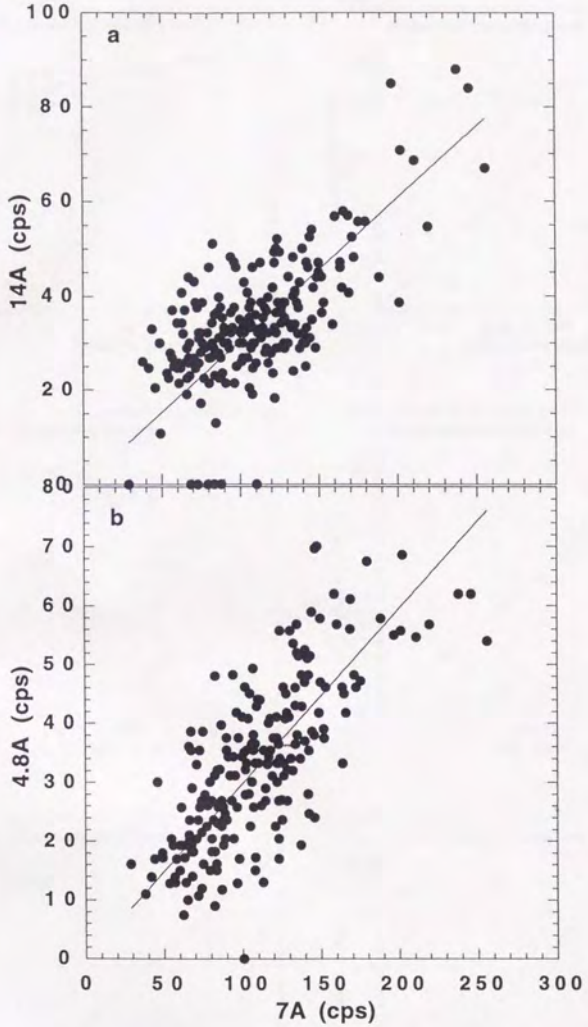

Figure III-1 Interrelationships beween diagnostic peaks of chlorite. a) 14Å versus 7Å, and b) 4.8Å versus 7Å.

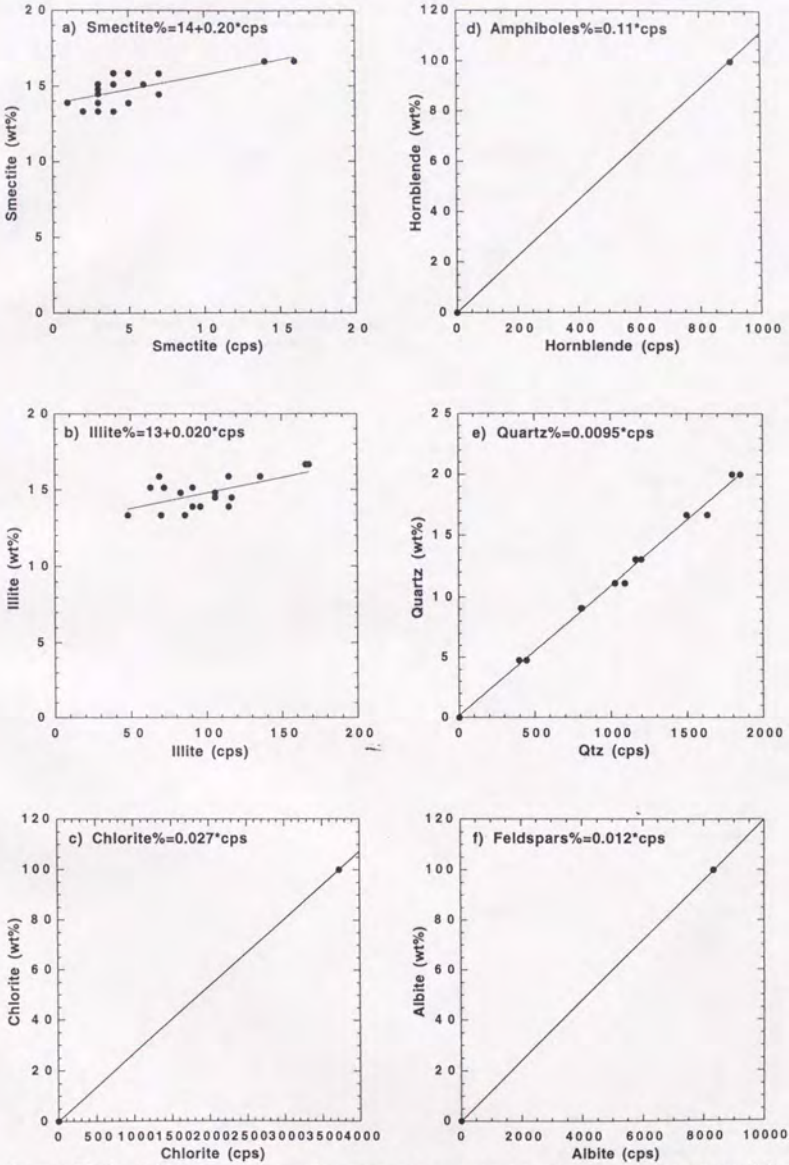

Figure III-2 Calibration curves and equations for smectite(a), illite (b), chlorite (c), amphiboles (d), quartz (e), feldspars (f), detrital amorphous (g), calcite (f), pyrite (g), and rhodochrosite (h).

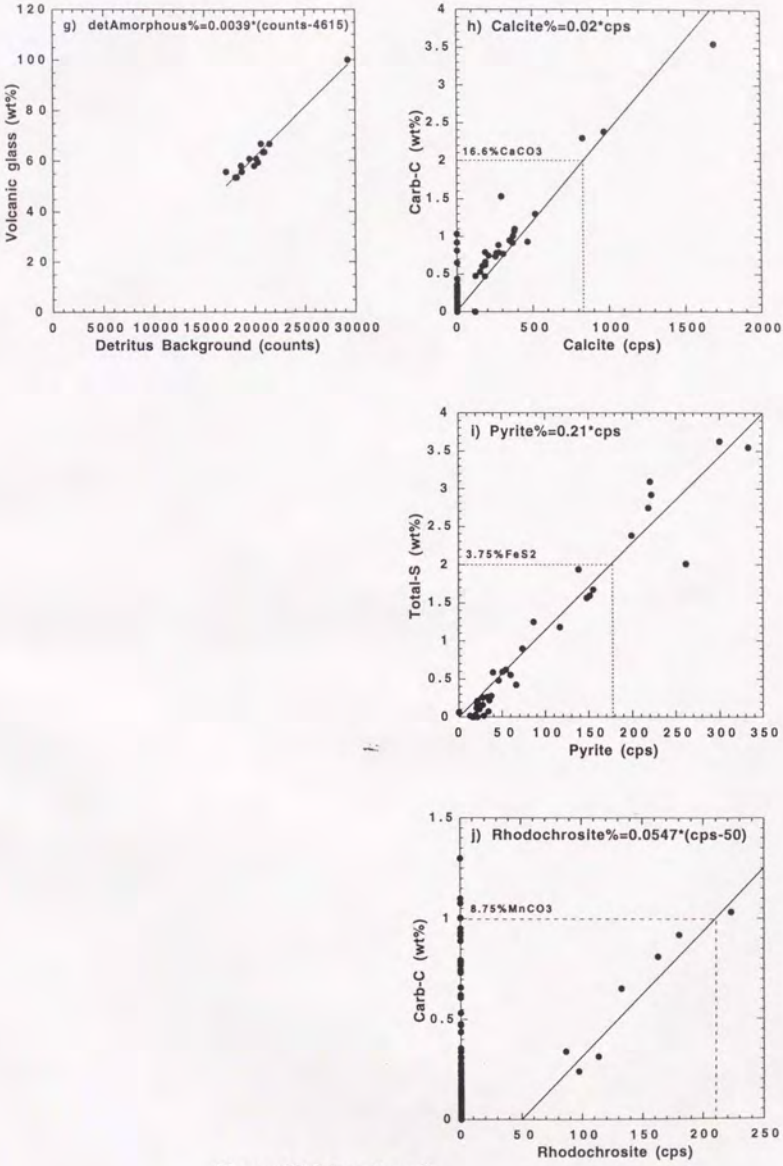

Figure III-2 (continued)

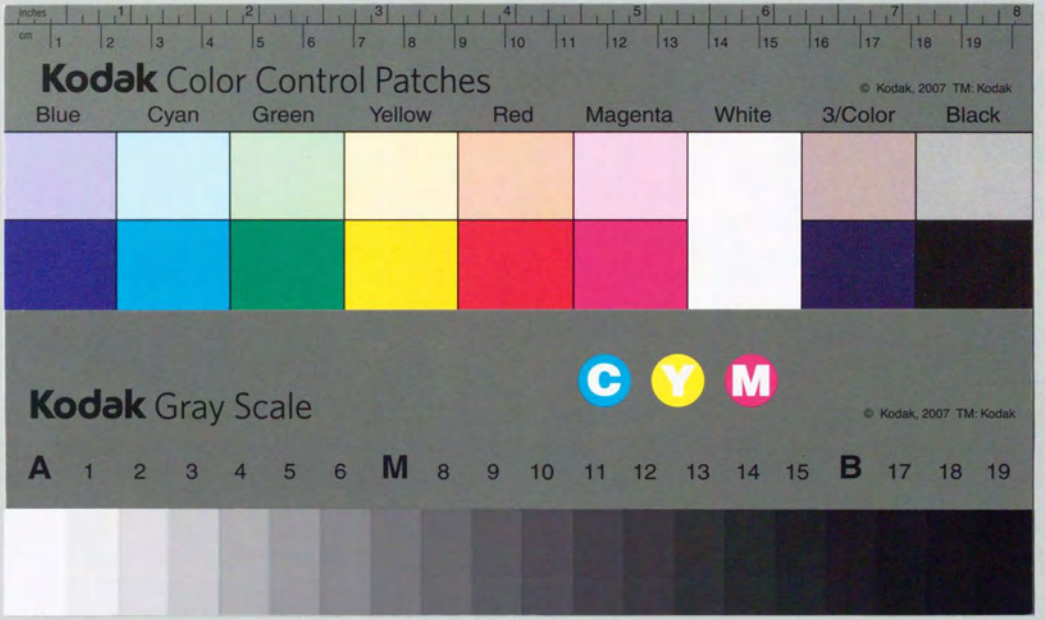
inches
cm
Kodak Color Control Patches
© Kodak, 2007 TM: Kodak
Blue
Cyan
Green
Yellow
Red
Magenta
White
3/Color
Black
C
Y
M
Kodak Gray Scale
© Kodak, 2007 TM: Kodak
A 1 2 3 4 5 6 M 8 9 10 11 12 13 14 15 B 17 18 19